Centre for Sensors, Instruments and
Systems Development
UNIVERSITAT POLITECNICA DE CATALUNYA

Shaping light to your needs

DOCTORAL THESIS

FOR OBTAINING THE DOCTORAL DEGREE

IN THE FIELD OF OPTICAL ENGINEERING FROM THE

TECHNICAL UNIVERSITY OF CATALONIA

UPC-BARCELONATECH

DEPARTMENT OF OPTICS AND OPTOMETRY

FACULTY OF OPTICS AND OPTOMETRY

NOVEL SYSTEM FOR MEASURING THE

SCATTERING OF THE CORNEA AND THE LENS

Author:

PAU SANTOS VIVES

Thesis Director:

DR. MERITXELL VILASECA RICART

Terrassa, 2018

A l'àvia i a l'Hèctor, Gal·la, Olau, Aleix i Mir

Assessment results for the doctoral thesis

Academic year:

Full name
_____

Doctoral programme
_____

Structural unit in charge of the programme
_____

Decision of the committee

In a meeting with the examination committee convened for this purpose, the doctoral candidate presented the topic of his/her doctoral thesis entitled _____

_____

_.Once the candidate had defended the thesis and answered the questions put to him/her, the examiners decided to award a mark of:

☐ FAIL ☐ PASS ☐ GOOD ☐ EXCELLENT

(Full name and signature)		(Full name and signature)	
Chairperson		Secretary	
(Full name and signature)	(Full name and signature)	(Full name and signature)	
Member	Member	Member	

_____, _____

The votes of the members of the examination committee were counted by the Standing Committee of the Doctoral School, and the result is to award the CUM LAUDE DISTINCTION:

☐ YES ☐ NO

(Full name and signature)	(Full name and signature)

Barcelona, _____

Supervisor's Certificate

Meritxell Vilaseca Ricart, associate professor at the Universitat Politècnica de Catalunya (UPC),

CERTIFY

that the work reported in the thesis entitled

Novel System for Measuring the Scattering

of the Cornea and the Lens

which is submitted by Pau Santos Vives in fulfilment of the requirements for the degree of Doctor by the Universitat Politècnica de Catalunya (UPC) has been carried out under my supervision within the framework of the PhD program in Optical Engineering.

_____

Meritxell Vilaseca Ricart

Agraïments

He dividit els agraïments entre la gent que ha aportat des d'un àmbit professional i les persones que ho han fet des d'un àmbit personal, matitzant que gairebé totes aquelles amb les que comparteixo un espai professional, també són importants fora de la feina. Sou moltes persones que heu fet posible aquesta tesi, seré més breu del que us mereixeu.

En primer lloc, i és la persona a qui més profundament li agraeixo haver-hi estat en tot el que implica el procés de la tesi (el suport durant la tesi) és a la Meritxell. Abans de començar el doctorat vaig preguntar a companys del màster i tothom em va dir que ets una grandíssima professora tant en coneixements com a persona. Els primers dies d'estar al Cd6, tots els companys i companyes que anava coneixent em deien exactament el mateix. Ara jo també tinc la sort de poder dir-ho. Gràcies per tot el que m'has ensenyat durant aquests anys. Gràcies per fer-ho sempre amb un somriure. És increíble la capacitat per poder amb tot i tirar-ho endavant des de l'excelència. Si has aconseguit que acabi la tesi, no dubtis mai que pots aconseguir tot el que desitgis.

Al JoAn, a qui puc considerar co-director de la tesi, que ha compartit amb mi els seus amplis coneixements sobre la òptica visual, l'ajuda imprescindible amb l'estadística i l'experiència al lab així com la seva humanitat.

Al Joan Carles, per tot el suport en l'àmbit clínic i aportacions essencials pel desenvolupament de la tesi.

A la Maria, per les hores invertides durant l'estudi clínic i les mesures amb les lents de contacte.

Al Jaume…*sobre espatlles de gegants*.

Al Fernando per la seva aportació en les simulacions i por totes les seves contribucions en el camp de l'òptica visual i sobretot en la técnica del Doble-Pas.

Al MD. Jorge Cazal, a tot l'equip del CIMA i del CUV per fer possible l'estudi clínic.

Al Xavi, un altre imprescindible per desenvolupar aquesta tesi. Sense les seves aportacions no hi hauria hagut ni sistema experimental ni prototip clínic.

A la Cristina i al Carlos Enrique, per tot el que vaig apendre en el projecte del HDA+, partint d'una idea inicial fins a arribar al prototip, passant pel disseny òptic.

Al Mikel, a la Clara i al Carles, per compartir l'aventura de Baltimore.

Al Tommaso, un placer vivir Hawaii contigo, las conversaciones sobre ciencia, sobre tecnología, sobre el futuro y el presente; las cervezas en la terraza y surfear cuando salía el sol. Y por lo que vendrá.

A tota la gent de Visiometrics. Que m'agradi la meva feina no es només per les tasques que he de desenvolupar, és sobretot per la gent amb la que comparteixo un objectiu comú.

Al Jan, per donar-me la oportunitat de l'oprtunitat de coneixer des de dins el món acadèmic i alhora del món industrial, cadascún amb les seves coses bones i dolentes, una experiencia d'un valor incalculable.

Al Càndid, per la llibertat i facilitats en cada pas que he donat.

Al Juan, gracias por toda la confianza que me has dado. No sé si eres consciente, pero tu forma de trabajar no tiene precio. Admiro tu forma de cuidar a las personas que trabajan contigo, sin importar la presión que tengas encima.

A l'equip de producció, Davids (Murillo, Martí i González), Judith, Antonio, Jasán. Mil gràcies per tota la feina que feu el dia a dia, per tirar de Visiometrics i pel bon humor que repartiu.

Al Sergiu, per conformar-te amb res que no sigui el millor possible.

A la Trini i l'Aida, gràcies per tot. Gràcies per fer-ho tot més fàcil.

A la Marta, per la teva capacitat d'analitzar amb profunditat totes les opcions i per la teva ètica. Al Luis, siempre riendo y transmitiendo felicidad, tienes que tener muy claro que llegarás donde quieras.

A tot l'equip d'enginyeria, David, Josué, Raúl R., Ricard, Jerry, Albert i Guillem. Amb els que compartim les hores. Gràcies pel bon ambient que aconseguiu sense deixar de ser competitius i mantenint un nivell professional altíssim.

Al Raúl C., un placer estar cada día a tu lado. Gracias por encontrar la forma de ayudar, siempre, aun cargando con Visiometrics en la espalda.

A l'Alex, des del primer día me has parecido una persona transparente y has demostrado unos conocimientos excepcionales sobre la difusión intraocular, la óptica visual y la ciencia. Eres una parte importante de esta tesis, lo sabes. Me ilusiona la idea de trabajar contigo los próximos años. Sé que aparte de pasarlo genial, tenemos mucho camino por recorrer.

Al Dr. Harilaos Ginis, καλημέρα celebrity. Fa falta més gent com tu, amb coneixaments tan extensos i profunds, i amb la facilitat i paciencia per compartir-los. Amb l'Alex sempre diem que *si lo dice Haris, será verdad*, i així és. Desitjo que compartim molts projectes en el futur per seguir aprenent.

Fora de l'àmbit professional, sense cap dubte, la persona més imprescindible en aquesta tesi ha estat l'Emi. Si no fos per tu això no hauria ni començat. Gràcies.

Al Valldu. A tots i totes les que feu possible aquest club i en especial al Gallego i al Ramon. Al primer per ser el motor incombustible, te echaremos de menos, disfruta y vuelve cuando quieras, aquí siempre tendràs la puertas obiertas. Al mister, per tantes coses que m'ha ensenyat, per la radicalitat dels seus raonaments i per la seva passió, que s'encomana.

A la Sara i al Sastre, per tots els dinars que acaben en sopar.

A l'Oriol i al Linus, cuidar-los com em cuiden ells a mi. (B)raves i buenas olas. I a tots els i la de física. Sou brillants.

A l'Eli, la Gladys i el Mario. Sois parte de esto y de mi vida, siempre os tengo presentes.

A la meva família, tan peculiar com meravellosa. Entre totes les definicions de família que he trobat, aquesta és la que més s'ajusta al concepte que tinc com a família: Un grup de gent que genuïnament s'estimen, confien, es cuiden i es busquen els uns als altres.

Als descarrilats del Zulo, això també és gràcies a TOTS vosaltres, per estar-hi SEMPRE. També encaixeu dins la definició de família. Al Sanuy, a l'Ander i l'Eloi, imaginar-me la vida sense vosaltres és impossible, hi sou des de que tinc memòria i no he conegut el món sense vosaltres, no us mereixeu que us agraeixi la Tesi, us mereixeu que us agraeixi haver crescut junts. Al Mendi, suposo que no ets conscient com d'important van ser les teves aportacions d'humor durant l'última etapa de la tesi, tot i la distancia m'he sentit molt a prop teu. Al Torre, referent absolut, tinc moltíssimes ganes d'insultar-te, però no ho puc fer aquí, espero que ho entenguis. Al Focu, pels riures infinits i pels suplements. Per les estones al Zulo, a

Pineda i tants altres moments inoblidables. Que no s'acabin mai. No em tireu gaire en cara haver-me posat monyes.

Contents

List of figures

List of tables

1 Introduction

According to the World Health Organization (WHO), 285 million people were estimated to be visually impaired worldwide in 2004, and 80% of them could be prevented or cured [1]. In 2017, another study estimated that 28 million people were blind and 216,6 million people had moderate to severe visual impairment [2]. In fact, vision plays a key role in human life: people with reduced visual acuity is 1.7 more likely to have a fall [3]; studies indicate that increasing uncorrected refractive errors had an increasingly detrimental effect on driving performance [4]; and one cause of scholar failure is visual impairment [5]. In 2012, the annual market of ophthalmic products was over 20 billion Euros. Even more, eye care products, diagnostic instruments and eye surgery exceeded 57% of revenues [6]. Therefore, research on human vision and eye optics has a direct impact on society as it can much contribute to improve people's life quality.

Properties of spatial vision, and specifically visual acuity, depend on the retinal image quality and brain processing. The retinal image is affected by three optical phenomena: diffraction, aberrations and scattering [7]. Diffraction is described by the Huygens-Fresnel principle for which in a propagating wave, each point can be understood as a point source of a spherical wave. When a wave encounters an obstacle with the size of the order of magnitude of the wavelength, interferences are produced due to phase summations.

Aberrations are caused by wavefront deformations. They can be classified in low-order and high-order aberrations (HOA) owing to the order of the Zernike polynomials in which they are often decomposed [8] (Figure 1.1). Low-order aberrations account for approximately 90% of the overall eye wavefront aberration. Myopia, hyperopia and astigmatism are of this kind and can be prescribed either using manifest subjective and objective refraction methods, while they can be corrected by means of glasses, contact lenses and refractive surgery. On the other hand, high-order aberrations such as coma, trefoil and spherical aberration cannot be easily corrected regardless the use of specific customized systems of refractive surgery.
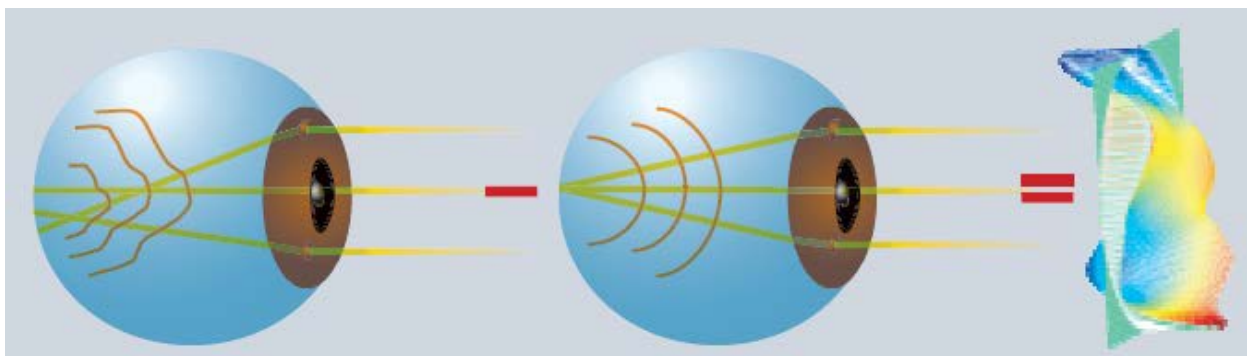
Figure 1.1. From left to right, aberrated wavefront, spherical wavefront and wave aberration map calculated as the difference between them (Source: Marcos 2005 [7]).

Whereas the two causes of retinal image distortion mentioned above are explained by the wave behaviour of light, scattering can be understood from its particle behaviour (i. e., photons). Thus, scattering is the deviation of photons or light rays due to photons' collisions because of media disturbances. And this may result in a veil of light over the retinal image (straylight); That is, the retina receives light at locations that do not optically correspond to the direction the light is coming from [9] (Figure 1.2).
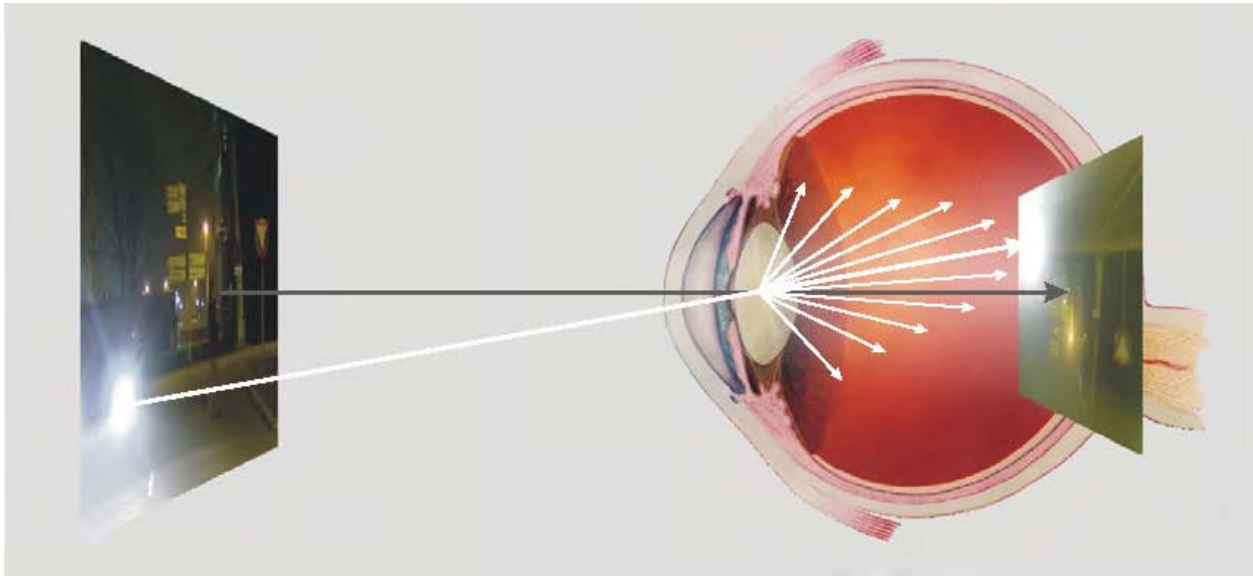
Figure 1.2. Illustration of retinal straylight with the image of the outside world (left) and its projection on the retina (right) (Source: van den Berg 2010 [10]).

This phenomenon is somehow very similar to what occurs in a game of billiard, when balls collide with each other influencing their trajectories. If the particles that produce the scattering are small compared with the wavelength, the phenomenon is called Rayleigh scattering. Within this domain, the scattered light intensity is proportional to λ^{-4}, where λ is the wavelength. The blue colour of the sky is an example of this; the white light coming from the sun is scattered by the atmosphere particles (blue light is the shortest visible wavelength). On the other hand, the scattering produced by particles with similar size to the wavelength is called Mie scattering. A well-known example of Mie scattering is the white colour of the milk, where all wavelengths are scattered in the same proportion.

Regarding the effect of scattering in the eye, it induces a luminous veil superimposed on the retinal image as commented above, which reduces the contrast and results in glare and hazy vision [11]. The cornea, a transparent tissue that constitutes the first and more powerful optical component of the eye (40 D [Dioptres]), and the lens, a biconvex structure with an optical power of approximately 20 D in far vision conditions, are the main sources of intraocular scattering (especially the last one).

Cataracts are responsible of 51% of world blindness and linked to a large amount of scattering produced in the lens [1]. They appear because of the denaturalization of proteins of the lens with age and, as a result, it

becomes opaque causing a dramatic increase of scattering [12]. Cataracts can be easily treated nowadays by means of surgery in which the lens is replaced by an artificial one. According to a review carried out by Gimbel and colleagues about the consequences of waiting for cataract surgery, a delay of 6 months in the surgery may result in a decrease of patient's vision and quality of life, the loss of driver's license, depression and adverse events including falls and fractures [13]. Consistent with this, as the WHO estimates, cataract surgery can allow people to increase their economic productivity 1500% of the cost of the surgery.

In this context, the assessment of intraocular scattering has been shown to be a potential tool to diagnose cataracts' severity. This is not a trivial issue since it is not possible to place a detector on the patient's retina. Traditionally, visual impairment due to scattering has been evaluated using clinical psychophysical tests such as visual acuity and contrast sensitivity charts with or without a glare source. However, there are some methods that deal with the assessment of backscattered light, such as the slit lamp. However, this light does not reach the retina as it travels away from it, and thus it does not affect vision. In the last years, other methods able to measure objectively the scattering of the whole eye by means of forward scattering (light reaching the retina and thus affecting vision) have also been proposed like double-pass (DP) technology.

Nevertheless, there is not yet any objective technique capable of measuring the intraocular scattering and determining from which part of the eye it is coming from, i. e., the cornea, anterior chamber, lens and vitreous.

Accordingly, the aim of this thesis is to develop a novel technique based on the Purkinje images for the objective and independent assessment of scattering caused by different parts of the eye. Specifically, we propose the analysis of the third (P3) and fourth (P4) Purkinje images formed by reflection of light by the first and second surfaces of the lens to do so. The hypothesis behind this is that P3 is affected by the light scattered in the cornea (and also in the anterior chamber), while P4 is affected by the former sources of scattering as well as that produced inside the lens.

In order to reach the goal of this thesis, the following stages have been completed:

1. Review of the methods to assess intraocular scattering.
2. Design and development of an optical-bench setup and a clinical prototype to acquire the Purkinje images.
3. Definition of parameters to account for scattering coming from different ocular structures, mainly the cornea and the lens.
4. Validation of the novel method at the laboratory level.
5. Validation of the novel method in a clinical environment.

This thesis is structured in nine chapters including this one as introduction.

Chapter 2 provides a description of the different topics covered by this work. It is dedicated to review the sources of scattering in the human eye and describe the state of the art of methods for its assessment. Finally, the theoretical basis of the Purkinje images formation and corresponding properties are also given.

Chapter 3 describes the experimental system developed. In the first section, optical simulations about the light distribution of the Purkinje images due to scattering in different ocular media are provided as well as relevant considerations to be taken into account as the basis to design the novel Purkinje system. Then a detailed description of the laboratory experimental setup as well as the proposal of novel parameters to measure scattering from the light distribution of the Purkinje images are given. The improvements needed to build the final prototype to work in a clinical environment are also discussed. Finally, the light-hazard calculations linked to safety issues are reported in detail.

Chapter 4 focuses on the validation of the technique proposed at the laboratory level. Two experiments were carried out for this purpose. Firstly, it was validated using artificial eyes with different levels of corneal and lens scattering. Secondly, we performed an experiment in-vivo, including eyes from a small group of volunteers of different ages.

Chapter 5 reports the outcomes of a clinical study that was conducted later. In this study, healthy eyes were included as a control group as well as others with cataracts and corneal disorders. Finally, the system was also validated with healthy young eyes with different levels of corneal scattering simulated by means of scattering-customized contact lenses.

Chapters 6, 7 and 8 contain the most relevant conclusions of this work and lines of future research and dissemination of the work done in this thesis.

Finally, the bibliography used in this thesis and the appendices containing the data sheets of components of the system, the instrumentation used, and the documentation related to ethical issues are presented.

2 State of the art

The quality of vision depends on the optics of the eye and the neural processing. As indicated in the introduction, the image formed on the retina by the ocular optics can be affected by diffraction, aberrations and scattering.

As a first approximation, the light scattering can be understood as changes in the trajectory of light due to collisions between photons and particles. However, it is a more complex process. From a classical approach, scattering is the deviation of an electromagnetic wave (incident ray) when it interacts with a scattering particle or surface. The interaction between the electric field of the incident light and the scatter particle results in a periodically oscillation of the electron orbits of the particle's molecules. Due to the oscillation, the distance between electrons (negative charge) and the nucleus (positive charge) changes, producing an induced dipole moment that acts as an electromagnetic radiation source. Therefore, the molecule emits light in different directions with respect to the incident light (scattering) [14]. If the emitted light is of the same wavelength as the incident light, the scattering is called to be elastic; if the wavelengths of the incident and emitted light are different, it is non-elastic scattering.

Scattering is also described by quantum optics. For simplicity, the description of the phenomena will be for a 2-level atom, although it can be applied to more complex systems. In this context, the lower energy state (E_0) is called ground state and the higher energy state (E_1) is called excited state. A photon that encounters an atom with the electron at the ground state can be absorbed if its energy ($\hbar\omega$) is the same as the difference of energies between the ground and excited states ($E_1 - E_0 = \hbar\omega$). If the photon is absorbed, the electron is excited to the upper level. However, due to uncertainty principle [15], energy and time cannot be definite simultaneously; in other words, the shorter the time interval is, the more energy values are allowed. This means that a photon can be absorbed even if its energy is not equal to the difference between levels ($E_1 - E_0 \neq \hbar\omega$). In this situation, the electron is excited to a virtual energy state for a short time. After this short time interval, the electron is de-excited to the ground state and a photon is emitted in a random direction. Thus, a photon is absorbed and emitted in a new direction as a bouncing between particles.

Two different frameworks have been developed to describe the theory of elastic light scattering: Rayleigh scattering (Lord Rayleigh (1842-1919)), which is valid for small particles; and Mie Scattering (Gustav Mie (1869-1957)), which is a solution for Maxwell's equations describing the scattering of a plane wave by a spherical particle. In fact, Rayleigh scattering is an approximation of Mie Scattering only valid for $\frac{2\pi r}{\lambda} \ll 1$ where r is the radius of the particle and λ is the wavelength of the incident wave in the surrounding media. Small particles are then defined as those following this inequality. Scattering intensity in the Rayleigh picture has a strong dependence on the wavelength ($I \propto \lambda^{-4}$); as a consequence, shorter wavelengths (bluish in the visible spectrum) are scattered more strongly than longer ones (reddish in the visible

spectrum). For larger particles, the scattering phenomenon is described by the Mie theory and there is no wavelength dependence.

Since scattering deviate photons from their initial trajectory, some of them entering in the human eye arrive at retinal locations that they should not reach and result in a veil of straylight over the retinal image. This has a significant impact on retinal image contrast for scenes containing a bright light source, such as those found in typical night driving [16] (Figure 2.1).

Figure 2.1. Simulated images without (left) and with scattering (right). Scattered light reduces retinal image quality owing to a decrease in the contrast of the retinal images.

2.1 Sources of intraocular scattering

Scattering in the eye can be produced in the tear film, the cornea and the crystalline lens, although aqueous and vitreous humours can also have a role.

Tear film is a liquid layer that protects the eye from the surrounding environment and the eyelid touch during blinking. It also provides nutrients to the cornea and allows having a good optical surface quality minimizing irregularities of the first corneal surface. A loss of homogeneity in the tear film due to local variations of its thickness [17] can have an impact on the retinal image. On the one hand, aberrations are introduced as long as the optical path depends on the tear film thickness, which means that for an irregular tear film the wave front is modified [18]. On the other hand, breaks in the tear film expose the irregular anterior surface of the cornea [19] increasing the scattering [20], [21]. Behrens and co-workers [22] proposed the term dysfunctional tear syndrome for dry eye disease. It affects 14% to 33% of the population worldwide [23], being the aging and the use of contact lenses the main causes.

The cornea is a convex-concave lens with a power around 40 D that has a structure built-up of collagen. The collagen fibres of the cornea are disposed in a transparent layer called stroma, in between the corneal epithelium and endotelium. It tends to absorb shorter wavelengths, especially ultraviolet (UV) (280 nm-315 nm), and blocks wavelengths above 2000 nm [24]. Mechanical distortion of the cornea as well as

damages and disorders of the epithelium, stroma and endothelium can cloud the cornea, inducing scattering and thus affecting the retinal image [25]. Farrell and colleagues [26] found a corneal scattering inversely proportional to the third power of the wavelength in in-vitro normal rabbit corneas. A more recent study [27] with enucleated eyes of pigs and rabbits found the same relation between cornea scattering and wavelength. Corneal edema due to surgery, infection and over-wear of contact lenses also affect corneal transparency and thus can cause intraocular scattering.

The crystalline lens, which is biconvex, has a variable optical power that allows focusing at different distances and achieving a good retinal image for near and far objects. It absorbs UV light, mainly from 300 nm to 400 nm (UVA). Because of the age and the denaturalization of proteins, the lens becomes opaque causing a dramatic increase of scattered light. In fact, it can be considered the main cause of intraocular scattering. Theoretical [28] and empirical [29] studies related to age determined that lens scattering does not exhibit wavelength dependence as the age increases. As described in the introduction, this common disease is called cataract, and can be treated by surgical replacement of the lens by an artificial one.

In turn, depending on the location of the lens opacification, cataracts can be classified from a morphological point of view as:

- Nuclear: the opacification is originated in the nucleus of the lens. It leads to a notable decrease of the retinal image quality.
- Cortical: the opacity appears at the equatorial zone of the crystalline lens. It might not affect the retinal image until intermediate stages of the cataract.
- Posterior subcapsular: in this case, the altered zone is the posterior crystalline capsule. The retinal image is generally highly affected by this kind of cataract.

The aqueous (between the cornea and the lens) and vitreous (between the lens and the retina) humours can be also a source of scattering [30] and might affect the retinal image under severe inflammatory processes (e. g., Tyndall's effect).

2.2   Methods to measure intraocular scattering

The current existing methods to measure or quantify intraocular scattering are presented in the following sections. The fundamentals of each method are described as well as the advantages and drawbacks. The methods are divided into subjective and objective. The first ones refer to those where the result or measurement strongly depends on the examiner criteria or the patient choice, which induce therefore high variability. In order to overcome this, objective methods to measure the intraocular scattering have been developed in the last years.

2.2.1   Subjective Methods

Clinically used methods to quantify scatter are based on psychophysical procedures, i. e., they need the active participation of the patient and thus, they are subjective. The most often used include from contrast sensitivity tests to more sophisticated systems such as the C-Quant instrument. Besides psychophysical tests, physicians also evaluate intraocular scattering of the eye by means of the slit lamp, which provides valuable information. In this case, the evaluation is strongly linked to the ophthalmologist criteria and therefore, this method is also considered as subjective. All them are described below.

Contrast sensitivity charts

This is one of the most widely used techniques to evaluate visual impairment. Essentially, the patients' contrast sensitivity refers to the minimum contrast that the visual system is able to distinguish for each spatial frequency (cycles per degree [c/d]). Figure 2.2 shows the typical contrast sensitivity function (CSF) obtained in adult population. It depends on the eye's optics but also on the neural process that takes places from the retina to the visual cortex. As it can be seen, the contrast sensitivity has a passband shape, being its maximum located at intermediate frequencies (4-10 c/d) while it is lower at higher and lower ones. The decrease at high frequencies is mainly caused by aberrations of the optics as well as photoreceptors density and size. The decrease at low frequencies is due to the lateral inhibition of ganglionar cells of the retina. The contrast sensitivity also depends on the level of illumination and other factors.
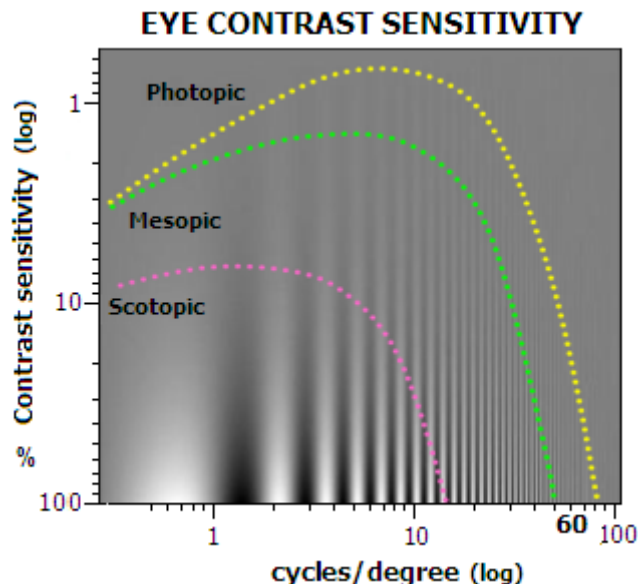
Figure 2.2. Typical contrast sensitivity function at photopic, mesopic and scotopic levels of illumination. The frequency (c/d) increases from left to right. The contrast increases from top to bottom.

CSF is often measured by means of tests including sinusoidal gratings with different spatial frequencies and contrasts [31]–[33], but it can also be evaluated using optotypes (letters or Snellen charts) with variable size and contrast [34].

As an example, Figure 2.3 shows the commercially available systems Vision Contrast Test System (VCTS) and CSV-1000. The first one has five different spatial frequencies (1.5, 3, 6, 12 and 18 c/d) and 9 different contrasts for each frequency. The second is a retro-illuminated screen that contains sine-wave gratings with spatial frequencies of 3, 6, 12 and 18 c/d and 8 different contrasts for each frequency.
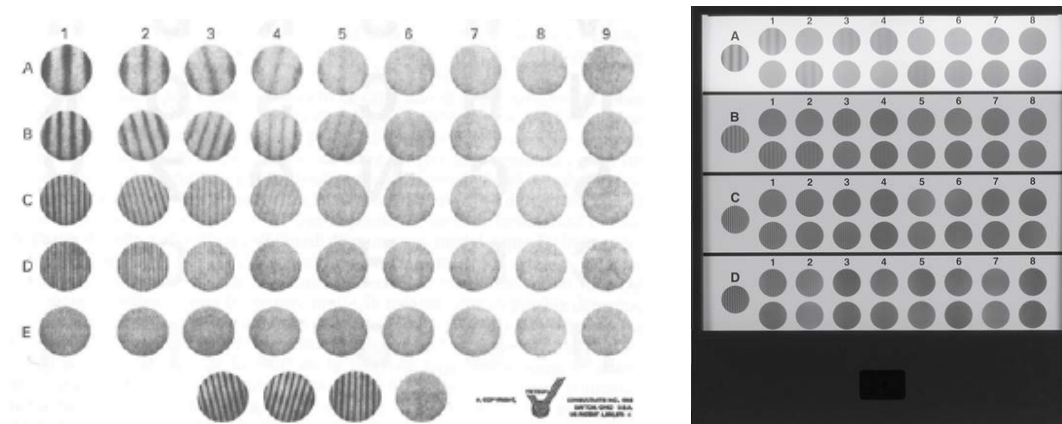
Figure 2.3. Vision Contrast Test System (left) and CSV-100 (right). Both include sinusoidal gratings with different contrast (columns) and frequency (rows). Orientation is used to evaluate if the patient can detect the grating or not in the first one while the second uses a two alternatives forced choice method.

Recently, computer generated charts have also been developed [35]. The advantage of displaying images on LCD (Liquid Crystal Device, an electronic display device where the luminance of each pixel is electronically controlled) monitors is the possibility of varying and control the contrast although sometimes specific displays are required as those typically used of 8-bit depth are above the human's contrast threshold.

It is worth noting that defocus mainly modifies the CSF at high frequencies, reducing therefore the CSF cut-off frequency (the highest perceived frequency at highest contrast), and therefore it is linked to the patient's visual acuity. However, intraocular scattering reduces homogeneously the CSF for all frequencies and this is the reason why in such case, the assessment of the visual acuity is not enough to analyse visual deterioration.

Sometimes, the effects of scatter on vision, which are basically glare, are also analysed by means of a contrast sensitivity test together with a bright source. Specifically, the CSF of the patient is compared with and without the presence of the source. There are commercial devices to perform this measure. The glare

testing system CSV-1000HGT (Vector Vision) is a retro-illuminated screen (Figure 2.4) similar to the CSV-1000 but containing a glare source.

Figure 2.4. CSV-100HGT, a contrast sensitivity test containing a glare source.

Another commercial instrument available is the Brightness Acuity Tester (BAT) [35] (Figure 2.5). The patient looks through the device, which can simulate different illumination conditions. In combination with contrast sensitivity tests, it provides the CSF and its variation under different illumination conditions.

Figure 2.5. Patient using BAT (Source: Holladay et al. 1987 [36]).

Equivalent veil luminance

At the beginning of the past century, an experimental scene to quantify the intraocular scattering [37], [38] was proposed. It relies on the fact that looking a target with the presence of a distant glare source is equivalent to look at the same target with the presence of a homogeneous background illumination. The goal of this method is to find the equivalent luminance (also called equivalent veil), L_v, which depends on the glare source used as well as the scattered light present in the patient's eye (Figure 2.6). The glare source is located at an eccentricity ϑ from the eye and produces an illumination E_{glare} at the pupil's plane.
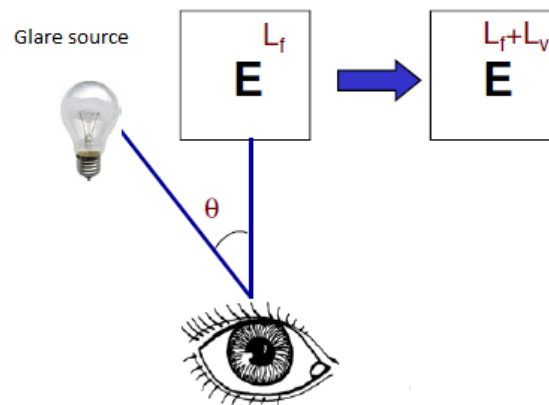
Figure 2.6. Schematic of the equivalent veil luminance fundamentals. L_f is the background and L_v is the equivalent background to reproduce the distant glare source effect.

Having a variable homogeneous background illumination, the patient is asked to choose the intensity needed to see the target similarly to the glare source situation. The more intraocular scattering, the more background intensity is needed to achieve the equivalent E_{glare} in the presence of the glare source. Empirically, it has been found that L_v for normal eyes can be calculated using the following equation (Equation 2.1):

$$L_v(\vartheta) = \frac{10E_{glare}}{\vartheta^2}$$
<div align="right">Equation 2.1</div>

Other equations to calculate L_v have been proposed including other factors like age, iris pigmentation or pupil size. In 2003, Vos [39] proposed the following one, which is now the general glare equation used:

$$\frac{L_v}{E_{glare}} = \frac{10}{\vartheta^3} + \left(\frac{5}{\vartheta^2} + 0.1 \cdot \frac{p}{\vartheta}\right) \cdot \left(1 + \left[\frac{age}{62.5}\right]^4\right) + 0.0025 \cdot p$$
<div align="right">Equation 2.2</div>

where p is the pigmentation factor and takes values from 0 to 1.2, being 0 a black eye and 1.2 a very light pigmented iris.

As it can be seen, age is a relevant parameter and has a deep impact on glare measurements. The reason is that with age, scattered light in the eye notably increases mainly due to opacification of the lens, which is

in charge of absorbing UVA along the whole life. Simultaneously, the crystalline lens has a period of growth throughout adulthood where new cells spread along the meridians, forcing older cells towards the nucleus and becoming compressed, which results in a loss in lens transparency [40].

This method was laborious and therefore unsuitable in the clinical practice, with large variations reported between results obtained in different groups [41].

Direct Compensation Method

The direct compensation method was presented by van den Berg in 1986 [42] in order to improve the uncertainties from the equivalent veil technique. In 1992, it was implemented in a portable device (straylight meter) by van den Berg and IJspeert [43].

The straylight meter was a 5 cm diameter tube containing concentric annulus of light-emitting diodes (LEDs) and a test patch at the centre (Figure 2.7). The working principle of the technique relied on the amount of scattered light emitted by the rings reaching the centre of the retina (where the image of the test patch is formed).
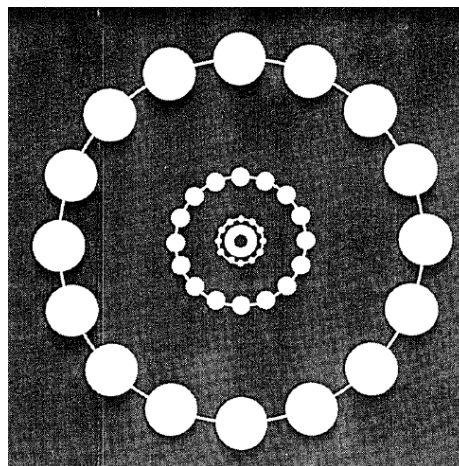
Figure 2.7. Schematic of straylight meter. Test patch at the centre of 1 degree of arc surrounded by a bright annulus of 2.5 degrees and three circumferences of light-emitting diodes at 3.5, 10 and 28 degrees, respectively. (Source: van den Berg et al. 1992 [43]).

To measure the straylight, the patient starts looking inside the tube with the test patch off while the modulation depth of the second ring (10 degrees of arc) increases until the patient is able to identify light flickering in the test. At this point, the modulation depth of the ring is increased 4 times and the test is illuminated with a counterphase modulation (when the ring turns off, the patch turns on and vice versa). The test intensity increases until the flickering is undistinguishable t the patient (Figure 2.8). The procedure is repeated for the rings positioned at 3.5 degrees and 28 degrees.
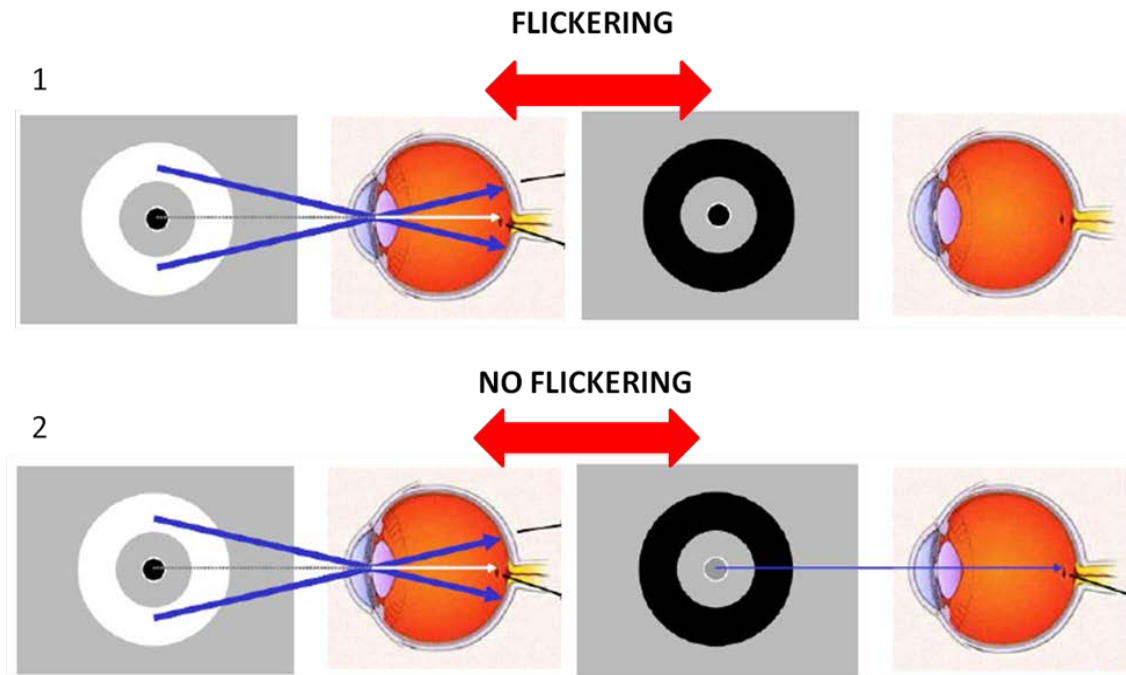
Figure 2.8. (Left) The ring is on and the test is off; note that a portion of light is reaching the central region of the retina due to scattering. (Right) The ring is off and the test is off (top) and on (bottom). (Top) the patient sees a flickering because the test is not compensating the scattered light from the ring. (Bottom) the test compensates for the scattered light and the patient cannot detect the flickering.

Studies about the aging effects [44], iris pigmentation [45] and the ratio between forward and backscatter in different kinds of cataracts [46] were published using this method. Forward scattering refers to scattered light reaching the retina (i. e., in the same direction of incident light) while backward scattering is that in the opposite (backward) direction. In the cited study, the authors found a significant correlation between age and scattering. Differences between light-blue and brown-dark eyes were reported, having the first ones more than two orders of magnitude of transmitted light. The results when comparing forward and backscatter showed that each kind of cataract (nuclear, cortical and posterior subcapsular) has a different and characteristic mean ratio between these quantities. However, there was a variation among individuals, especially for cortical and posterior subcapsular cataracts. The publication concluded that, as a rule, forward scatter cannot be derived from backscatter. As it will be seen in the end of this section, the slit-lamp method, which is widely used clinically, provides information of backscattered light. Consequently, new methods for the assessment of forward intraocular scattering are still being developed nowadays.

Although the direct compensation method was important in the research of intraocular scattering, it has some drawbacks. It uses high intensity visible light, which is not comfortable for patients. Furthermore, there is no control of measurement reliability since there is no reference to check the patient's answer (the contrast sensitivity charts have different orientations for each grating in order to check the veracity of the

answer) [47]. And sometimes it is not clear for patients to determine when the flickering disappears. This is the reason why it is no longer used.

Compensation Comparison Method

As commented above, in the direct compensation method it is often not easy to identify the light intensity needed to compensate for the flickering. Accordingly, a modified version of this technique was later developed where a "two alternatives forced choice" was introduced to solve this issue [48], [49]. In this new approach, just one half (randomly chosen) of the central test is illuminated with counterphase modulated light (Figure 2.9). The patient must choose which one of the two halves is flickering more strongly (note that the two halves could flicker, but they will have different "flickering intensity"), which is an easier task.

The compensation comparison method has been implemented in a commercial device called C-Quant (Oculus Optikgeräte GmbH,Wetzlar, Germany).
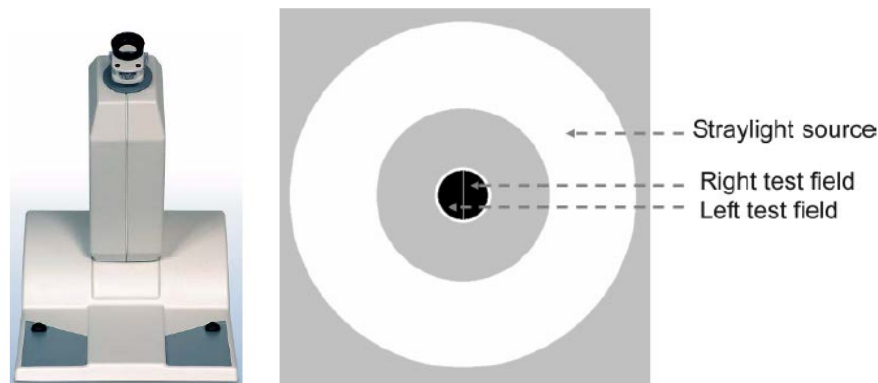
Figure 2.9. Commercial device (left) and schematic of the field of view in the C-Quant device (right) (Source: Franssen et al. 2005 [49]).

By definition, if the patient determines that the flickering side is the half without compensation, the result is 0; if the patient determines that the flickering side is the half with compensation, the result is 1. The results are fitted with the psychometric function in order to minimize human error [49].

This psychophysical method is able to measure the effect of intraocular scattering in the patient's vision (including optics and neural contribution). Even the two alternatives forced choice is a huge improvement for the reliability of patients' decision, subjective measurements could still induce to false-negative or false-positive results. Another drawback of this method is that for many of the patients with cataracts, who are the most affected by scatter, it is difficult to perform the demanded task.

Slit lamp biomicroscope

The combination of a microscope and a slit lamp (light source) is a widely used method to explore clinically the anterior segment of the eye. It requires the skills of the clinician and usually the dilation of the patient's pupil if the lens is to be observed. Physicians usually use it as a means of grading cataracts. A cataract grade

classification called Lens Opacities Classification System III (LOCS III) [50] was created from slit lamp images (Figure 2.10) trying to diminish the intrinsic variability of the method depending on the examiner's criterion used. LOCS III is the third generation of cataract grade classification for slit lamp images. It includes 6 levels of nuclear opalescence (NO) and colour (NC) for nuclear cataracts, and 5 levels for cortical (C) and posterior subcapsular (P) cataracts. The improvements from LOCS II to LOCS III are equal intervals between standards, an increase of standard images, the incorporation of decimal grading and a reduction of tolerance limits.

It is worth noting that slit lamp images are obtained with backscattered light. In-vitro studies in human donor lenses showed that forward and backscatter have different behaviour, which might depend on the particle size [51], [52]. Accordingly, forward scatter cannot be derived from backscatter [46] although they are somehow related.
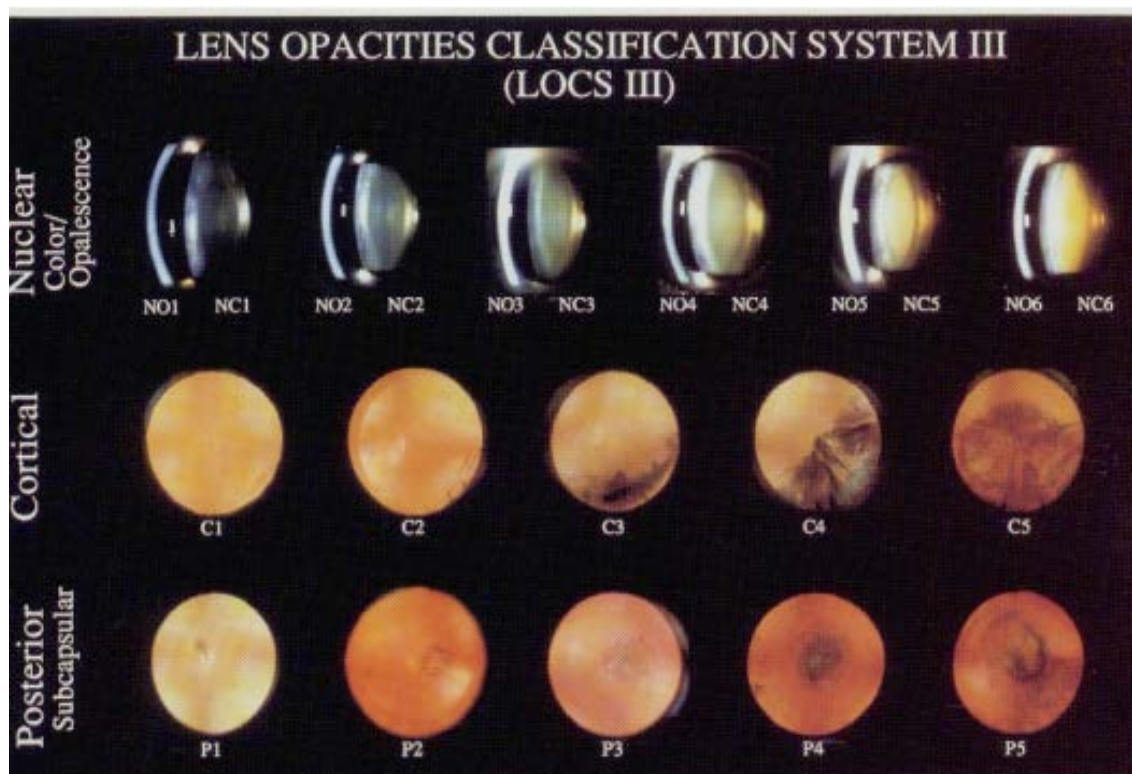
Figure 2.10. The LOCS (Lens Opacities Classification System) III standard (Source: Chylack et al. 1993 [50]).

2.2.2 Objective Methods

A review of the up-to-date objective techniques used to quantify intraocular scattering is presented in the following pages. As formerly mentioned, they try to overcome the variability that subjective methods show seeking to find methods that neither require the active participation of the patient nor the examiner.

Scheimpflug cameras

For a lens and image planes that are parallel, the focus plane is also parallel to them. If a planar object is parallel to the lens and the image plane, it can coincide with the focus plane. However, if the object is not parallel, just a region of the object will be in focus (Figure 2.11). The Scheimpflug principle introduced in 1904 by Theodor Scheimpflug [53] is a geometrical description to focus an object when it is not parallel to the image plane. It determines the position and orientation of the planes in order to achieve a planar object to be completely in focus.
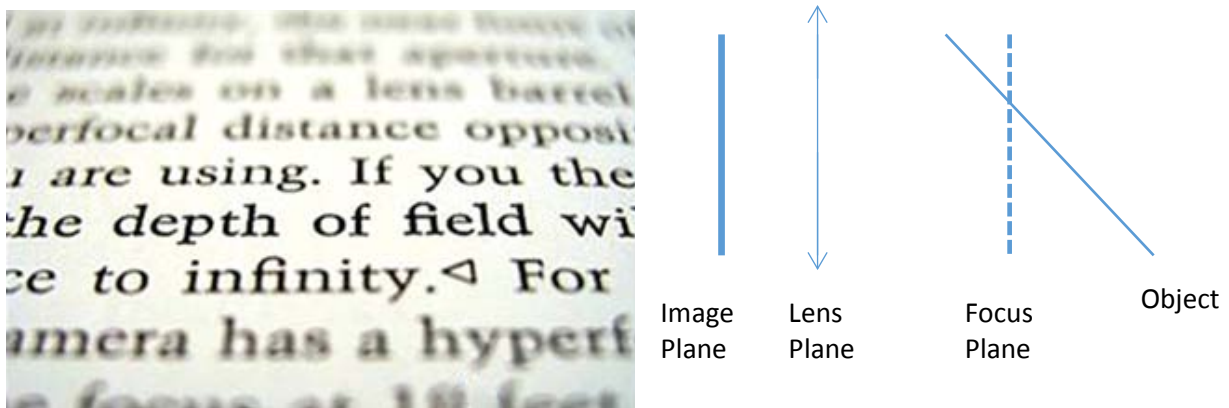
Figure 2.11. Example of non-parallel object and image planes where just an object section is in focus. Real image (left) and schematic of planes (right) (Source: Jain et al. 2009 [54]).

In a Scheimpflug camera, the slit beam (the light used to illuminate the eye section), the objective lens, and camera sensor are positioned in such a way that a cross-section of the object (in our case the eye) appears in focus [55] (Figure 2.12).
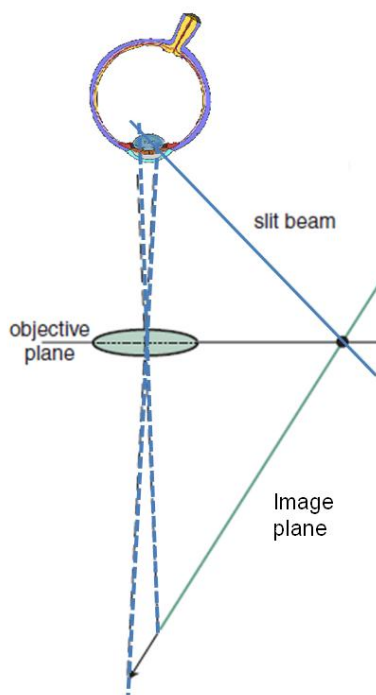
Figure 2.12. Optical design of the Scheimpflug camera to view the cross-section of the eye.

Vivino and co-workers developed a Scheimpflug slit lamp camera system for quantitative densitometric applications of ocular structures [56]. According to Beer studies [57], the medium concentration is proportional to the optical density (OD). The Scheimpflug slit lamp camera system was used to find a correlation between OD and cataracts. The system was designed to objectively measure OD in three different anatomical parts of the lens (anterior, nuclear and posterior) (Figure 2.13).
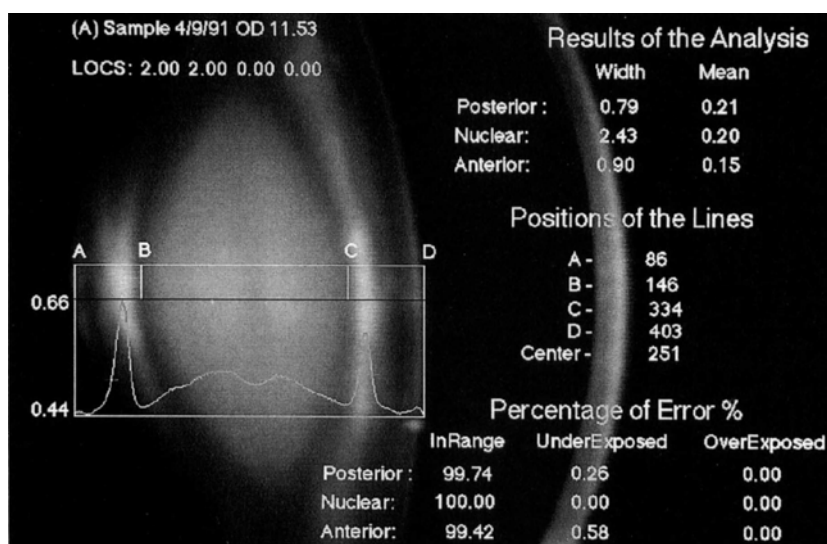
Figure 2.13. Output obtained with the Scheimpflug slit lamp camera system. Width is the layer's width in mm, Mean is the OD and the Percentage of Error % corresponds to the saturated and underexposed pixels for each anatomical part of the lens. The LOCS score is determined by a physician, not by the Scheimpflug system (Source: Vivino et al. 1993 [56]).

In recent studies, the Scheimpflug system has been compared with the LOCS III scale [58]. Authors have reported a positive linear correlation between the Scheimpflug-measured lens nuclear density and the LOCS III grading scores for nuclear opalescence (NO) and nuclear colour (NC) (r = 0.734 and 0.719, respectively).

According to the former results, the Scheimpflug technique can be used as an objective numerical value for cataract grading. Moreover, this technique is able to distinguish opacities of different anatomical parts of the lens. Nevertheless, measurements are obtained using backscattered light, similarly to the slit lamp technique, and thus outputs can differ from those obtained with the scattered light reaching the retina [46], which is actually impairing patient's vision.

Dynamic light scattering (DLS)

The objective techniques described so far have a macroscopic approach. Dynamic light scattering (DLS) analyses the eye properties in a microscopic scale. The eye is illuminated by coherent light and the scattered light is recorded by a photodetector (Figure 2.14). The eye molecules are assumed to have a Brownian motion (i. e., random walk) [59]. The light intensity scattered by the eye molecules fluctuates since the relative position between molecules changes with time. In other words, for constant illumination intensity, the recorded intensity has small variations in time due to the molecules movement. In order to obtain information about the recorded signal, the autocorrelation is computed (Equation 2.3):

$$g^2(\tau) = \langle I \rangle [1 + \beta exp(-2\Gamma\tau)]$$ Equation 2.3

where I is the average recorded intensity, β is an empirical constant, Γ is related with the diffusion coefficient (by means of the wavelength, scattering angle and refractive index) and τ is the time shift. A more detailed description can be found elsewhere [60].
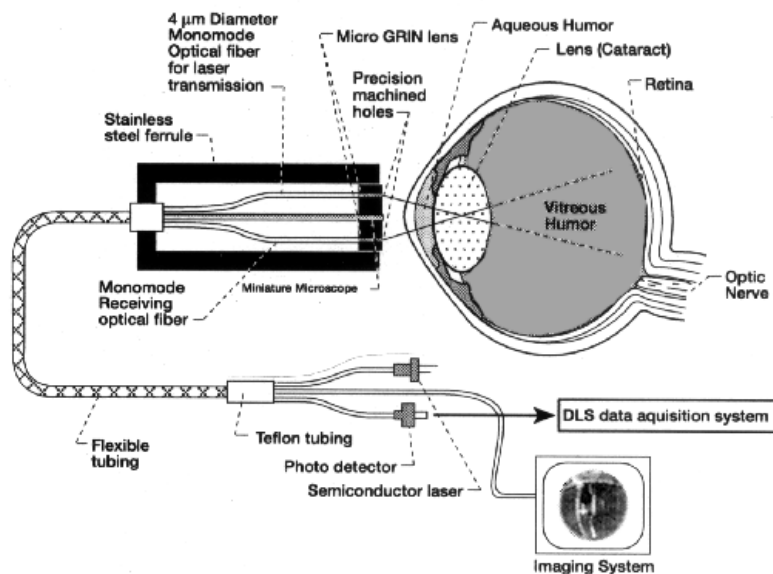
Figure 2.14. Schematic drawing of NASA's fiber-optic eye diagnostics device (Source: Ansari et al. 2004 [60]).

The autocorrelation can be understood as the comparison between the signal and the signal itself shifted in time (Figure 2.15).
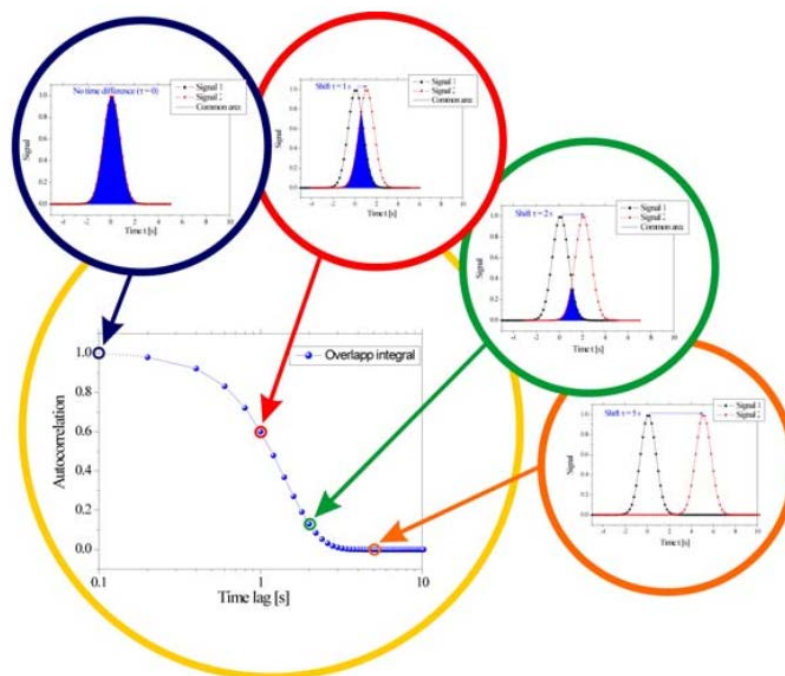
Figure 2.15. Example of the autocorrelation curve. The signal is compared by itself shifted in time (Source: Schwille et al. 2001 [61]).

Since the intensity changes are caused by the molecules movement, the decay of the autocorrelation curve is related with their diffusion coefficient. Light intensity scattered from slow particles fluctuates slowly, while light intensity scattered from fast particles fluctuates rapidly. Moreover, from the Stokes-Einstein relationship it is known that the diffusion coefficient of a spherical particle in an aqueous solution is inversely proportional to the particle hydrodynamic radius [62]; knowing the diffusion coefficient, the particle size can therefore be calculated.

In a recent study [63] using DLS, it was shown that the particle size distribution in normal eye's tears is smaller than 50 nm in diameter, while the size distribution for aqueous-deficient dry eyes is up to 300 nm in diameter. Therefore, the authors concluded that aqueous-deficient dry eyes is likely to be a protein conformational disease.

Studies have shown that DLS is also sensitive in early cataract detection [64]–[66]. Ansari and co-workers [67] compared Scheimpflug images with particle size distributions measured with DLS (Figure 2.16). To compare the two methods, they studied cold cataracts in calf eyes. Cold cataracts refer to cataracts that appear as temperature decreases, providing a complete control on the cataract degree. The results showed

that when the temperature drops, the particle size distribution changes while the OD units calculated from the Scheimpflug images do not change until 11ºC. Accordingly, it was shown that DLS is more sensitive than Scheimpflug images to detect early cataracts.
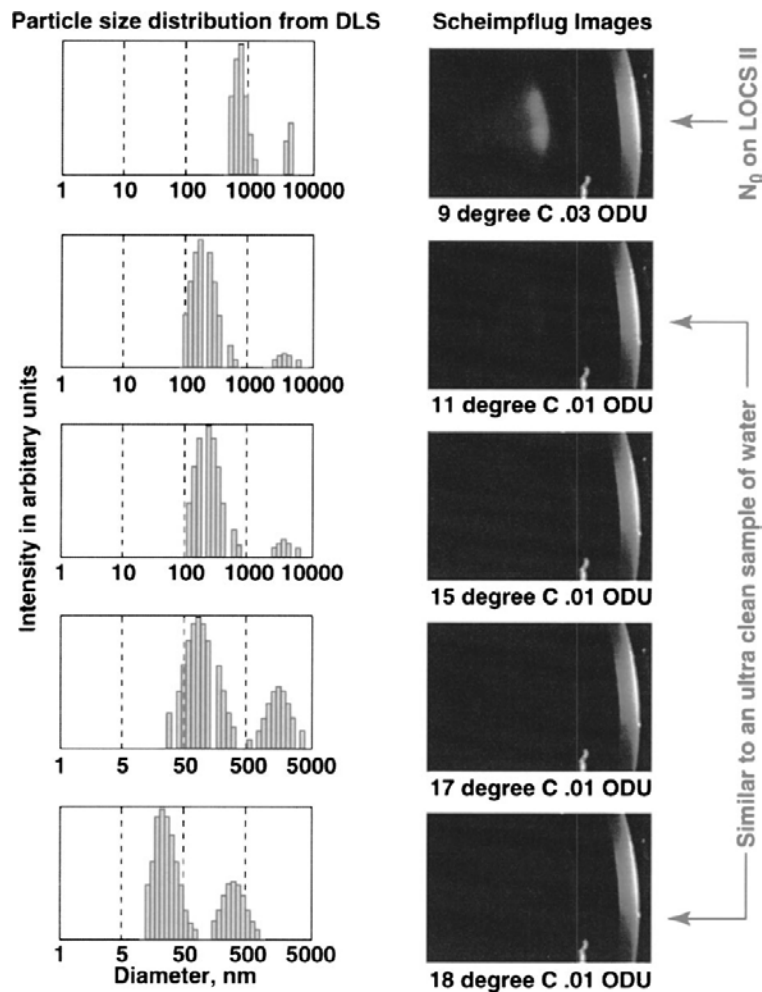
Figure 2.16. Comparison of DLS and Scheimpflug images in calf eyes with induced cold cataract. (Left) Particle size distribution from the DLS measurements. (Right) Scheimpflug images. Temperature increases from top to bottom (Source: Ansari et al. 1998 [67]).

However, DLS is not the best technique when dealing with eyes with high degree of opacity. Fluctuations in the intensity signal are mainly caused by a particle going in or out of the illumination volume. A high opacity implies a high concentration of scatter particles. The higher the concentration, the more probability of having more than one particle going in or out of the illumination volume at the same time, which makes the analysis of intensity fluctuations impossible. Additionally, for the calculations of the particle size, a constant lens refraction index and viscosity are assumed while nowadays, it is not clear how the lens viscosity changes due to cataract formation [60].

In summary, DLS provides information about the size distribution of particles but it does not measure scattering affecting the retinal image. However, it has been shown that the size distribution is related with eye diseases like aqueous-deficient dry eye and cataracts.

Shack-Hartmann (SH) wavefront sensor

The Shack-Hartmann (SH) wavefront sensor was designed to measure wave aberrations. Using a micro-lenses array, a light beam is decomposed into several smaller beams and thus a camera detects a grid of points (Figure 2.17). This grid of points is compared with a grid formed by a perfect free-aberration planar wavefront. From the displacement of each point with respect to the point from the perfect beam, the wavefront and the Zernike polynomials can be calculated.
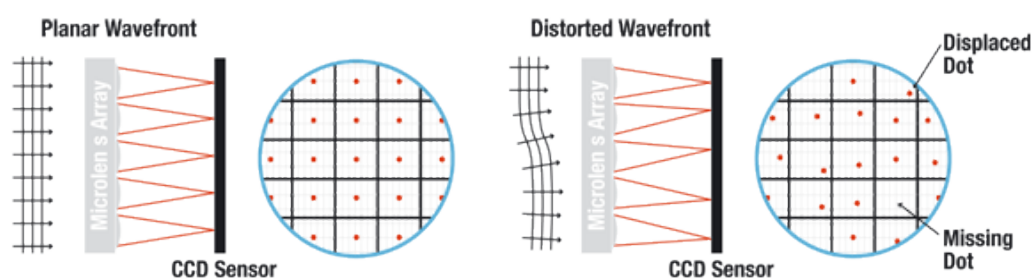
Figure 2.17. Planar wavefront and its regular grid on the CCD sensor (left) and distorted wavefront and its irregular grid on the CCD sensor (right) (Source: www.thorlabs.com).

To measure the aberrations of the eye, a collimated beam is sent to the pupil; the light is reflected at the retina and separated from the illumination path using a beam splitter (BS 2), and finally reaches the micro-lenses array (ML array). The ML array decomposes the beam into several smaller beams and they are detected by a camera. A second camera (pupil control) is used to align the system with the patient's pupil. The ML array is located at a pupil's conjugate plane by means of a telescope (L1 and L2). The CCD (charge-coupled device) sensor is placed at the focal plane of the ML array and therefore it is at a plane conjugated with the retina (Figure 2.18).
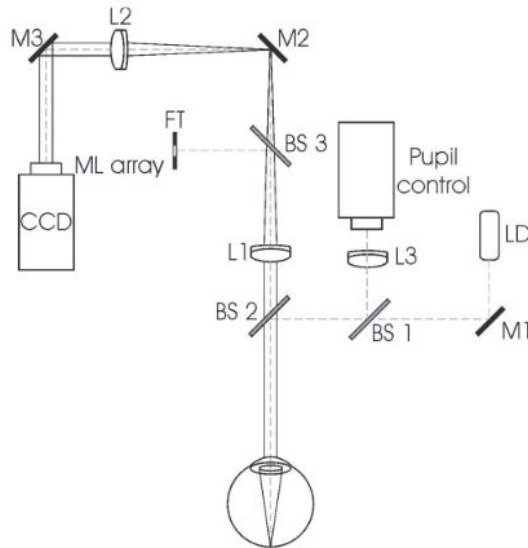
Figure 2.18. Schematic of a SH setup. BS are beam-splitters, M are mirrors, L are lenses, FT is a fixation test, LD is a laser diode and ML is a micro-lenses array (Source: Díaz-Doutón et al. 2006 [68]).

Although SH was designed to provide information about aberrations, researchers tried different strategies to measure intraocular forward scattering by means of this technique. Donnelly and colleagues [69] studied the intensity distribution pattern formed by each lens. Their hypothesis was that the tails of the distribution contained information about the intraocular scattering (Figure 2.19).
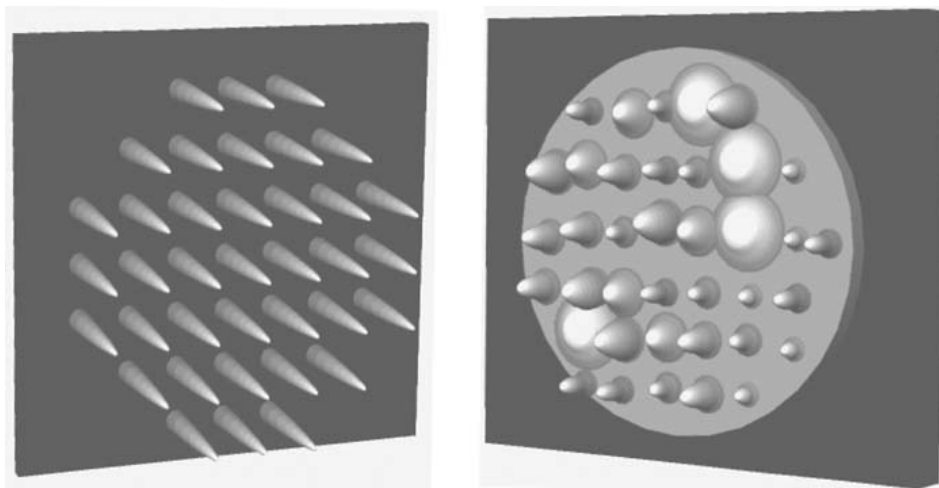
Figure 2.19. Simulation of a SH image limited by diffraction (left) and from an optical system with scattering (spreading of intensity distribution) and aberrations (displacement of the points with respect to a squared grid (right) (Source: Donelly et al. 2004 [69]).

Mihashi [70] explored two different strategies. The first one was to calculate the local contrast at each spot. The hypothesis relies on the fact that scatter spreads the light intensity distribution. A free-scatter media

should have a larger intensity contrast than a scatter media (Figure 19). The contrast was defined with the following equation (Equation 2.4):

$$Contrast = \frac{I_{max} - I_{min}}{I_{max} + I_{min}}$$

Equation 2.4

The results that these authors obtained showed a contrast difference between cataractous and non-cataractous eyes. The inverse contrast in eyes with cataracts (5.04 ± 3.06 inverse contrast units) was significantly larger than the one found in normal eyes (1.57 ± 0.56) and keratoconic eyes (1.83 ± 0.79).

The second way to assess intraocular scattering from SH measurements was about to compare the width of the simulated intensity pattern distribution of each spot taking into account the measured aberrations, which includes the system aberrations, and the width of the measured intensity pattern, which includes the system aberrations and scattering. The authors found that the width of the intensity distribution, i. e., the Point Spread Function (PSF), in cataractous eyes (81.8 μm ± 65.2 μm) was also significantly larger than that in normal eyes (9.3 ± 4.3 μm) or keratoconic eyes (30.0 μm ± 20.1 μm). They concluded that both methods were successful in distinguishing between cataractous and normal eyes. However, no objective classification values to quantify the amount of scatter were provided.

Double-Pass (DP) technique

The fundamentals of the Double-Pass (DP) technique [71] are straightforward. A light beam is focused on the retina and the reflected light is recorded using a camera. All information of the eye's optics is included in the recorded image intensity distribution.

The mainstream setup for the DP technique (Figure 2.20) uses a diode laser with a spatial filter as a point light source. An infrared wavelength of 780 nm is often chosen for the patient's comfort. The entrance pupil (EP) is used to control for the beam diameter and it is placed at the pupil's conjugated plane. By means of a Badal system, the spherical refraction of the eye is compensated (two lenses (L3, L4) and two mirrors (M4 and DF) where the distance between them can be modified). A 50-50 beam-splitter (BS2) is placed between the entrance pupil and the first lens of the Badal system. In the first pass (the light going from the light source to the eye) the beam is transmitted through the beam-splitter (BS2) to the Badal. In the second pass (the light going from the eye to the camera), the light is reflected by the beam-splitter (BS2) to the exit pupil (ExP). After the Badal, the image of the point source is formed on the retina through the optical system of the eye, where it is reflected and repeats the same path in the opposite way until it is recorded with the camera (CCD1) (note that the detector is optically conjugated with the retina). In order to reduce the speckle pattern, a vibrator is included in a mirror to break the light coherence in the first pass. A fixation target (FT) and another camera (CCD2) to align the eye are commonly used.
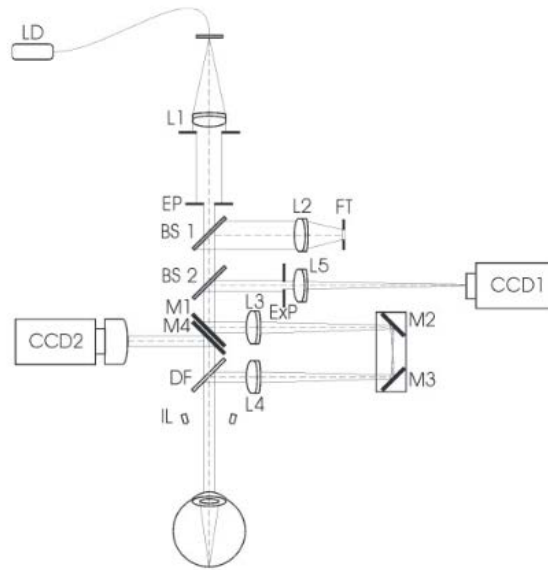
Figure 2.20. Schematic of a DP system. LD is the laser diode, L are lenses, EP is the entrance pupil, BS are beam splitters, FT is the fixation target, ExP is the exit pupil, M are mirrors, CCD1 is the DP camera, CCD2 is the pupil camera to align the patient's eye, IL are infrared LEDs to illuminate the pupil, DF is a dichroic mirror and L3, L4, M2 and M3 are the lenses and mirrors of the Badal system (Source: Díaz-Doutón et al. 2006 [68]).

The amplitude distribution of intensity at the retina (first pass) is the convolution of the object and the impulse function of the eye (Equation 2.5) (Figure 2.21). Since the source is a point object in the first pass (Equation 2.6), the intensity distribution at the retina is the PSF. The PSF in the first pass (PSF') depends on the diffraction (entrance pupil size), eye aberrations and intraocular scattering as follows:

$$A'(x',y') = h'(x',y') \otimes A(-x,-y) = h'(x',y') \otimes \mathbb{I} \qquad \text{Equation 2.5}$$

$$I(x',y') = |A'(x',y')|^2 = |h'(x,y)|^2 = PSF' \qquad \text{Equation 2.6}$$

where I is the intensity distribution, A is the amplitude distribution at the object plane, A' is the amplitude at the image plane, h' the impulse function of the eye.

For the second pass, the object is the retinal image (PSF') and the image recorded with the camera is the convolution of the retinal image and the impulse function of the eye (Equation 2.7).

$$I''(x'',y'') = \left|h''^{(x,y)}\right|^2 \otimes I'(x',y') = PSF''(x,y) \otimes PSF'(-x,-y) \qquad \text{Equation 2.7}$$

where I'' is the intensity distribution at the detector, h'' is the impulse function of the eye (now the pupil is the exit pupil) and PSF'' is the PSF of the second pass [72].
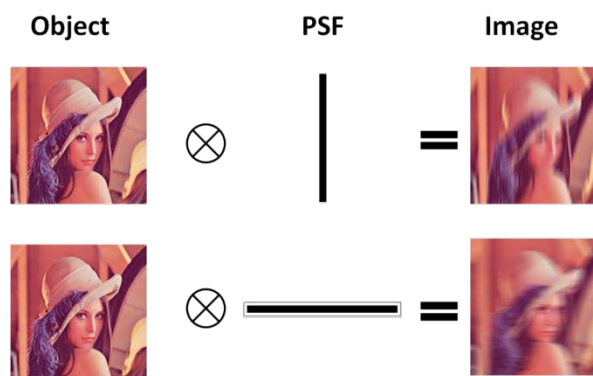
Figure 2.21. Example of image formation from the convolution of an object and the PSF of an optical system.

According to this, the final recorded DP image depends on the PSF of the eye's optics. This means that the DP image contains information about the diffraction, aberrations and intraocular scattering.

For a small entrance pupil (2 mm of diameter), the image in the first pass is almost not affected by the eye's optics and is determined by the pupil's diffraction. Therefore, the retinal image can be calculated and deconvolved from the DP image in order to assess the PSF of the second pass, i. e., the PSF of the eye. Then, the image of the second pass corresponds to the correlation of the first pass image (which is known as it is assumed to be limited by diffraction) with the actual ocular PSF, which contains information of aberrations (higher-order) and scattering.

On the other hand, the modulus of the Fourier Transform of the PSF is the Modulation Transfer Function (MTF). The MTF indicates how the contrast decreases through an optical system for each spatial frequency. Note that for a frequency of 0 c/d the contrast cannot decrease; for this reason, the MTF is always normalized at this value (it has a value of 1 at 0 c/d). The ocular MTF has a low-pass shape: its maximum value is for 0 c/d and it decreases as the frequency increases due to aberrations, scattering and diffraction. Using the convolution theorem, the MTF of the eye's optics can be retrieved by dividing the MTF of the DP image by the diffraction limited MTF as described elsewhere [72].

Figure 2.22 shows a comparison between a healthy young eye and the same eye with 4 D of induced astigmatism and how the MTF decreases as the aberrations increase. The MTF meaning is similar to that of the CSF explained in the contrast sensitivity charts section. However, it should be reminded that the CSF includes the optical but also the neural processing while the MTF only depends on the optics of the eye (Equation 2.8):

$$CSF = MTF \cdot CSF_{Neural\ Process}$$

Equation 2.8
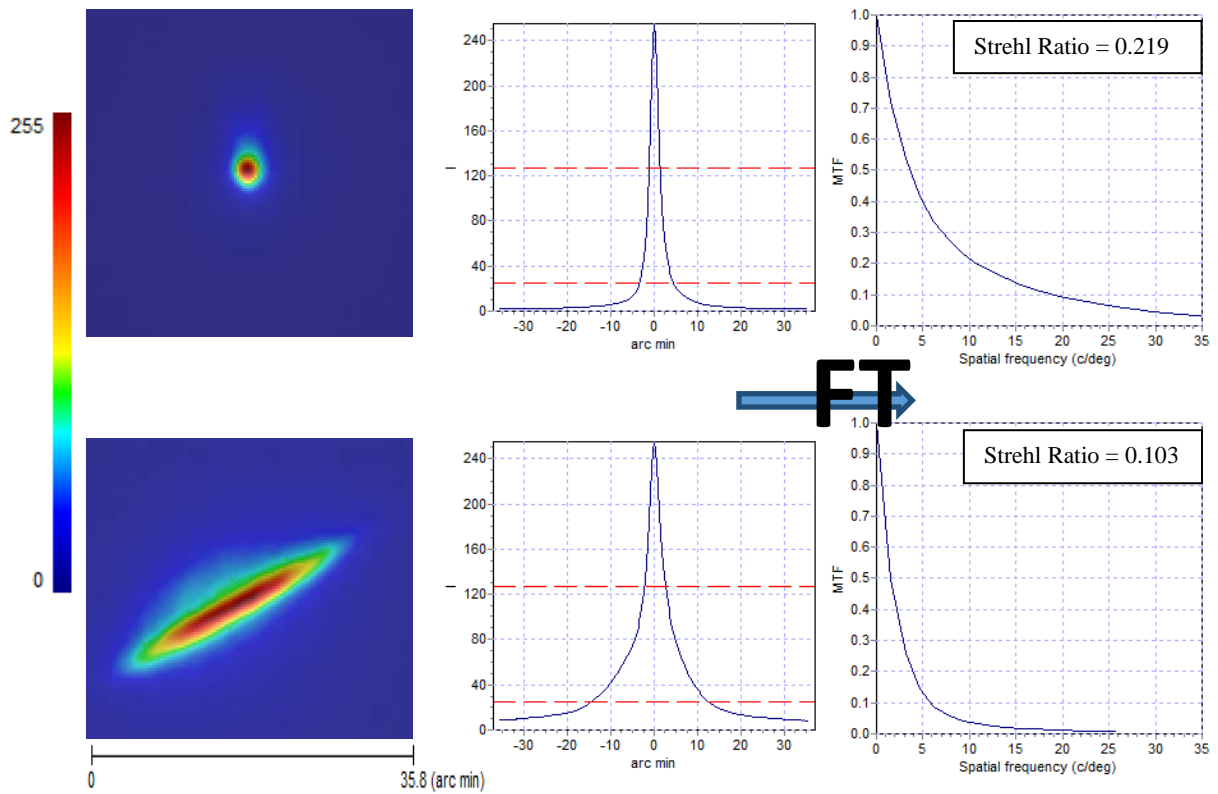
Figure 2.22. (Left) DP images in pseudocolor. (Centre) Averaged radial profile of the DP image (the intensity is in arbitrary units). (Right) Averaged radial profile of the MTF. The top images correspond to a young healthy eye and the bottom ones to an eye with 4 D of astigmatism (FT: Fourier Transform).

A commercial device based on the DP technique was developed some years ago (Visiometrics S.L., Cerdanyola del Vallès, Spain) for clinical use, under the name of HD Analyzer (Figure 2.23). This device acquires the DP image of the patient's eye and provides the corresponding MTF curve. From them, several parameters to analyse the ocular optical quality are computed such as the MTF cut-off frequency and the Strehl ratio. This last parameter is computed in the instrument in two dimensions as the ratio between the areas under the MTF curve of the measured eye and that of the aberration-free eye [73]–[75].

Figure 2.23. The HD Analyzer (Visiometrics S.L).

Besides the former parameters, the instrument also measures the Objective Scattering Index (OSI). This is a parameter proposed by Artal and colleagues from the LOUM (Laboratorio de Óptica, Universidad de Murcia, Murcia, Spain) in collaboration with the CD6 (Center for Sensors, Instruments and Systems Development, Universitat Politècnica de Catalunya, Terrassa, Barcelona, Spain) [76] to quantify the intraocular scattering from DP images. OSI has been defined as the ratio between the intensity recorded in an annulus ring of 12 minutes of arc (') to 20' and the intensity at the central part (circle of 1' of diameter) of the normalized DP image (Figure 2.24).

As commented above, the DP images are affected by ocular aberrations and intraocular scattering. The ring size was justified from the fact that the central part of the PSF of the human eye is dominated by aberrations and that scatter is only present in areas far away from it. This can be considered a good approach if the eye is not highly aberrated. Of course, to perform the measurements, the low-order aberrations of the eye must be corrected. Actually, the defocus effect on the OSI has been studied, and it has been found that uncorrected values over 1.0 D should be avoided [61].
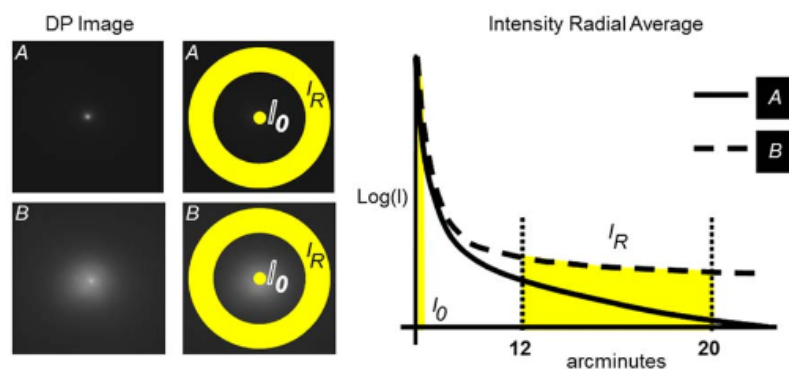
Figure 2.24. DP images and the radial intensity average for two different scattering levels: low scattering (A) and high scattering (B). The regions I_R and I_0 (in yellow) are used to compute the OSI (I_R/I_0) (Source: Artal et al. 2011 [76]).

The same authors also proposed a cataract classification from the OSI values: $OSI < 1$ Healthy eye, $1 \leq OSI < 3$ Early cataract, $3 \leq OSI < 7$ Mature cataract, and $7 \leq OSI$ Severe cataract. Later, Vilaseca and co-workers conducted a clinical study to validate the OSI [77]. They compared the OSI values in 188 eyes with nuclear, cortical and posterior subcapsular cataracts, which were previously graded with the LOCS III classification system at the slit lamp, and reported good agreement between both methods (Figure 2.25).
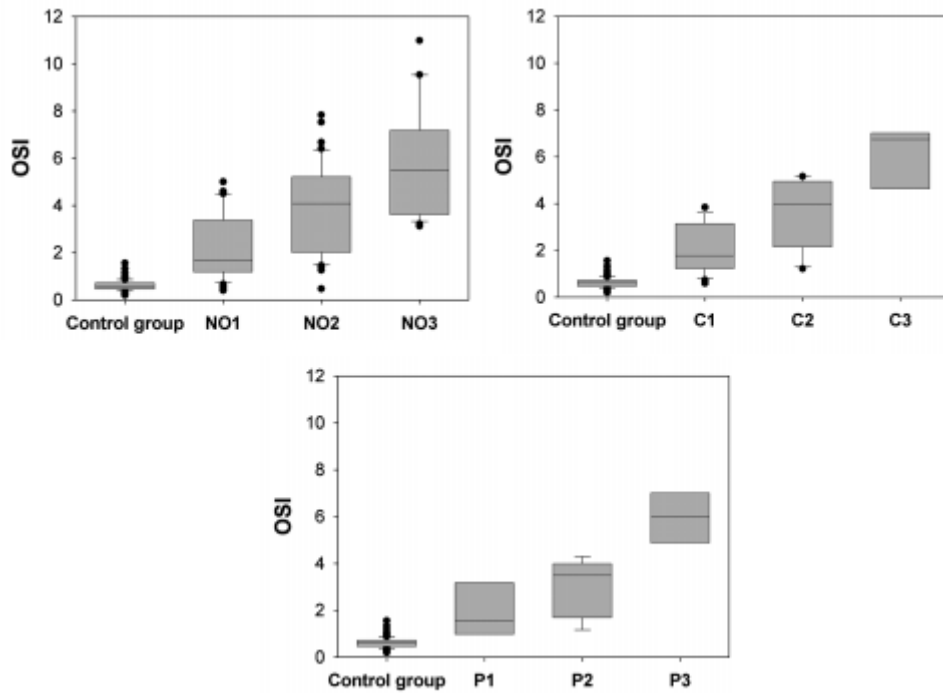
Figure 2.25. Box plots showing the correlation between OSI and LOCS III classification system for nuclear (NO), cortical (C) and posterior subcapsular (P) cataracts (Source: Vilaseca et al. 2012 [77]).

Other authors [78] also compared the DP technology with a Scheimpflug system for cataract grading in eyes with age-related nuclear cataract (Figure 2.26).
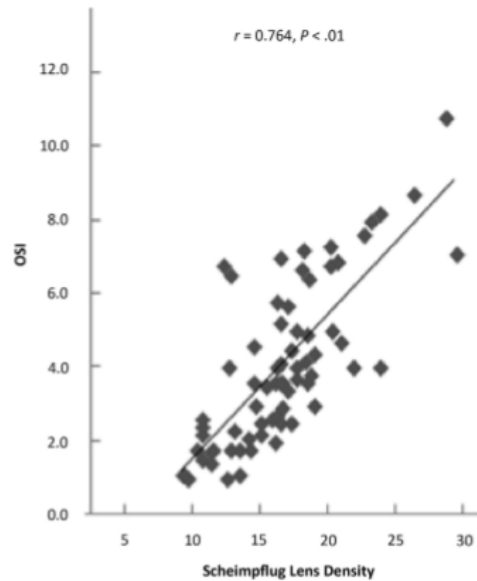
Figure 2.26. Relationship between the Objective Scattering Index (OSI) and Scheimpflug lens density (Source: Lim et al. 2014 [78]).

The results showed that OSI was in general well correlated with Scheimpflug lens density (OD) (r = 0.764). However, for the same Scheimpflug OD value, some specific individuals showed OSIs from 1 to 7, which is a significant clinical difference.

The former results indicate that in general the DP technique can be considered an objective and reliable method to measure intraocular scattering. Moreover, it deals with forward scattering, and thus, it is expected to provide information directly related with scattering impairing patient's vision.

However, criticisms have been made to this technique because infrared light (780 nm) penetrates easily into the choroid, where diffusion and back reflection occur, and this artifact is added to the recorded DP image; however, the use of near-infrared light in the DP imaging device increases the patient's comfort during image acquisition. Despite the fact that the 12'-to-20' ring included in the computation of OSI is affected by the artifact of infrared light diffusion in the choroid, this can be considered a relatively constant background [79], [80].

It is also remarkable to mention that DP images, and all the other techniques explained, provide the intraocular scattering assessment from the whole eye. Thus, nowadays it is still not possible to know from which part of the eye the scattering comes from.

Accurate reconstruction of the wide-angle PSF

Ginis et al. [81] have recently developed a new method to measure intraocular scattering. Although the principle behind it is similar to that of a DP pass setup, they have incorporated an extended light source in a way to reconstruct the wide angle PSF of the eye. The main idea of this technique is projecting consecutive

uniform light disks (increasing their radius) on the eye instead of using a narrow laser beam. The disks are generated by a liquid crystal modulator, which is illuminated by a xenon lamp. The intensity at the centre of the reflected disks is measured by an electron multiplying CCD camera (Figure 2.27), which depends on the intensity of the uniform projected disk and the scattered light from the non-central parts of the disk to the centre.
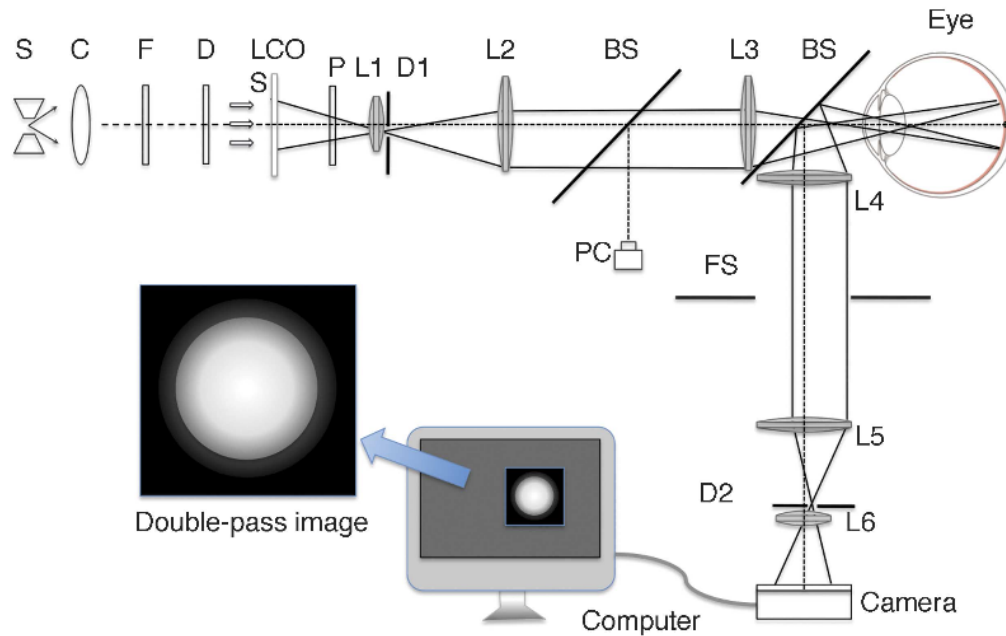
Figure 2.27. Schematic of the experimental setup. S is the light source, C is a collimating lens, F are green filters, D is a diffuser, LCOS is a liquid crystal spatial light modulator (used to project disks with different radius), Lx are lenses, Dx are diaphragms, P is a linear polarizer, BS are beam splitters, PC is the pupil camera and FS is a field stop (Source: Ginis et al. 2012 [81]).

Being the extended light source a disk with uniform intensity I_0, the recorded image of the light reflected by the retina is the convolution of the projected disk with the DP PSF (PSF_{dp}). The intensity at the centre of the recorded image is given by (Equation 2.9):

$$I_c(\vartheta) = I_0 \int_0^{\vartheta} 2\pi\varphi PSF_{dp}(\varphi)d\varphi \qquad \text{Equation 2.9}$$

where I_c is the intensity at the centre of the recorded image and ϑ is the radius of the projected disk (Figure 2.28).
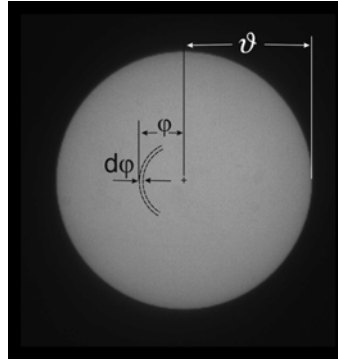
Figure 2.28. Example of an image of a uniform disk imaged through an optical system with rotationally symmetric PSF that includes scattering (Source: Ginis et al. 2012 [81]).

The intensity at the centre of the recorded image is the compromise between the lost intensity from the centre of the projected disk due to the scattering and the gain intensity due to the scattered light from each point of the disk. To better understand this, two extreme cases can be considered:

1. When the radius of the projected disk tends to 0, it is just a point and the situation is the same as in the DP technique where the recorded image is the PSF_{dp}.
2. When the radius of the projected disk tends to infinity, due to the law of energy conservation, the intensity at the centre of the recorded disk should be I_0.

In an experimental situation where the analysis spans several degrees (i. e., about 10 degrees (°)), it is a reasonable approximation to assume that effectively all the energy of the PSF is taken into account and therefore, all measurements of I_c can be normalized with respect to the largest available disk. After the normalization, the intensity at the centre is as follows (Equation 2.10):

$$I_c(\vartheta) = \int_0^\vartheta 2\pi\varphi PSF_{dp}(\varphi)d\varphi \qquad \text{Equation 2.10}$$

And the derivative is:

$$PSF_{dp}(\vartheta) = \frac{1}{2\pi\vartheta}\frac{dI_c(\vartheta)}{d\vartheta} \rightarrow PSF_{dp}(\vartheta_n) = \frac{1}{2\pi\vartheta_n}\frac{I_c(\vartheta_{i+1})-I_c(\vartheta_i)}{\vartheta_{i+1}-\vartheta_i} \qquad \text{Equation 2.11}$$

where $\vartheta n = \frac{\vartheta_{i+1}+\vartheta_i}{2}$. $PSF_{dp}(\vartheta)$ is calculated by varying the radius of the projected disk and measuring the intensity at the centre of the recorded disks.

Ginis and colleagues showed that the DP PSF at a given angle (e. g., 5°) can be used as a measure of intraocular scattering. The reconstruction of the wide angle PSF was tested in two young eyes (GP and JB), one of them wearing gas-permeable contact lenses to generate different amounts of scattering (CL and CL5) and was compared with an artificial eye (alone and with a diffusing filter - the Black Pro Mist 1 scatter filter) (Figure 2.29).
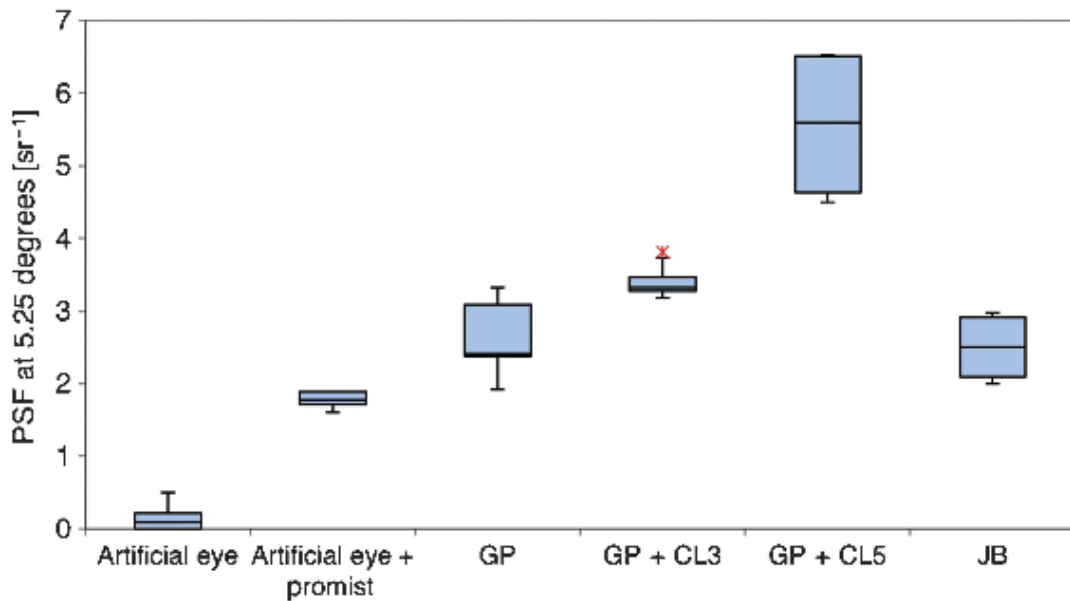
Figure 2.29. Box plot showing the experimental results obtained for an artificial eye and human eyes using contact lenses to generate scattering (Source: Ginis et al. 2012 [81]).

Measuring the intraocular scattering with an extended light source permits to have enough sensitivity at large angles, which is not possible in the traditional DP technique due to the low intensity far away from the centre. Measuring at larger angles avoids the error introduced by the eye's aberrations.

Moreover, this novel technique uses green light instead of near infrared as illumination source. This technique was used to measure the intraocular scattering using 6 different wavelengths from 500 to 650 nm [82]. The results showed that for small angles the wavelength dependence on the measured scattering matches with the transmittance spectrum of haemoglobin. The conclusion was that using reddish wavelengths could introduce errors in the measured intraocular scattering due to the retina reflectance. On the other hand, since the human eye is more sensitive to green light, its use could be uncomfortable for patients and usually drops are needed for pupil dilation to perform such measurements.

Sigma

Sigma (University of Murcia, Spain) is a commercial instrument used to measure the intraocular scattering based on a modified DP system similar to the wide-angle reconstruction explained in the previous section (accurate reconstruction of the wide-angle PSF method) and optimized in terms of speed and clinical use [83]–[85] (Figure 2.30).
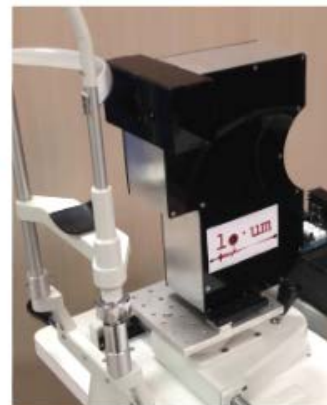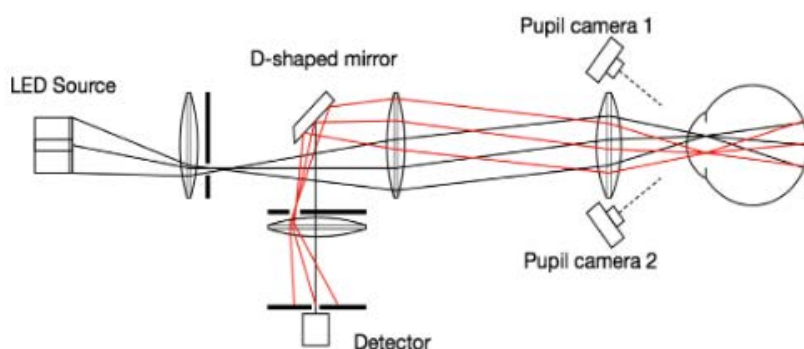
Figure 2.30. Schematic of the setup (left) and clinical device (right). It uses 520 nm-LEDs as a light source, two cameras that have their axes intersecting at the pupil plane and a silicon photomultiplier as a detector (Source: Ginis et al. 2014 [83]).

This compact optical integration instrument to measure intraocular straylight projects a disk (3º) and an annulus (3º to 8º) with uniform intensity unlike to varying the radius of the projected disk. The disk and the annulus light are square-wave temporally modulated with different frequencies for each zone. The intensity at the centre of the reflected disk is measured with a silicon photomultiplier device. Part of this intensity is from the disk and due to scattering part is from the annulus. The contribution from the disk and the annulus is calculated from the Fourier transform of the signal (Figure 2.31).
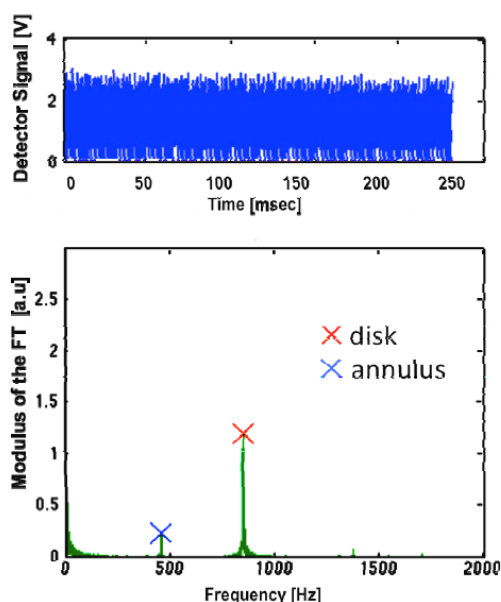
Figure 2.31. Measured signal (top) and modulus of its Fourier transform (bottom). The Fourier transform gives the contribution from the disk and the contribution from the annulus to the measured intensity (Source: Ginis et al. 2014 [83]).

As in the previous section, the intensity at the centre of the disk is given by the following equations (Equation 2.12 and 2.13):

$$I_d(\vartheta) = I_0 \int_0^{\vartheta_1} 2\pi\varphi PSF_{dp}(\varphi)d\varphi \qquad\qquad \text{Equation 2.12}$$

$$I_a(\vartheta) = I_0 \int_{\vartheta_1}^{\vartheta_2} 2\pi\varphi PSF_{dp}(\varphi)d\varphi \qquad\qquad \text{Equation 2.13}$$

where I_0 is the uniform intensity of the illumination source, I_d and I_a are the contributions from the disk and annulus in the detected signal and ϑ_1 and ϑ_2 are the inner and outer angular size of the annulus.

The PSF value at the middle of the annulus can be calculated using Equation 2.11 as follows:

$$PSF_{dp}(\vartheta) = \frac{1}{2\pi\vartheta}\frac{1}{I_0}\frac{dI_c(\vartheta)}{d\vartheta} \rightarrow PSF_{dp}(\vartheta_n) = \frac{1}{2\pi\vartheta_n}\frac{1}{I_0}\frac{I_c(\vartheta_2)-I_c(\vartheta_1)}{\vartheta_2-\vartheta_1} \qquad \text{Equation 2.14}$$

where $\vartheta n = \frac{\vartheta_2+\vartheta_1}{2}$, $I_c(\vartheta_2)= I_a + I_d$ and $I_c(\vartheta_1)= I_d$. Moreover $I_0 = I_c(\vartheta_2)= I_a + I_d$ since we assume that $\lim\limits_{\vartheta\to\infty} Ic(\vartheta) \rightarrow I_0$ (Equation 2.15).

$$PSF_{dp}(\vartheta_n) = \frac{1}{2\pi\vartheta_n}\frac{1}{\vartheta_2-\vartheta_1}\frac{I_a}{I_a+I_d} \qquad\qquad \text{Equation 2.15}$$

Using the value of the PSF in the Stiles-Holladay equation (Equation 2.16) [37], [38] the following expression is obtained to account for straylight (S):

$$S_{dp} = \vartheta_n^2 PSF_{dp} \qquad\qquad \text{Equation 2.16}$$

This method was tested and validated in 10 eyes with no pathologies using 4 different grades of photographic diffusing filters placed in front of them to simulate scattering (Figure 2.32).
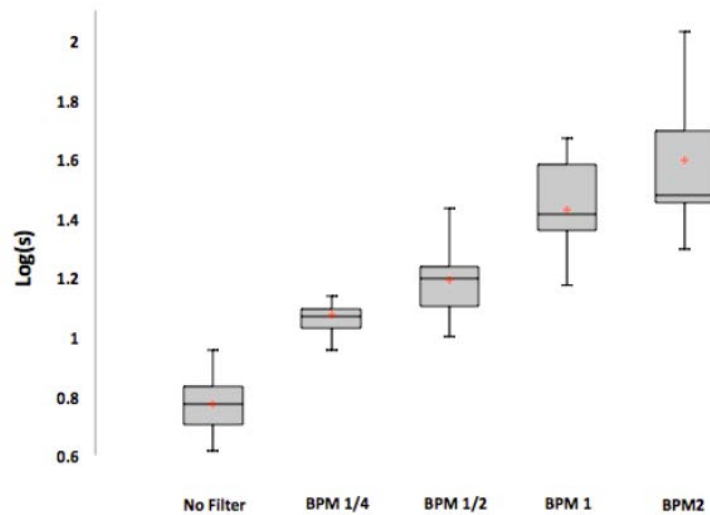
Figure 2.32. Log(S) for the ten eyes using different photographic filters (Source: Ginis et al. 2014 [83]).

This technique allows measuring the intraocular scattering and prevents artefacts from the eye aberrations and retina reflection. It is critical to reflections, so that the optical design is built in a way that allows separating the illumination and recording paths. The use of dilating drops is needed in some cases for pupil dilation. Since it is not needed to project disks with different radius, there is an optimization in terms of speed. However, powerful electronics to modulate the light source are required.

Purkinje imaging system

Up to our knowledge, a system based on Purkinje images has also been proposed as a means of assessing anterior segment intraocular scattering [67]. Since in the next section a detailed analysis of the Purkinje images is given, this system will be described there (section 2.3).

2.3   Purkinje Images

The Purkinje images refer to any of the images that can be seen reflected from the eye of a person who is looking at an illuminated object. They are formed by reflection of light from the different optical ocular structures (Figure 2.33). Therefore, there are 4 Purkinje images corresponding to the different eye optical surfaces:

- First surface of the cornea (first Purkinje image, P1)
- Second surface of the cornea (second Purkinje image, P2)
- First surface of the lens (third Purkinje image, P3)
- Second surface of the lens (fourth Purkinje image, P4)
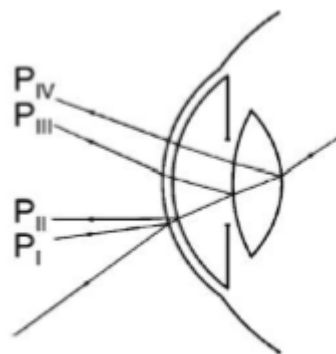
Figure 2.33. Drawing of the Purkinje images (Source: Jóźwik et al. 2014 [86]).

To calculate the position and size of the first Purkinje image corresponding to a given object, the first corneal surface is considered to be a spherical mirror as follows:

$$s' = \frac{r \cdot s}{2s - r}$$ Equation 2.17

$$M = \frac{-s\prime}{s}$$ Equation 2.18

where *r* is the radius of curvature of the surface, in this case the anterior corneal surface, *s* is the distance between the object and the surface (corneal apex), *s'* is the image position with respect to the surface and *M* is the magnification. Note that for the P1 calculation, *s* is negative and *r* is positive, *s'* is positive and *M* is positive.

The second Purkinje image is calculated assuming that the second surface of the cornea is a mirror. Therefore, to calculate the size and position of P2, the image formed when the light is refracted through the first corneal surface must be firstly calculated (Equations 2.19 and 2.20). Then the image formed by reflection from the posterior corneal surface is computed using equations 2.17 and 2.18 again.

$$\frac{n\prime}{s\prime} = \frac{-n}{s} + \frac{(n'-n)}{r}$$ Equation 2.19

$$M = -\frac{ns\prime}{n\prime s}$$ Equation 2.20

where *n* and *n'* are the refractive indexes of the first and second media, respectively.

To compute the third and fourth Purkinje images, the same process must be repeated considering the reflections from the two surfaces of the lens and the preceding refractions.

Assuming the Le Grand theoretical eye model, for the first Purkinje image, n is the refractive index of the air (n = 1) and n' that of the cornea (n' ≈ 1.377); for P2, n is the corneal refractive index and n' is that of the aqueous humor (n' ≈ 1.337); for P3, n is the refractive index of the aqueous humor and n' is that of the lens (n' ≈ 1.420); and finally, for P4, n is the lens refractive index and n' is that of the vitreous body (n' ≈ 1.336) [87], [88].

The theoretical position and size of the Purkinje images depend on the distance between the object and the eye as well as the distance between the cornea and the lens, and the object size. Figure 2.34 shows the positions of the Purkinje images assuming again the Le Grand theoretical eye model and a distance of 500 mm between the object and the eye. As it can be seen, P1 (green) and P2 (pink) are almost at the same plane, at 3.87 and 3.58 mm from the corneal apex, respectively; P3 (blue) is the farthest Purkinje image, 10.61 mm far away from the corneal apex; and P4 (purple) is inverted and close to P1 and P2, at 4.32 mm from the corneal apex.
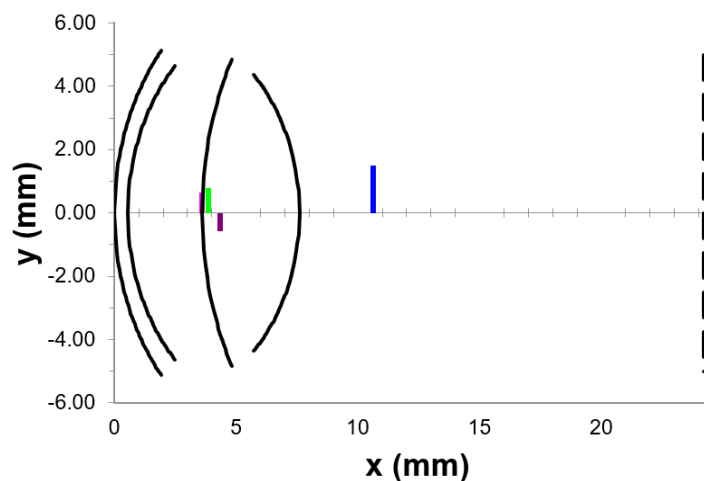
Figure 2.34. Locations of the Purkinje images assuming the Le Grand theoretical eye model and a distance of 500 mm between the object and the eye (x is taken from the corneal apex).

On the other hand, figure 2.35 shows the Purkinje image sizes as a function of the distance between the object and the eye (object size = 1 mm). Note again that P4 is the only inverted Purkinje image.
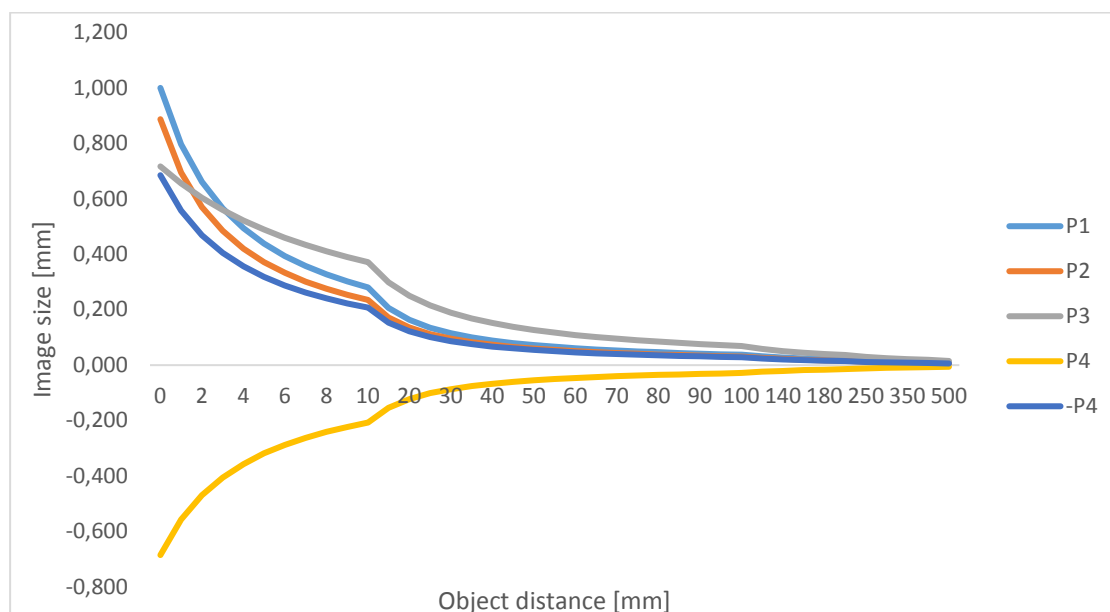
Figure 2.35. Purkinje images size as a function of the distance between the object and the eye.

The first and second Purkinje images overlap due to the small corneal thickness (~550 µm) and almost the same radii of curvature of the anterior and posterior corneal surfaces. Moreover, from the Fresnel equations [89] (Equations 2.21, 2.22 and 2.23), it is obvious that the intensity of P1 is orders of magnitude above the

intensity of P2 (~100 times), which makes very difficult to detect the P2 light distribution. P3 and P4 have a similar intensity, around 30 times lower than P1 (these rough intensity estimations have been done assuming light arriving at the eye with a normal incidence of light onto the surface (0º)).

$$R_s = \left| \frac{n \cos\theta_i - n_2 \sqrt{1 - \left(\frac{n}{n'} \sin\theta_i\right)^2}}{n \cos\theta_i + n' \sqrt{1 - \left(\frac{n}{n'} \sin\theta_i\right)^2}} \right|^2 \qquad \text{Equation 2.21}$$

$$R_p = \left| \frac{n \sqrt{1 - \left(\frac{n}{n'} \sin\theta_i\right)^2} - n' \cos\theta_i}{n \sqrt{1 - \left(\frac{n}{n'} \sin\theta_i\right)^2} + n' \cos\theta_i} \right|^2 \qquad \text{Equation 2.22}$$

$$R = \frac{R_s + R_p}{2} \qquad \text{Equation 2.23}$$

where R is the reflectance, the subscripts s and p denote the state of polarization of light, n and n' are the refractive indexes of the first and second media, respectively, and θ_i is the angle of incidence.

Purkinje-based systems for ocular applications

Different patterns and light sources have been used by researchers to deal with Purkinje images for several applications related with the eye. Shapes ranging from a point [90] to a semicircle of LEDs [86] have been used for different purposes, including the assessment of the tilt and decentration of intraocular lenses (Figure 2.36) [91]–[93], to demonstrate that the accommodative ciliary muscle function is preserved in older humans [94], and even for measuring the intraocular scattering from the fourth Purkinje Image [90]. Since the goal of this thesis deals with the assessment of scattering from a system based on Purkinje images, this last study is described in detail below.
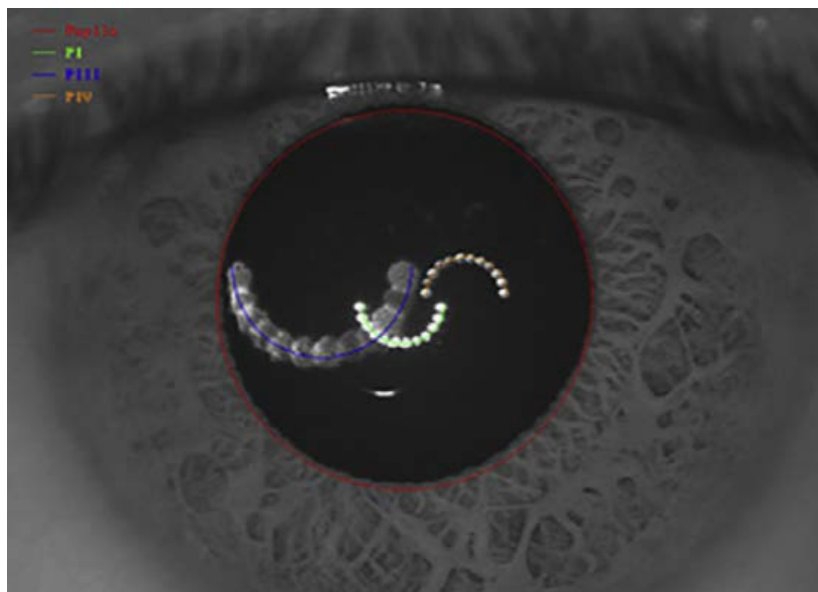
Figure 2.36. Purkinje reflexes used for the assessment of the tilt and decentration of intraocular lenses (Source: Maedel et al. 2017 [92]).

As commented, in the experiment by Bueno et al. [90], a Purkinje-based system was used to measure the contribution of the anterior segment to the total intraocular scattering of the eye.

In this system, the fourth Purkinje image (P4) of a point source object was acquired with a camera and posteriorly analysed. The P4 image (Figure 2.37) is the light reflected by the posterior surface of the lens so that the scattering caused by the retina is assumed to be not included in it.
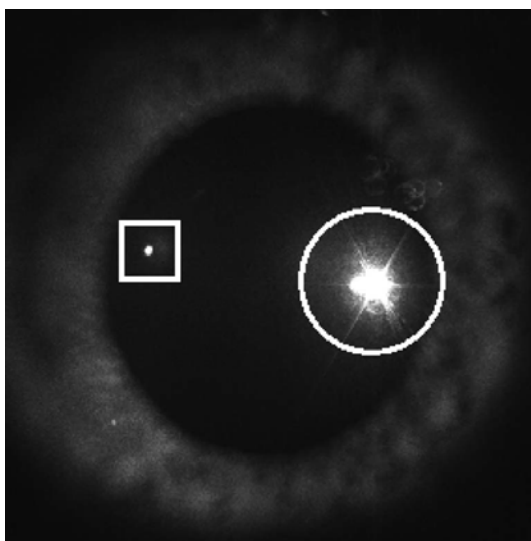
Figure 2.37. First (circled) and fourth (squared) Purkinje images of a living human eye (Source: Bueno et al. 2007 [90]).

To acquire the Purkinje images (Figure 2.38), the eye was illuminated with a He-Ne laser. To quantify the amount of scattering produced in the anterior segment of the eye, P4 was acquired in two different

experimental conditions, which provided saturated and non-saturated images (this was achieved by means of a removable neutral density filter, RNDF).
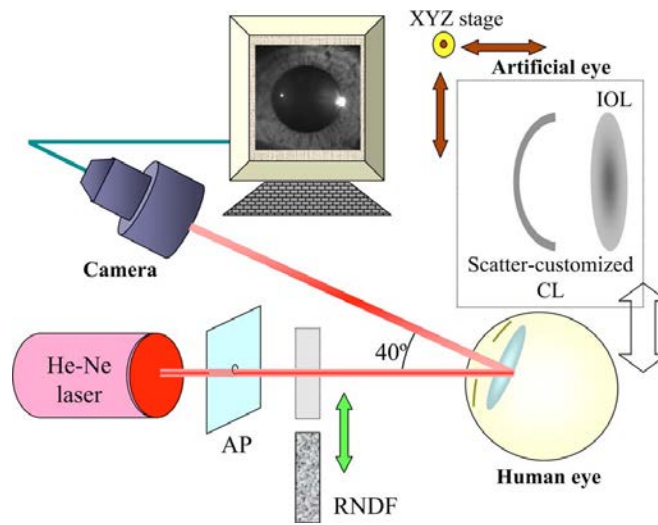
Figure 2.38. Schematic of the experimental setup used to acquire the P4 image. AP is the entrance pupil and RNDF is the removable neutral density filter (Source: Bueno et al. 2007 [90]).

For each image taken (saturated and non-saturated) the radial profile was plotted and normalized. Next, the area under the radial profile was computed (from 0 mm to 0.24 mm). To compute the area of the saturated image, the pixels with intensity 1 (after the normalization) were excluded. The amount of scattering was then given by a so-called *Parameter Of Scattering* (POS) (Equation 2.24):

$$POS = \frac{k'_{sat}}{k'_{nonsat}}$$

Equation 2.24

where k'$_{sat}$ and k'$_{nonsat}$ are the radial profile areas for the saturated and the non-saturated Purkinje images.

This technique was tested in an artificial eye and two additional eyes wearing customized contact lenses to simulate scattering. Eight normal young eyes without scattering were used as control group. Scattering increments were detected as shown in Figure 2.39.
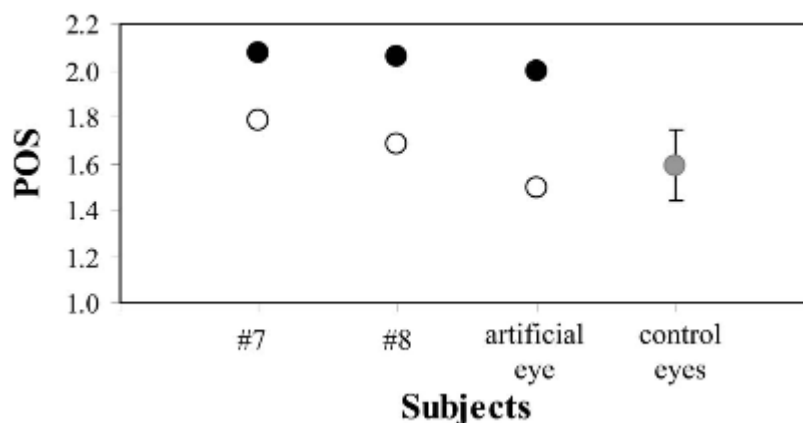
Figure 2.39. Measured POS for normal young eyes (#7 and #8) wearing scattering customized contact lenses (white black spots correspond to different contact lenses) and for the artificial eye. The averaged POS value for 8 young normal eyes is also included (Source: Bueno et al. 2007 [90]).

As the authors pointed out, this technique is able to measure the amount of scattering produced in the anterior segment of the eyes, avoiding the contribution from the retina. However, it is not trivial to implement this procedure in a commercial instrument since not all eyes saturate the image for the same laser power. Although Bueno and colleagues explained the experimental method, they did not provide an objective quantity of saturation. Another question not answered yet is the precision of the Purkinje imaging system to measure scattering. In the study, it was shown to provide similar values of scattering in normal young eyes and to be sensitive enough to differentiate between a naked normal eye and the same one wearing customized diffusing contact lenses.

3 Experimental setup

In this thesis, we propose the use of Purkinje images to quantify independently the scattering of the cornea and the lens. Specifically, we propose a methodology based on the analysis of the third (P3) and fourth (P4) ones formed by reflection of light on the first and second surfaces of the lens, respectively. The experimental system developed to acquire these Purkinje images is explained in this chapter.

Some preliminary considerations as well as the design of the stimulus chosen according to the features of the Purkinje images are firstly described; then, we show the experimental setup developed to validate the method at the laboratory level by means of new parameters of scattering; finally, the improvements made to build an appropriate prototype for a clinical environment are presented as well as safety issues that must be taken into account.

3.1 Preliminary considerations and design of the stimulus

As seen in the former chapter, instruments such as the HD Analyzer make use of the ocular PSF to measure the scattered light in the eye. It is well known that the central part of the PSF is dominated by the effects of aberrations while the wide-angle PSF (> 1°) is more influenced by intraocular scattering [81], [95], [96] (Figure 3.1). Therefore, in order to avoid effects of aberrations, a setup able to measure the light distribution at angles above 1° is desirable.
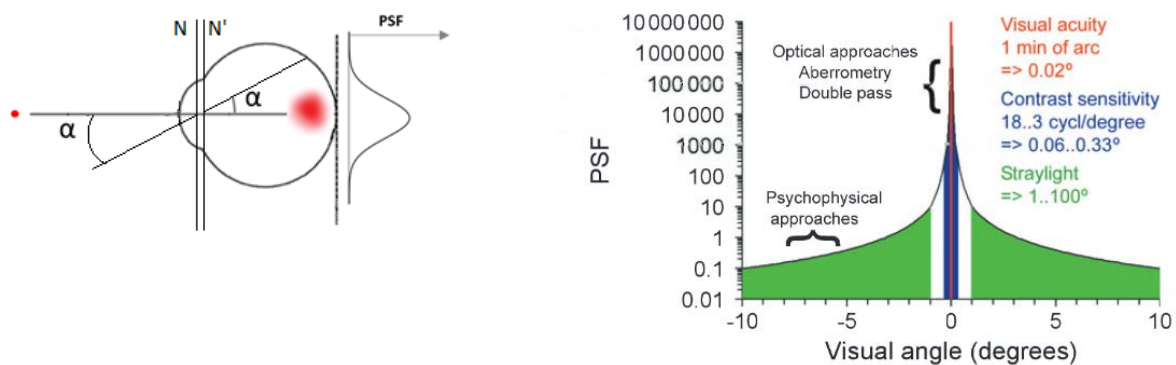
Figure 3.1. (Left) Red point, which represents a point light source, and the corresponding image on the retinal plane (red circle), which is the ocular PSF. *N* and *N'* denote the nodal planes of the eye's optics and *α* is the visual angle. (Right) PSF of the healthy young eye according to the Commission Internationale de l'Éclairage (CIE) standard with different domains indicated. (Source: van den Berg *et al*. 2009 [95])

Other instruments such as the C-Quant use a central disk and a peripheral annulus glare source subtending an angle (α) larger than 1° that creates a veiling glare at the center, which is used to quantify intraocular scattering (Figure 3.2).
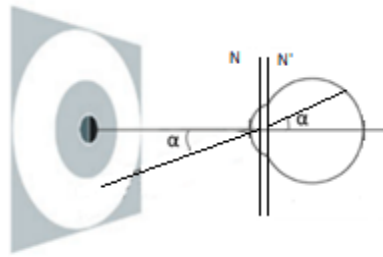
Figure 3.2. Stimulus used in the C-Quant instrument with a central disk divided into two halves and a circular annulus.

Instead of a disk plus and an annulus, in our setup we decided to use a stimulus with a vertical pattern composed of two slits - built on an opaque plate - permitting light to pass through (Figure 3.3). The use of a 1-dimensional pattern makes it easier to avoid overlapping among Purkinje images, although this also depends on the angle between the stimulus and the detector as well as the visual axis.

The selected pattern allowed us to measure the light intensity for each Purkinje image corresponding to the two slits as well as to a central dark fringe between them, in which only scattered light is expected to be.
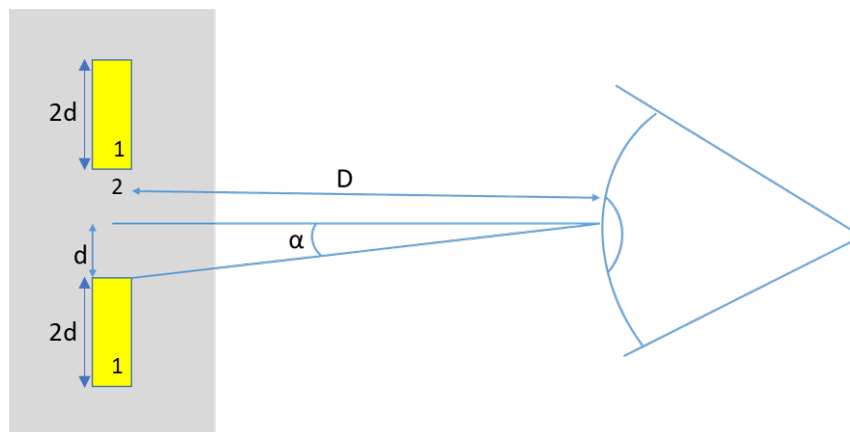
Figure 3.3. Schematics of the stimulus used: visual angle (α), distance between slits or fringe size (2d) and distance between the eye and the stimulus (D). For the sake of simplicity, the distance between the corneal apex and the nodal point is neglected. The grey rectangle represents an opaque object and the yellow rectangles are slits through which light passes to create the Purkinje images (1). The space between the yellow rectangles is what we call dark fringe (2).

Drawing a parallel from the CIE standard [95], which states that visual angles beyond 1° account for scattering, the ratio between the slits size (2d) and the distance between the test and the eye (D) should be in agreement with the limit of equation 3.1:

$$1^\circ < \ \alpha = \tan^{-1}\left(\frac{d}{D}\right)$$ Equation 3.1

Accordingly, we decided to place the stimulus at a distance of D = 90 mm from the eye, being the two slits of 5 mm with a separation between them of 5 mm (d = 2.5 mm). Therefore, the angle used in our system was of ~1.6º (> 1 º as suggested in the literature when dealing with the PSF). Nevertheless, it is important to note that we do not evaluate the light distribution at the retina but at the Purkinje images planes, whose locations depend on the distance between the object and the eye, and the specific locations of the surfaces of the eye's optics.

A slit width of 3 mm was chosen in order to avoid overlapping among Purkinje images while, at the same time, not having diffraction effects. Additionally, we decided to use an angle of 40º between the light source and the eye. The visual axis formed an angle of 20º with the detector (Figure 3.4). We experimentally checked that with these angles, Purkinje images (P1, P3 and P4) did not overlap at the detector plane.

In order to make the centering of the Purkinje images easier, especially the third and the fourth, we also added two extra horizontal slits at the external parts of the stimulus (top and bottom). However, only the two vertical slits were used for the assessment of scattering. Moreover, in order to make the vertical slits uniform in terms of luminance, diffusers were attached to both sides of the opaque plate.
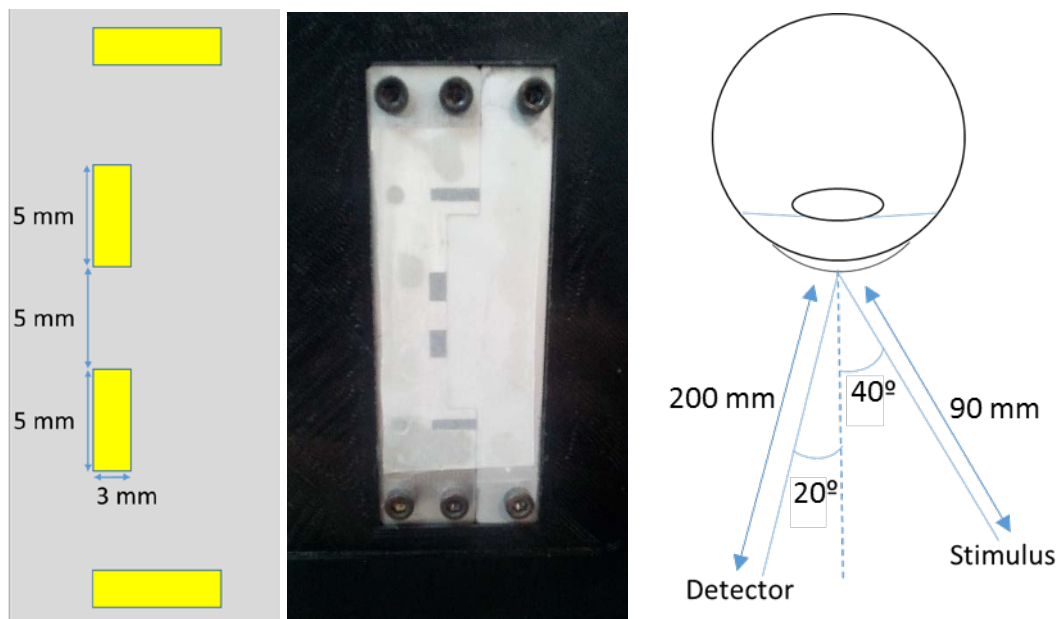
Figure 3.4. Schematics of the stimulus to create the Purkinje images (left) and real stimulus (center). Yellow rectangles represent the illuminated slits through which light passes. Distances and angles between detector, stimulus and eye (right).

If one considers the total length of the stimulus used for the scattering assessment to be of 15 mm - i. e., the 2 slits plus the central dark fringe - and the actual distance between the stimulus and the eye (90 mm), the corresponding Purkinje images sizes are of P1 = 0.62 mm, P2 = 0.51mm, P3 = 1.15 mm and P4 = 0.47 mm. Therefore, they are much smaller than 4 mm, a standard pupil size. The horizontal image sizes corresponding to a slit width of 3 mm are of P1 = 0.12 mm, P2 = 0.10 mm, P3 = 0.23 mm and P4 = 0.10 mm, also much below 4 mm. So that, all images will be inside the pupil.

Furthermore, their axial positions in the eye are 3.73 mm, 3.50 mm, 10.14 mm, and 4.25 mm from the corneal apex (Figure 3.5). P3 and P4 are separated about 6 mm and the last one is inverted.
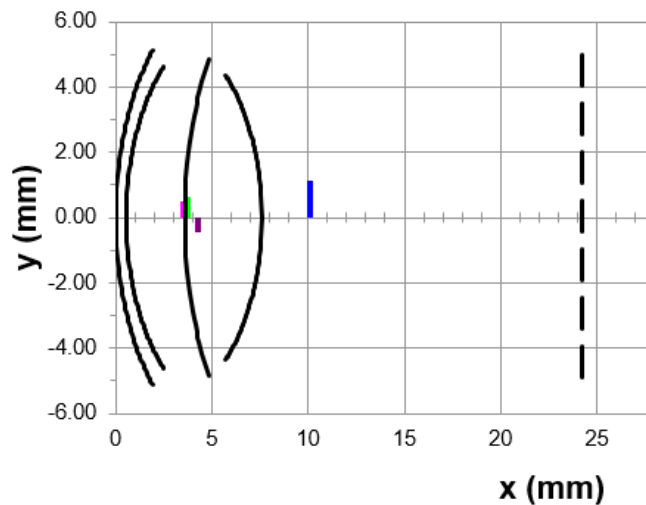
Figure 3.5. Schematics in which the Purkinje images sizes and positions with respect to the surfaces of the eye's optics are shown. P1 in pink, P2 in green, P3 in blue and P4 in purple. The dashed black line corresponds to the retina.

In order to analyze the effect of scattering on the light intensity distribution of the Purkinje images, we performed some preliminary simulations before building our experimental setup on the optical bench. The optical design software Zemax (Radiant Zemax, Redmond, U.S.A.) was used for this purpose. The intraocular scattering was simulated using the mie.dll bulk scattering library and defining particles properties (size, refractive index and density) as suggested in the literature for corneal [97] and lens [98] scattering (Table 3.1). We used the Liou-Brennan eye model [99] and a wavelength of 550 nm. The light source was simulated using two rectangles of the same sizes as we selected for the stimulus (3 mm x 5 mm) and we placed a diffusor attached to the rectangles. We simulated a detector system with a pixel size of 8x8 µm and 1004(H) x 1002(V) pixels attached to a telecentric lens with similar properties to those finally used in the experimental setup (see next section). However, we used paraxial lenses instead of the actual ones (Figure 3.6).

Table 3.1. Scatterer particles parameters.

	Size [μm]	Density [cm^{-3}]	Refractive index
Cornea	7,2	10^7	1,2
Lens	3	10^6	1,49
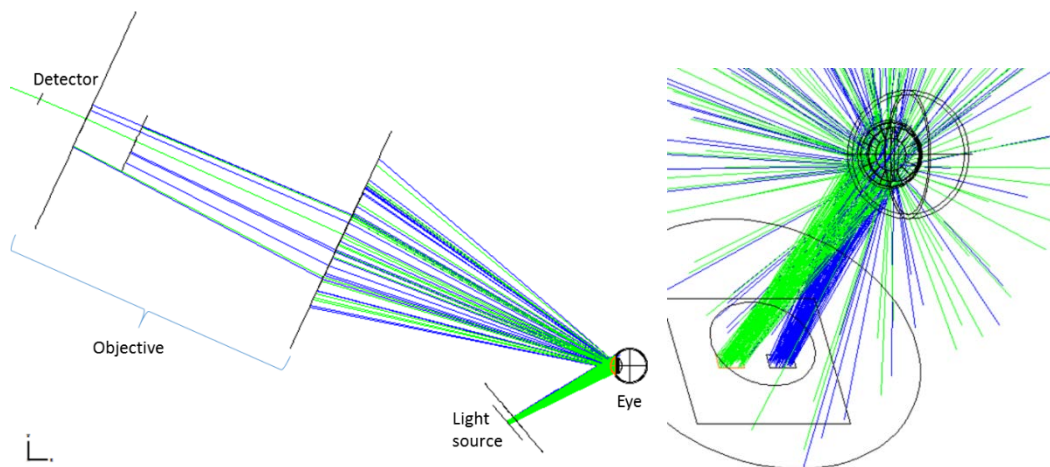
Figure 3.6. Simulated optical layout from Zemax (left). Simulated rectangles as a light source and Liou-Brennan eye model (right). Light emitted by one rectangle is represented with green lines and the light emitted by the other rectangle is represented in blue.

The simulated Purkinje images are shown in Figure 3.7. It can be seen that their intensity distribution depends on the intraocular scattering and its origin. When there is corneal scattering, P3 and P4 images are both affected by scattering. However, when it comes from the lens, P3 is unaffected while the P4 intensity distribution is influenced.

Therefore, these simulations support our initial hypothesis, i. e., that the P4 image depends on the corneal and lens scattering, but that P3 is only influenced by scattered light produced in the cornea.
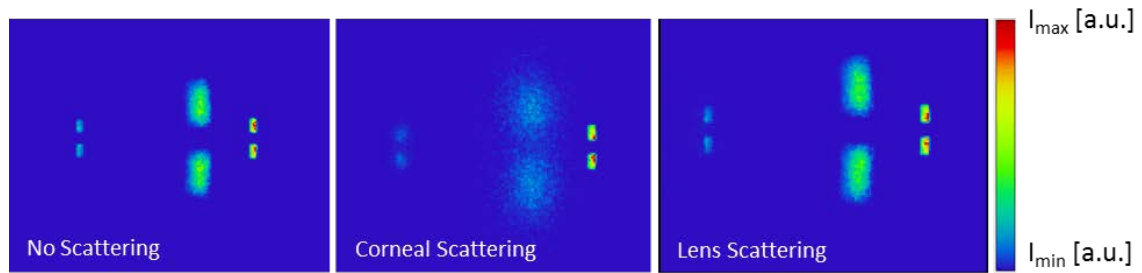
Figure 3.7. Intensity distribution of the simulated Purkinje images (from left to right, P4, P3 and P1).

3.2 Optical bench setup and contrast computation

Based on the former considerations, Figure 3.8 shows the layout of the experimental setup developed to create and acquire the Purkinje images.
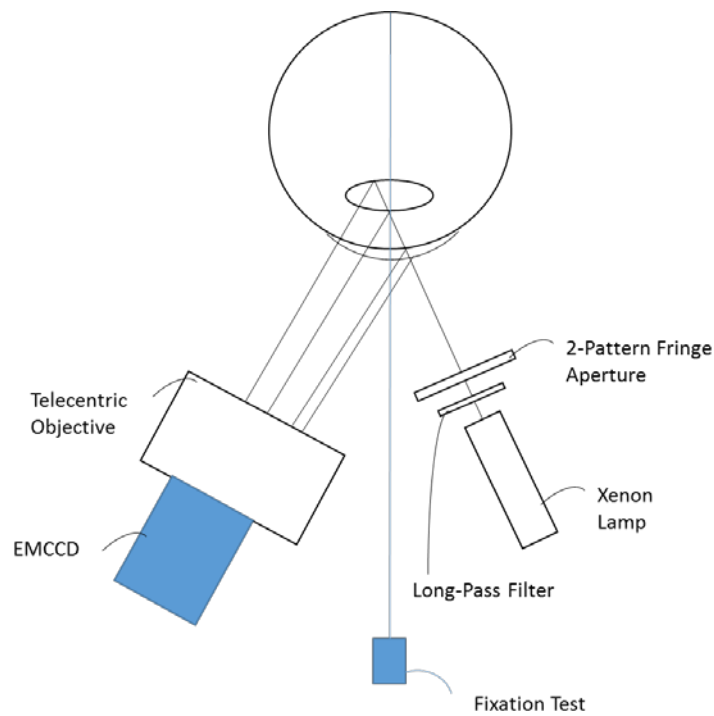
Figure 3.8. Layout (top view) of the Purkinje setup (EMCCD: Electron-multiplier CCD camera).

The light source used was a xenon lamp (Hamamatsu Photonics, Hamamatsu, Japan) whose light is projected towards the opaque plate with the two slits (3mm x 5mm each slit) to create the Purkinje images profile (Figure 3.9). As commented in the former section, we used diffuse light and diffusors attached to

the anterior and posterior surfaces of the opaque plate were used for this purpose. Thanks to them, the slits have a homogeneous luminance.

A long-pass filter (with a cutoff frequency of 760 nm) that lets the near infrared (NIR) pass through while blocking visible light – avoiding therefore pupil's contraction - was placed between the xenon lamp and the opaque plate. Therefore, Purkinje images are formed by means of NIR radiation.
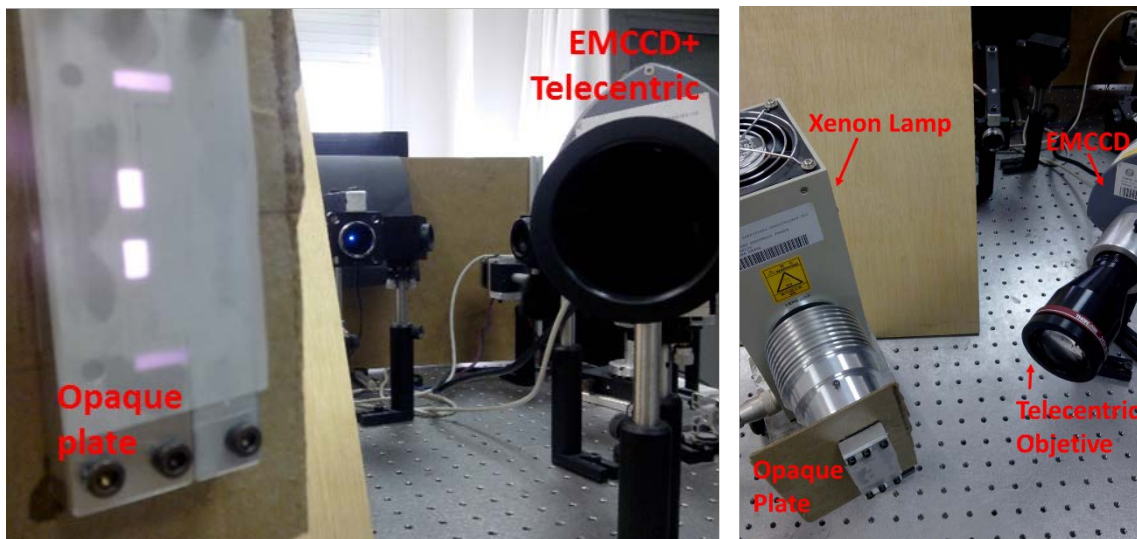
Figure 3.9. (Left) Front view of the experimental setup, i. e., from the patient's point of view. At the left side of the picture, the opaque plate with the 2-slit pattern used to create the Purkinje Images. The two external horizontal slits are just a guide to center the images, while the two vertical slits are used to compute the contrasts from which the intraocular scattering is assessed. (Right) Top view of the experimental setup.

The Purkinje images were recorded by means of a 14 bits electron-multiplier-CCD (EMCDD) camera (Luca, Andor Technology, Belfast, United Kingdom) with a pixel size of 8x8 µm and 1004(H) x 1002(V) pixels. The camera was attached to a telecentric objective lens (MVTC23024, Thorlabs GmbH, Munich, Germany) that gives the necessary depth of field (11 mm) and magnification (0.243x) to acquire all Purkinje images at the same time, and to compensate for the distortion associated with different positions (Figure 3.10). P1 and P2 overlap because the similar radii of curvature of the anterior and posterior surfaces of the cornea and the small corneal thickness.
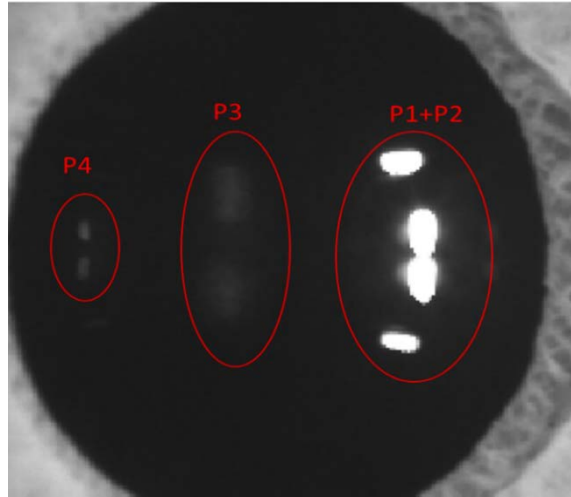
Figure 3.10. Purkinje images of a healthy eye. P1 and P2 overlap and P1 saturates.

A chinrest was also attached to the optical table of the laboratory, and used to minimize patients' movements during measurements while simultaneously improving comfort.

Figure 3.11 shows the Purkinje images taken with the described optical bench setup using the artificial eye OEMI-7 (Ocular Instruments Inc., Bellevue, WA, USA), and the vertical intensity profile of the fourth Purkinje image. Note that the light from the anterior and back surfaces of the cornea (P1 and P2) and the lens (P3 and P4) are acquired simultaneously.

For the scattering assessment, the portion of photons that change their initial trajectory compared with the total amount of photons must be measured. To do so, we decided to use the Michelson contrast definition. In fact, two contrasts for each Purkinje image were calculated (Equations 3.2 and 3.3), since there are two maximums and one minimum in the intensity profile, corresponding to the vertical slits and the central dark area (dark fringe).

$$Contrast_1 = \frac{I_{max1} - I_{min}}{I_{max1} + I_{min}}$$ Equation 3.2

$$Contrast_2 = \frac{I_{max2} - I_{min}}{I_{max2} + I_{min}}$$ Equation 3.3

where I_{max} and I_{min} are the maximum and minimum intensity (see Figure 3.11, Right).

To compute the intensity profile of each Purkinje image, we manually selected an area big enough that included one isolated Purkinje image (see yellow rectangle in Figure 3.11). The profile intensity was then calculated as the maximum pixel value for each row inside the selected area: the first value of the intensity profile corresponds to the maximum value along the first row inside the selected region, the second value of the intensity profile corresponds to the maximum value of the second row inside the same area, and so forth.
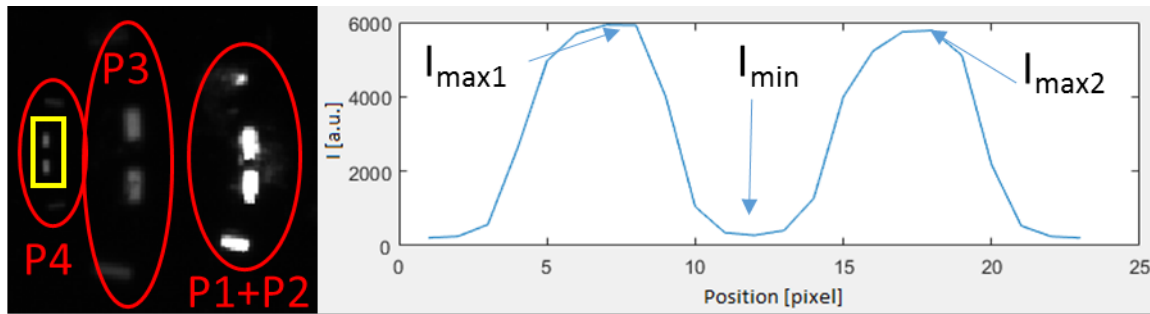
Figure 3.11. (Left) Four Purkinje images of an artificial eye (OEMI-7). The first one (P1) is much brighter than the others and because of this, it is always saturated when the dynamic range of the camera is optimized to record the other three images. P1 and P2 appear superimposed. (Right) Intensity profile of the P4 image in arbitrary units. It is the maximum intensity of each row corresponding to the area delimited by the yellow rectangle (i. e., the intensity value of the position 0 is the maximum intensity value of the first row inside the yellow rectangle).

Then, the final contrast value for each Purkinje image (P3 and P4) was calculated as the average of the two former ones. For an ideal system free from scattering, I_{min} would be 0, and then the contrast would be 1. The greater the scattered light, the higher the I_{min} with respect to I_{max}; and thus, the contrast decreases as scattering increases.

A series of Purkinje images were acquired with the same artificial eye using several exposure times in order to preliminary evaluate the performance of the proposed method and the influence of the intensity of the light source on the parameters based on the contrast. As an example, Figure 3.12 shows the results for the third Purkinje image contrast (P3). Besides the naked eye, combinations of it plus several commercial filters previously validated by others researchers were used to simulate different amounts of scattering. Specifically, we used the filters Black Pro Mist 1 (BPM1) and Black Pro Mist 4 (BMP4) (Tiffen, New York, USA) to simulate an eye with a low amount of scattering and the effect of an early cataract, respectively [100].

As expected, the computed contrasts decreased with the use of filters and were constant with the exposure time, meaning that the outcome of our system is independent of the light exposure as it is a relative measure. The BMP4 filter was linked to the smallest contrast, as it includes the highest amount of scatter.
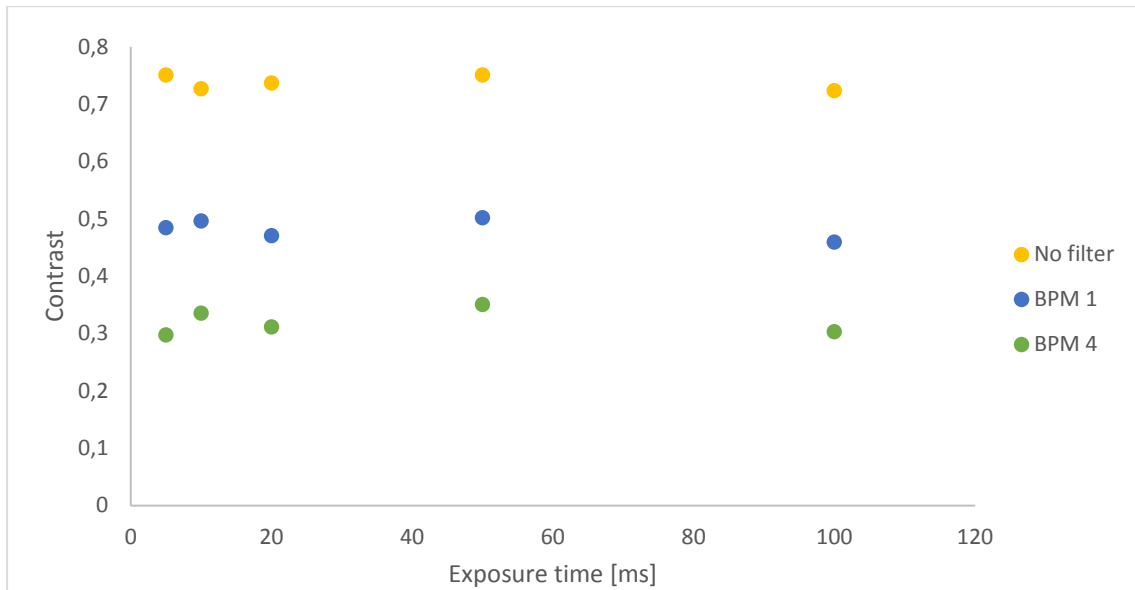
Figure 3.12. Contrast of the third Purkinje image (P3) of the artificial eye (OEMI-7) as a function of the exposure time. In yellow the contrast obtained for the naked eye, in blue the contrast when the BPM 1 filter is placed in front of the eye, and in green the contrast when the BPM 4 filter is placed in front of the eye. Each point is the average of the two computed contrasts for each image.

3.3   Clinical prototype

Some aspects of the optical bench setup were improved to make it useful for a clinical environment. Firstly, we added a low intensity LED with an emission peak at 470 nm (M470F3, Thorlabs GmbH, Munich, Germany) as a fixation target. This minimized the eye movements along the measurement process. The wavelength and low intensity of the LED were chosen according to the eye's sensitivity, which is rather low at this wavelength, avoiding pupil's contraction and improving patient's comfort. The LED was controlled with the DC4100 - LED Driver (Thorlabs GmbH, Munich, Germany).

Furthermore, an additional long-pass filter was also included in the system (with a cutoff frequency of 760 nm). It was placed next to the telecentric objective lens in order to block the blue light from the fixation LED.

We also added a stepper motor (Nanotech, Feldkirchen, Germany) to control for the distance between the system and the patient's eye to properly acquire the images. The system was mounted on a breadboard attached to the stepper motor, which allowed the system to be moved as a whole.

We enclosed the whole system inside a black box and for aesthetic reasons we replaced all handmade holders and light blockers for 3D printed pieces, which helped to preserve optical elements from dust and from being touched by patients (Figure 3.13).

Finally, a couple of 3-D printed grab bars was also added for the patients' comfort and to minimize even more their movement during measurements.
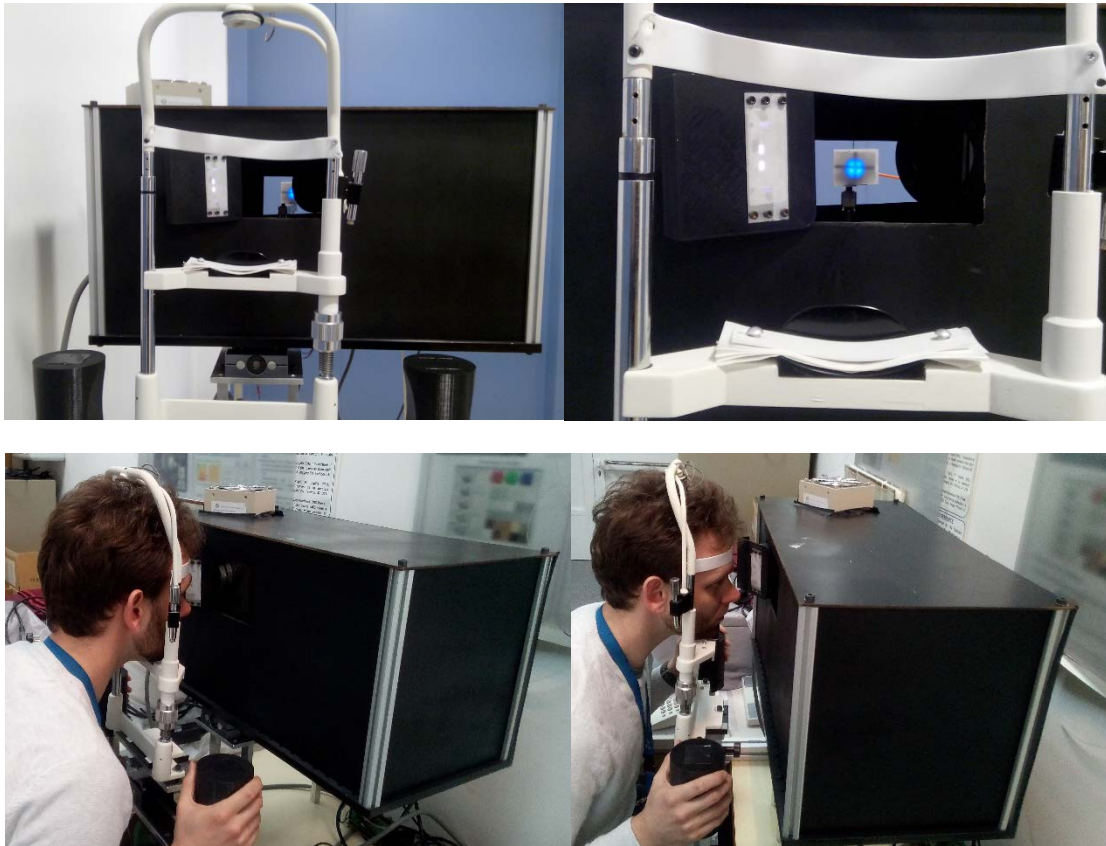
Figure 3.13. Several views of the clinical prototype. The fixation target used (blue) can be seen in the images at the top.

The acquisition of images was carried out by the open source µManager software (Open Imaging, San Francisco, USA), which permitted adjusting the exposure time of the camera [101]. The stepper motor was controlled by the SD243_v1.0 software developed by microPaP Engineering S.L. (Terrassa, Spain).

To ensure that all Purkinje images were acquired at the best focus position, a routine was developed to perform a scanning process along different distances between the system and the eye allowing few images to be recorded at each position. The scan started and finished with clearly defocused images while in the middle some sharp ones were available (Figure 3.14 top). According to this scanning process, the contrasts of all acquired images were then computed as previously explained (section 3.2), and the highest contrast was taken as the correct one for each of the Purkinje images. In some cases, the highest contrast for the P3 and P4 images did not correspond to the same position (Figure 3.14 bottom).
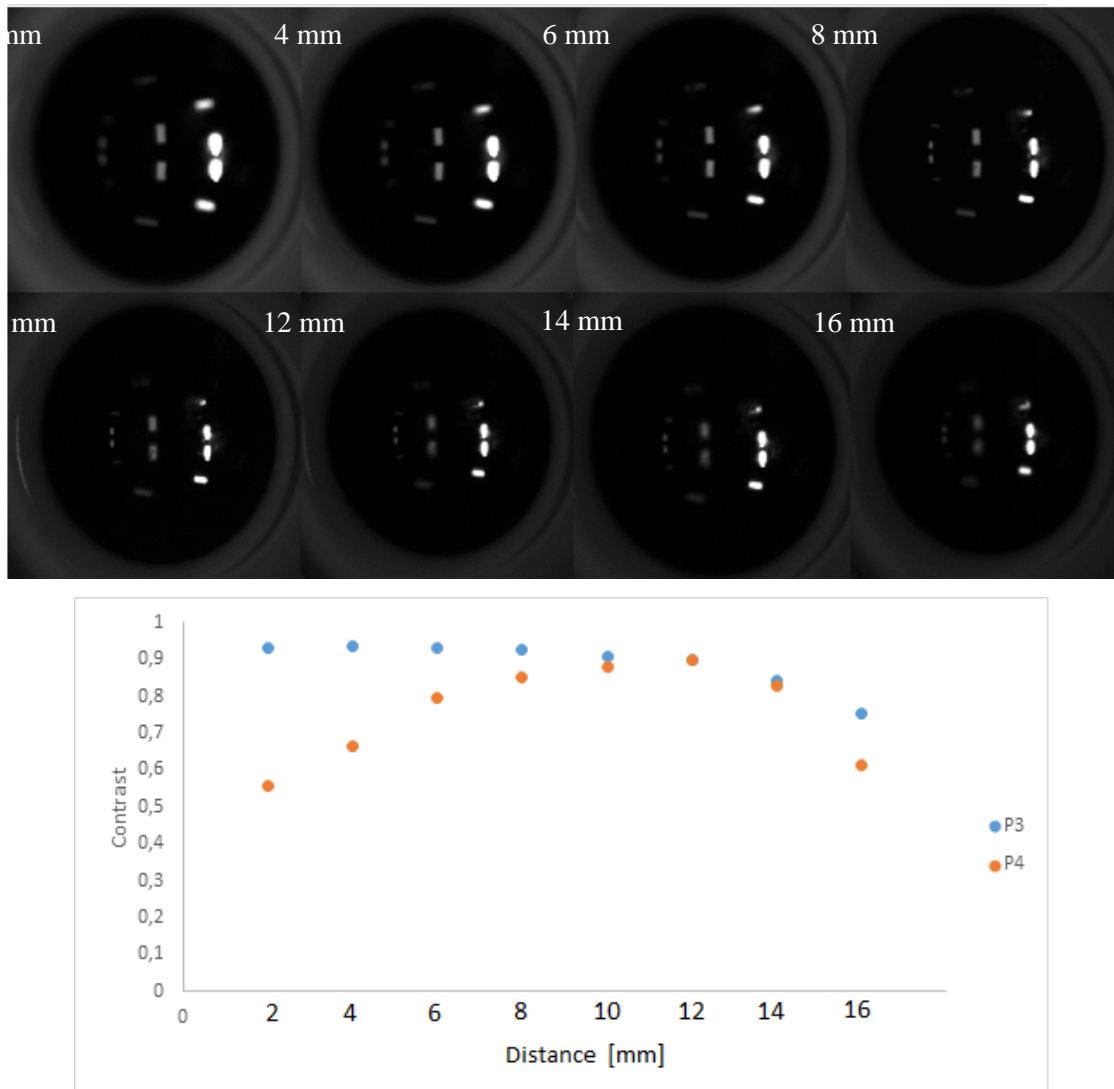
Figure 3.14. (Top) Purkinje images from an artificial eye (OEMI-7) taken at different distances between the eye and the system along the scanning process. (Bottom) Corresponding Purkinje contrasts (P3 and P4) as a function of the distance from the first image.

3.4 Safety issues

The standard ISO 15004-2:2007 "Ophthalmic instruments -- Fundamental requirements and test methods -- Part 2: Light hazard protection" [102] specifies fundamental requirements for optical radiation safety for ophthalmic instruments and is applicable to all ophthalmic instruments that direct optical radiation into or at the eye and for which there is a specific light hazards requirement section within their respective national standards.

According to this standard, ophthalmic instruments can be classified into either Group 1 or Group 2 in order separate those instruments that are not capable of presenting a potential hazard from those which do.

To determine if our system was inside the established limits to be classified as an ophthalmic instrument for which no potential light hazard exists, we performed the calculations shown below. Firstly, the corneal and lens irradiance for non-weighted infrared radiation was calculated as only radiation above 760 nm (from the xenon lamp and the long-pass filter) is emitted by the clinical prototype, as it is indicated in table 3.2 of the ISO 15004-2:2007 "*Limit values for continuous wave instruments*":

Table 3.2. Group 1 limit values for continuous wave instruments (Table 2, 5.4.1.4 of the ISO 15004-2:2007).

	Parameter	Wavelength (nm)	Equation	Limit
5.4.1.4	Unweighted corneal and lenticular infrared radiation irradiance, E_{IR-CL}	770 to 2500	$E_{IR-CL} = \sum_{770}^{2500} E_\lambda \times \Delta\lambda$	20 mW/cm^2

where E_{IR-CL} is the unweighted corneal and lenticular infrared radiation irradiance, E_λ is the spectral irradiance and $\Delta\lambda$ is the summation interval.

The spectral irradiance was measured by means of the spectrophotometer Spectro 320 (Instrument Systems GmbH, Munich, Germany) at the plane where the cornea is positioned during the clinical measurements and the cumulative spectral irradiance was calculated from 770 nm to 2500 nm when the xenon lamp was switch on. The result was of 0.504 mW/cm^2, below the limit established by the standard for Group 1 (20 mW/cm^2).

According to the emission range of our system and the same standard, the other limit that needs to be taken into account is the thermal hazard for the infrared and visible radiation of the retina. To calculate the thermal irradiance of the retina by weighted infrared and visible radiation, the following calculations must be carried out:

Table 3.3. Group 1 limit values for continuous wave instruments (Table 2, 5.4.1.6 of the ISO 15004-2:2007).

Parameter	Wavelength (nm)	Equation	Limit
5.4.1.6	R(λ) weighted retinal visible and infrared radiation thermal irradiance, E_{VIR-R}	380 to 1400	$E_{VIR-R} = \sum_{380}^{1400} E_\lambda \times R(\lambda) \times \Delta\lambda$	0.8 W/cm²

where E_{VIR-R} is the weighted retinal visible and infrared radiation thermal irradiance and $R(\lambda)$ is the visible and infrared radiation thermal hazard weighting function (Table 3.4).

As reported in the standard, in this case the values of the retinal spectral irradiance, E_λ, must be determined from the spectral radiance of the ophthalmic instrument, L_λ. To do so, the spectral irradiance at the corneal plane, $E_{\lambda-C}$, must be multiplied by the squared distance between the eye and the stimulus ($D = 90$mm) and divided by the area of the stimulus ($A = 15$mm²):

$$L_\lambda = \frac{E_{\lambda-C} \cdot D}{A}$$

Equation 3.4

The spectral irradiance values on the retina are then calculated by multiplying the spectral radiance values by the pupil's area and dividing it by the square of the pupil-retina distance (Equation 3.5). The standard indicates that the pupil's area, A_p, through which the light passes during the normal use of the ophthalmic instrument must be determined. In this thesis, a value of 8 mm of diameter was used to check for danger in the worst case, and a pupil-retina distance, D_0, of 17 mm was considered, as it is specified in the ISO 15004-2:2007.

$$E_\lambda = \frac{L_\lambda A_p}{D_0{}^2}$$

Equation 3.5

Table 3.4. Spectral weighting functions for the retinal hazard analysis.

λ (nm)	R(λ)	λ (nm)	R(λ)	λ (nm)	R(λ)
380	0,00625	785	0,68	925	0,35
385	0,0125	790	0,66	930	0,34
390	0,025	795	0,65	935	0,33
395	0,05	800	0,63	940	0,32
400	0,1	805	0,62	945	0,32
405	0,2	810	0,6	950	0,31
410	0,4	815	0,59	955	0,31
415	0,8	820	0,58	960	0,3
420	0,9	825	0,56	965	0,3
425	0,95	830	0,55	970	0,29
430	0,98	835	0,54	975	0,28
435-700	1	840	0,52	980	0,28
705	0,98	845	0,51	985	0,27
710	0,95	850	0,5	990	0,26
715	0,93	855	0,49	995	0,26
720	0,91	860	0,48	1000	0,25
725	0,89	865	0,47	1005	0,25
730	0,87	870	0,46	1010	0,24
735	0,85	875	0,45	1015	0,23
740	0,83	880	0,44	1020	0,23
745	0,81	885	0,43	1025	0,22
750	0,79	890	0,42	1030	0,22
755	0,78	895	0,41	1035	0,21
760	0,76	900	0,4	1040	0,21
765	0,74	905	0,39	1045	0,2
770	0,72	910	0,38	1050-1400	0,2
775	0,71	915	0,37		
780	0,69	920	0,36		

By doing all this, the value obtained for the R(λ) weighted retinal visible and infrared radiation thermal irradiance was of 0.003 W/cm^2, much below the limit established for Group 1 (0.7 W/cm^2).

Moreover, the irradiance of the fixation test (blue LED emitting at 470 nm) when measured at the corneal plane was of 1.41 μW/cm^2. To measure the irradiance of this LED we used a power meter (PM160, Thorlabs GmbH, Munich, Germany). Repeating the calculations that we made for the xenon lamp, we obtained a value of R(λ) weighted retinal visible and infrared radiation thermal irradiance of 0.3 mW/cm^2, orders of magnitude below the limit value again (0.7 W/cm^2).

Thus, it was demonstrated that the instrument developed in this thesis complies with the standard to be classified in Group 1 and that it does not present potential hazard.

4 Validation of the system at the laboratory level

As commented formerly, the goal of this thesis was to develop a system to objectively measure the intraocular scattering and separate the contribution from the cornea and the lens. For this purpose, we developed the system already described to acquire the Purkinje images. Our hypothesis was that the third Purkinje image, since it is the reflection from the anterior lens surface, is mainly affected by the scattering from the cornea and the anterior chamber of the eye, while the fourth Purkinje image is also affected by the lens scattering. The validation of the system at the laboratory level and methodology proposed are described in this chapter.

4.1 Validation with artificial eyes

As a proof of concept of our experimental setup based on the Purkinje images, we firstly tested it using artificial eyes with different levels of corneal and lens scattering.

4.1.1 Methods

We used two artificial eye models. The first one was the commercial artificial eye OEMI-7 (Ocular Instruments Inc., Bellevue, WA, USA), which is a compact eye model with the same sizes, radii of curvature and refractive indexes as the human eye (Figure 4.1).
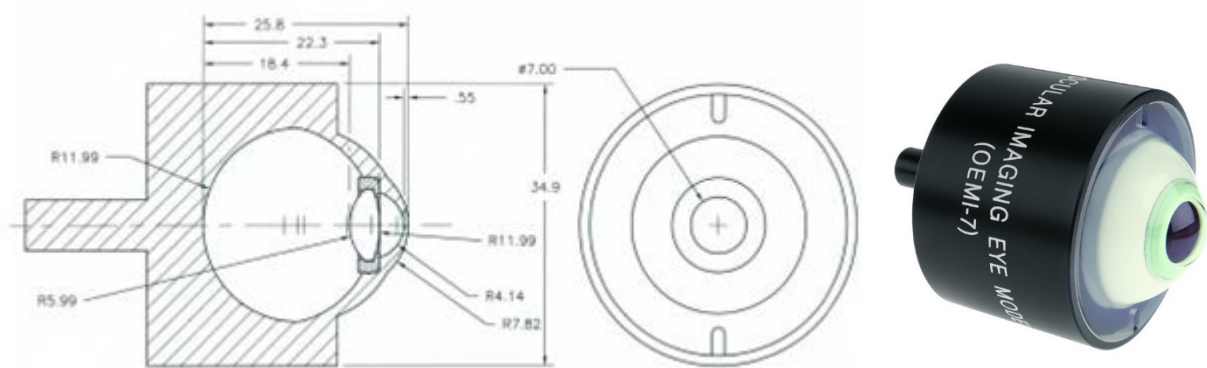
Figure 4.1. Schematics of the commercial artificial eye OEMI-7 (left). General view of the OEMI-7 commercial eye model (right)(Source: Argawal et al. 2016 [103]).

The second artificial eye used was a customized model. In fact, we used the cornea from the Eyetech Laser Eye Model LE-110 (Eyetech Ltd., Morton Grove, Ill., USA); however, a couple of concentric plano-convex lenses ACL2520U and ACL1512U (Thorlabs GmbH, Munich, Germany) were placed together inside the eye by attaching their planar surfaces one to each other to emulate the human lens shape (Figure 4.2).

Additionally, we printed a holder by using the Witbox 2 3D printer (BQ, Madrid, Spain) to place the artificial cornea and lens in the desired positions.
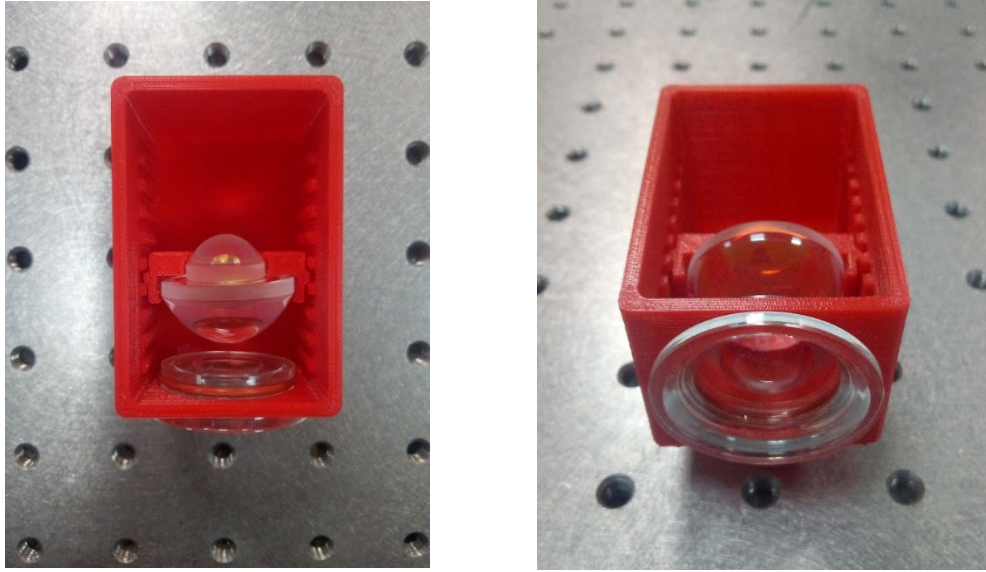
Figure 4.2. Customized artificial eye. Cornea from Eyetech, artificial lens made by two plano-convex lenses (Thorlabs) and a 3D-printed holder.

We used several commercial filters, previously validated by others researchers to simulate different amounts of corneal and lens scattering. Specifically, we used the filter Cinegel 3020 (c3020) (Rosco, Stamford , USA) with properties similar to a mature cataract [104], and the filters Black Pro Mist 1 (BPM1) and Black Pro Mist 4 (BMP4) (Tiffen, New York, USA) with optical characteristics that resemble ocular cataracts; specifically, they are used to simulate an eye with a low amount of straylight and the effect of an early cataract, respectively [100].

With the OEMI-7 model, several levels of corneal scattering were achieved by placing the filters in front of the eye. Specifically, we simulated five levels of corneal scattering by using the following: the OEMI-7 model without filters (naked OEMI-7), the OEMI-7 plus the BPM1 filter in front of it (BPM1 OEMI-7), the OEMI-7 plus the BPM4 filter (BPM4 OEMI-7), the OEMI-7 plus one single sheet of the c3020 filter (c3020 OEMI-7) and, finally, two sheets of c3020 were placed together in front of the eye model (Double c3020 OEMI-7).

With the customized eye from Eyetech we simulated lens scattering by placing the filters in between the two plano-convex lenses. In this case, three different levels of scattering were achieved by using the eye model without filters (naked customized artificial eye), and one and two sheets of the c3020 in between the plano-convex lenses (c3020 customized artificial eye; and double c3020 customized artificial eye).

We performed three measurements for each described condition with the optical bench Purkinje setup and the P3 and P4 contrasts corresponding to the third and fourth images were computed as described in chapter

3 (Section 3.2). The reported results are the average of the three individual measurements for each particular scattering condition as well as the corresponding standard deviation (SD).

4.1.2 Results

Figure 4.3 shows the Purkinje images from the OEMI-7 artificial eye and their corresponding intensity profiles for the naked eye and in the presence of the c3020 filter, respectively. As expected, the more scattering, the less contrasts in the third (P3) and fourth (P4) Purkinje images.
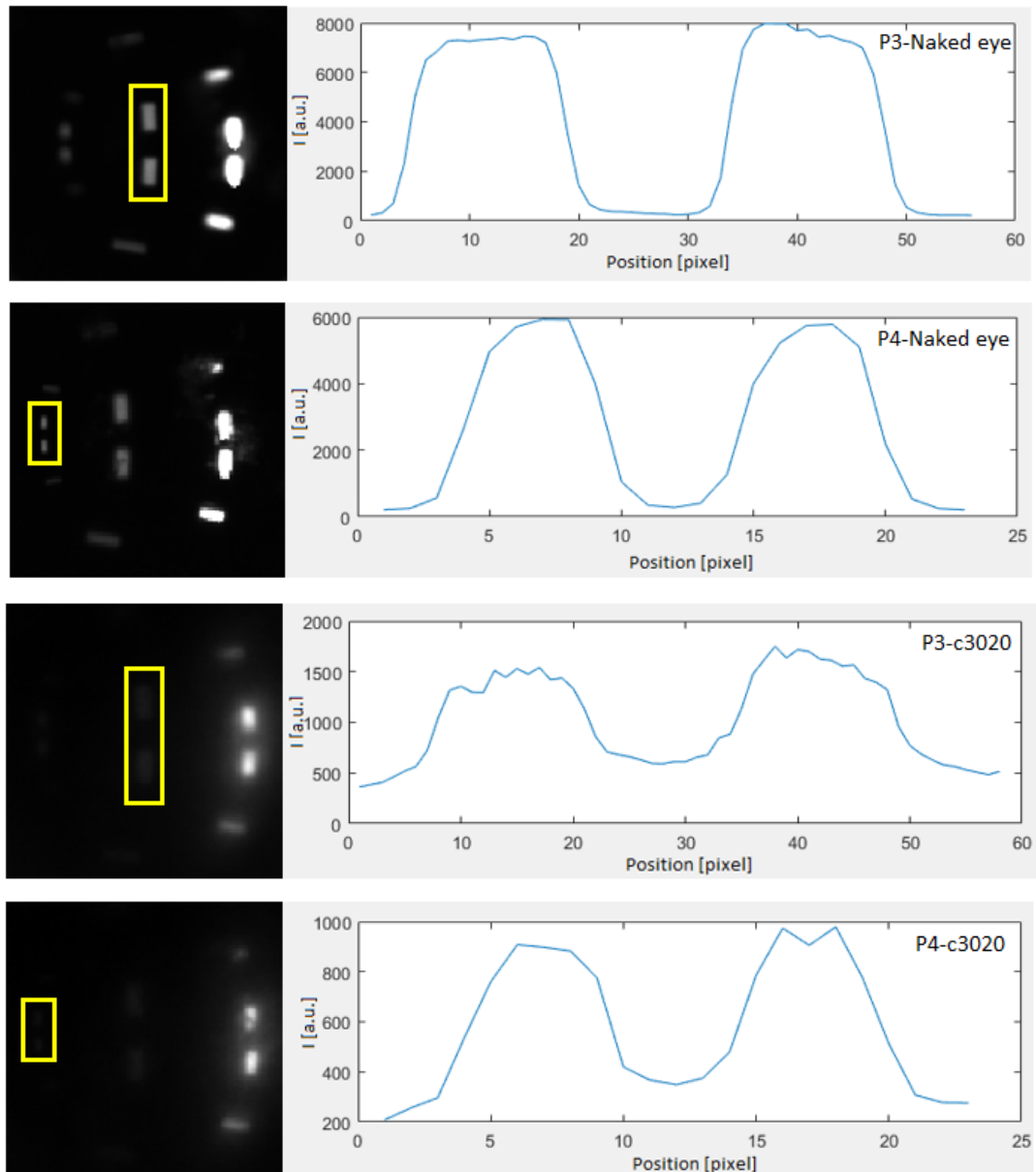
Figure 4.3. Purkinje images from the OEMI-7 model and corresponding intensity profiles. From top to bottom: contrasts of P3 naked eye, P4 naked eye, P3 c3020 and P4 c3020. The first Purkinje image is saturated so that P3 and P4 are within the dynamic range of the camera. The intensity profile plotted is the maximum pixel value per each row inside the yellow rectangle of the corresponding image.

Figure 4.4 shows the scatterplots of the measured Purkinje contrasts by using the OEMI-7 eye model for the several simulated levels of corneal scattering. As it can be seen, P3 and P4 contrasts decrease as the corneal scattering increases. Similarly, Figure 4.5 shows the results for the customized artificial eye and different filters to induce lens scattering. In this case, the P4 contrast decreases as the lens scattering increases while the P3 contrast remains constant. The numerical results of the former validations are summarized in Table 4.1.
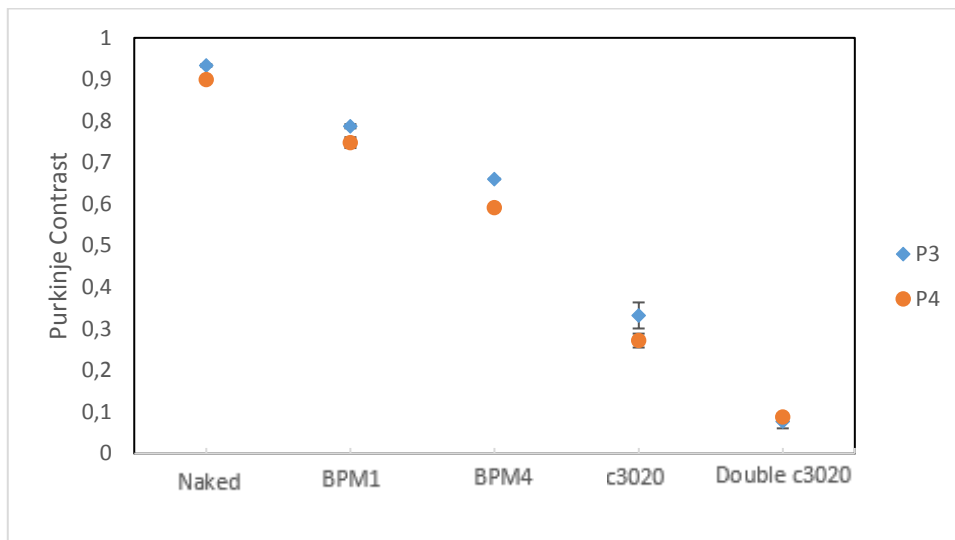
Figure 4.4. Scatterplot of the measured Purkinje contrasts using the OEMI-7 eye model for different levels of simulated corneal scattering. In blue, the P3 contrast and in orange, the P4 contrast. Error bars are the standard deviation of the mean (SD).
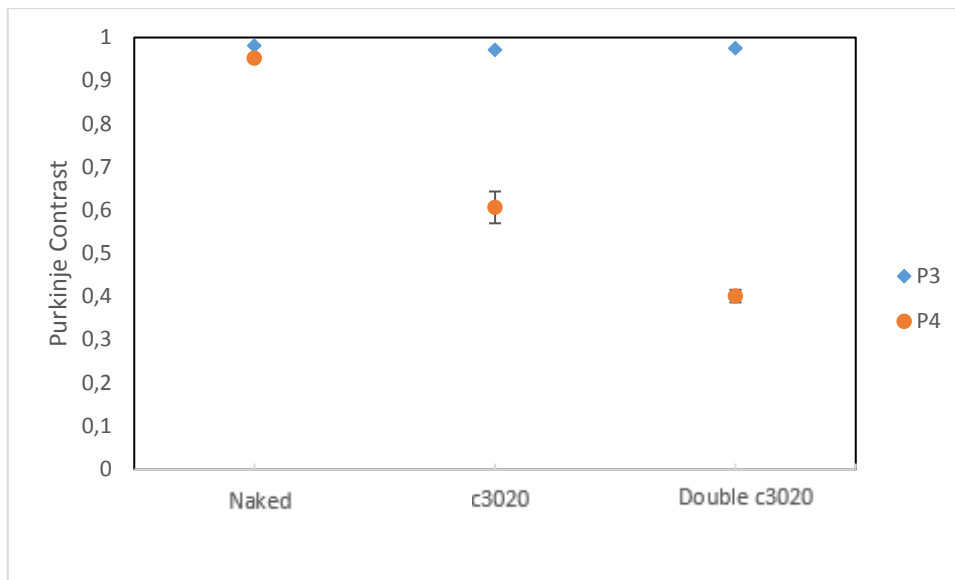
Figure 4.5. Scatterplot of the measured Purkinje contrasts using the customized artificial eye for different levels of simulated lens scattering. In blue, the P3 contrast and in orange, the P4 contrast. Error bars are the standard deviation of the mean (SD).

Table 4.1. Results of the measured Purkinje contrasts (P3 and P4) in artificial eyes with different levels of corneal and lens scattering. The Mean ± SD (standard deviation) are given.

	P3		P4	
Corneal scattering				
Naked OEMI-7	0.93	± 0.00	0.90	± 0.00
BPM1 OEMI-7	0.79	± 0.01	0.75	± 0.01
BPM4 OEMI-7	0.66	± 0.00	0.59	± 0.00
c3020 OEMI-7	0.33	± 0.03	0.27	± 0.02
Double c3020 OEMI-7	0.08	± 0.02	0.09	± 0.01
Lens scattering				
Naked customized artificial eye	0.98	± 0.00	0.95	± 0.00
c3020 customized artificial eye	0.97	± 0.00	0.61	± 0.04
Double c3020 customized artificial eye	0.98	± 0.00	0.40	± 0.01

These preliminary results validate the initial hypothesis of this thesis. When simulating corneal scattering, the contrast of both Purkinje images (P3 and P4) decreased. On the other hand, when the scattering filters were positioned at the lens plane, thus simulating the nature of cataracts, P3 contrast was kept constant regardless the amount of scattering, while the P4 contrast drastically decreased as a function of scattering. Therefore, it is clear that P3 is affected by the scattering from the cornea and unaffected by that from the lens, while P4 contrast is affected by both, that is, corneal and lens scattering. Therefore, the method proposed allows one to know where the scattering comes from.

4.2 In-vivo validation

In this section, we move a step forward by testing the Purkinje system developed in-vivo, that is, with real eyes. The on-bench system was used to measure several real eyes as a means of validating its usefulness before going to a clinical environment. The main outcomes are described next.

4.2.1 Methods

In this preliminary analysis, we measured 13 eyes of 13 volunteers (6 females and 7 males) recruited from the staff of the CD6 (Center for Sensors, Instruments and Systems Development) and colleagues (age 51.2 ± 13.6 years, range [30, 71]).

The measurement protocol included the assessment of intraocular scattering by means of the following instruments: the Scheimpflug camera Galilei 6 (Ziemer, Biel, Switzerland), HD Analyzer (Visiometrics

S.L., Cerdanyola del Vallès, Spain) and our optical bench experimental setup to acquire the Purkinje images and compute P3 and P4 contrasts.

All measurements were taken in a dark room and without pupil dilation. Firstly, we measured the scattering with our experimental setup. Patients were asked to put the head on the chinrest. To ensure that the best focused image was obtained, we performed a scanning process for each patient varying the distance between the system and the eye, and few images were registered at each position. The reported Purkinje contrasts are the average of the 3 images with highest contrasts obtained. Purkinje images affected by the eye lips were excluded as well as those in which the fourth Purkinje image was on the pupil boundary (small pupils).

Then, we acquired DP images by means of the HD Analyzer. Because optical quality might be dependent on tear film quality, measurements were taken just after the patient blinked. The spherical refractive error was automatically corrected by the DP system (from -8.00 to +6.00 D with an accuracy of 0.125 D), whereas astigmatism was corrected with an external cylindrical lens (with an accuracy of 0.25 D) to obtain the best possible retinal image. We did three consecutive measurements and the reported OSI value is the average of these individual measurements. DP measurements of patients with a pupil diameter smaller than 4 mm were excluded from the analysis.

Finally, we took images using the Galilei 6 to check for corneal transparency. The dual camera configuration captures two Scheimpflug slit images from opposite sides of the slit beam and simultaneously tracks decentration due to eye movements [105]. The reported densitometry is the highest value found in the cornea. The lens densitometry was not analyzed since the pupil was not dilated.

4.2.2   Results

In this study, eyes with abnormal large values of corneal densitometry were artificially classified as eyes with a certain degree of corneal opacification (37.7 of corneal densitometry against an averaged corneal densitometry of 28.1 ±1.8 for the rest of the volunteers) (Figure 4.6). A previous study on 445 healthy participants found a mean corneal densitometry that is in agreement with our laboratory-sample classification (25.81 ± 5.14) [106]. Eyes with large OSI values and transparent corneas were artificially classified as eyes with cataracts (2.9, 3.6 and 4.9 OSI against an OSI average of 0.75 ±0.4 for the rest of volunteers). Overall, we had 9 healthy eyes, 3 with cataracts and 1 with corneal opacification (Table 4.2).
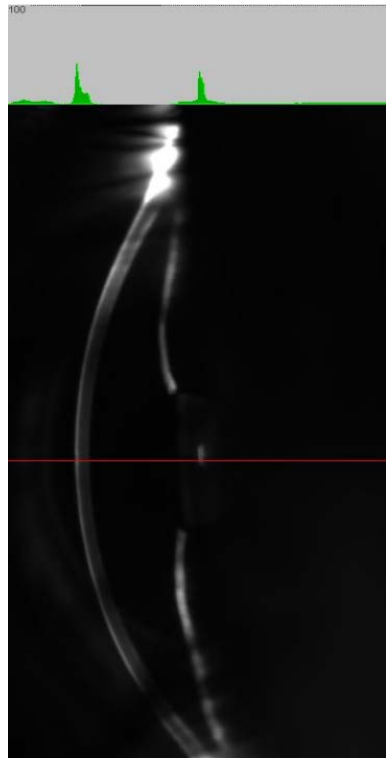
Figure 4.6. Image of the eye with a corneal densitometry of 37.7 taken Scheimpflug camera Galilei 6. In green the densitometry profile corresponding to the red line.
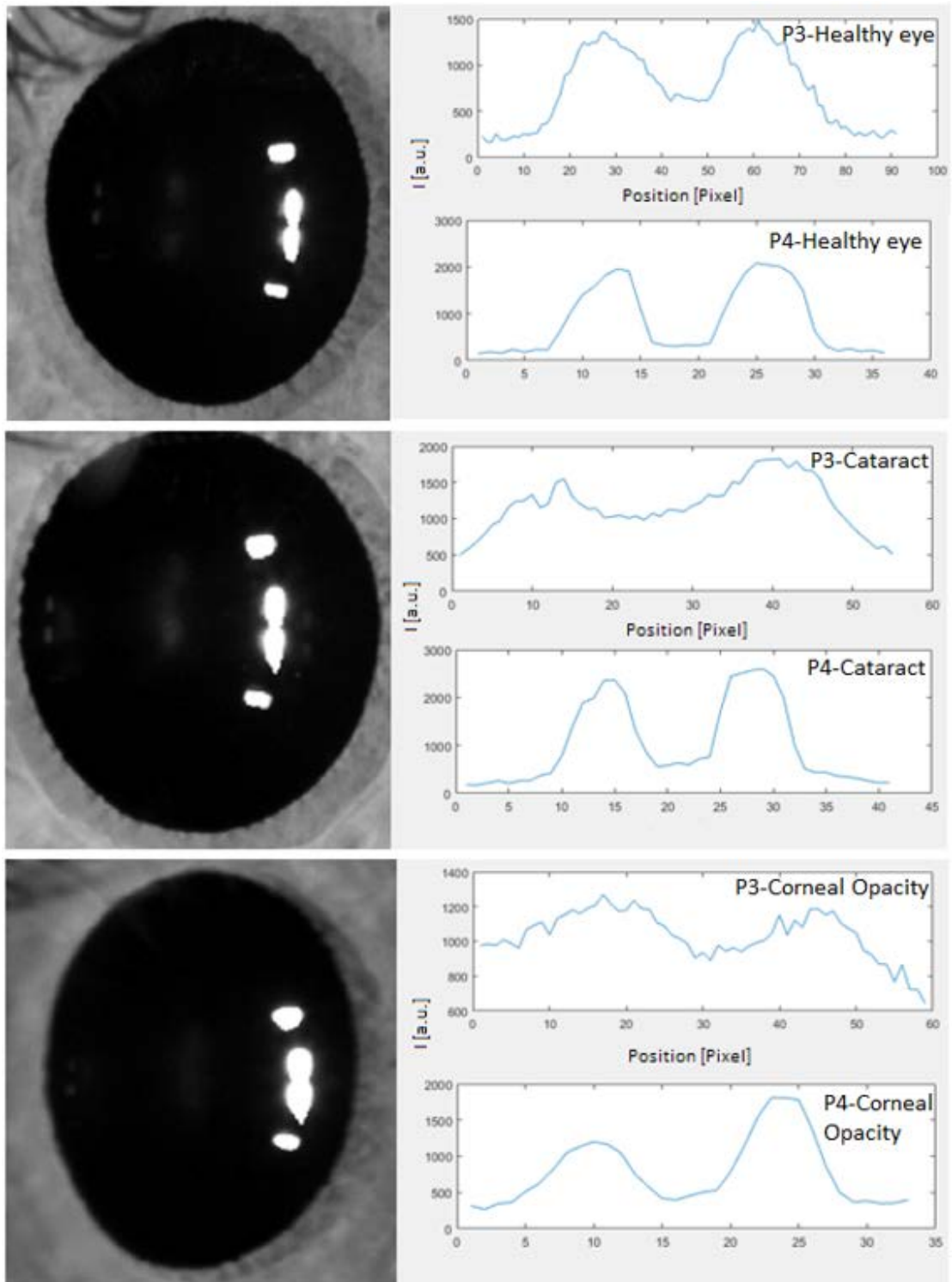
	Healthy eye	**Cataract**	**Corneal opacity**
P3	0.43	0.24	0.15
P4	0.69	0.62	0.59

Figure 4.7. Purkinje images (left) from a healthy eye (top), eye with a cataract (middle) and eye with a corneal opacification (bottom), and the corresponding P3 and P4 intensity profiles (right). The values of P3 and P4 contrasts are also given.

Table 4.2. Intraocular scattering values for healthy eyes, and with corneal opacifications and cataracts: contrast of the Purkinje Images (P3, P4), OSI and corneal densitometry. The mean ± SD are shown as well as the range (minimum and maximum values) (NA: Not Applicable as only 1 eye is available).

	Mean ± SD [Range]					
	Healthy eyes		**Corneal opacification**		**Cataracts**	
P3	0.45 ± 0.05	[0.39 , 0.53]	0.15 ± 0.0	[NA]	0.30 ± 0.09	[0.24 , 0.40]
P4	0.69 ± 0.05	[0.61 , 0.75]	0.59 ± 0.0	[NA]	0.58 ± 0.04	[0.53 , 0.62]
OSI	0.75 ± 0.44	[0.33 , 1.8]	0.73 ± 0.0	[NA]	3.79 ± 1.02	[2.9 , 4.9]
Densitometry	28.52 ± 1.77	[27 , 32]	37.67 ± 0.0	[NA]	26.5 ± 0.71	[26 , 27]

It is worth noting that in general P3 contrasts were lower than P4 contrasts although the reflectance of both were expected to be about the same order of magnitude ($R_{P3} \sim R_{P4} = 7 \times 10^{-4}$) (refer to the state of the art for more information). This may be due to the fact that the size of the P3 is larger than the P4, so that the same amount of light is more widespread. Also, the posterior lens surface is smoother and the anterior surface looks like ground glass (orange peel effect) (Figure 4.8) [107]. The reflection of the posterior lens surface is done on the endothelial layer (the lens capsule, which is a cellular layer); this surface is considered to be smoother than the anterior lens surface and, therefore, this gives rise to a better quality of the fourth Purkinje image [108], from which a more marked profile is obtained in terms of intensity profile.

Another possible artifact could come from the position where the Purkinje images are formed. As we commented in section 2.3, P3 is formed much closer to the retina than the other Purkinje images, which are indeed closer to first surface of the lens; and even a telecentric objective lens with enlarged depth of field was used to acquire at the same time both images, P3 could be more influenced by defocus resulting in a lower contrast. Moreover, the fact that P3 is formed by the reflection on a rough surface made it difficult the subjective task of focusing this image.
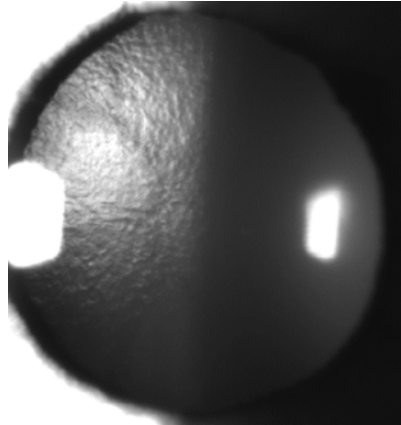
Figure 4.8. Image of the first surface of the human lens taken with a slit-lamp. The roughness of the anterior lens surface (orange peel effect), where the light is reflected to form P3, can be clearly seen.

Interestingly, the eye with corneal opacification was not linked to a large value of OSI. On the contrary, eyes with cataracts had large OSI values.

Figure 4.9 shows P3 and P4 contrasts obtained with our experimental setup as a function of age. As with the artificial eyes, the one with corneal opacification has P3 and P4 contrasts diminished with respect to healthy eyes. However, eyes with cataracts were also linked to lower P3 and P4 contrasts. It should be reminded that P3 was expected to remain constant in this last case.

Therefore, these results suggest that the P3 contrast in in-vivo eyes is not only affected by corneal scattering as assumed as initial hypothesis. In fact, Navarro et al. reported that the roughness of anterior lens surface is age dependent [107], which can affect the measured P3 contrast.
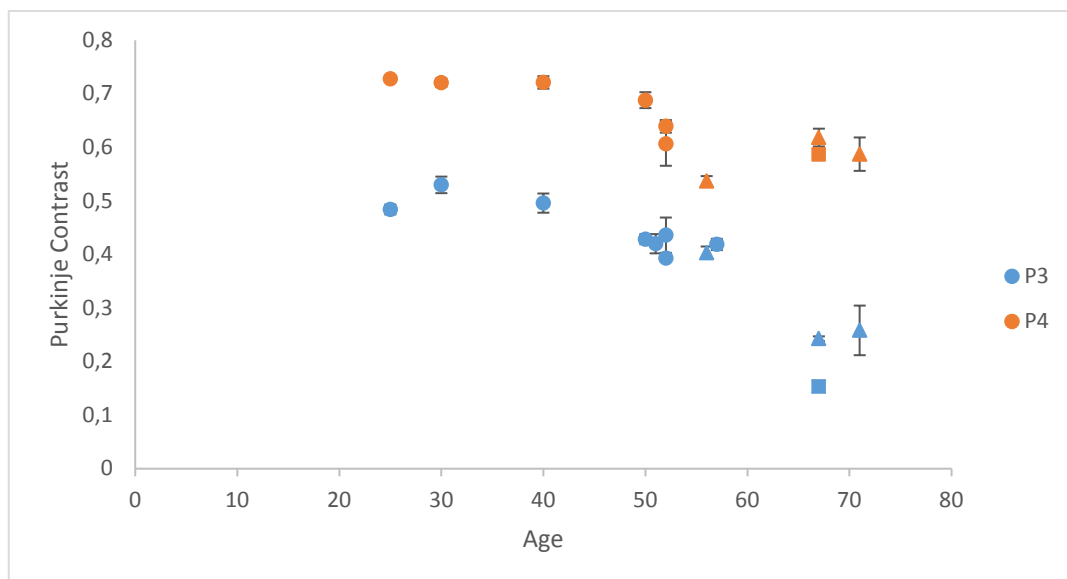
Figure 4.9. Purkinje contrasts as a function of age. P3 contrast, in blue, P4 contrast in orange. Healthy eyes are represented with a circular marker, eyes with cataracts with a triangle and the eye with corneal opacity with a square.

To study this in more detail, data was classified among groups of age decades: <50, between 50 and 60 and > 60 years old (Figure 4.10).
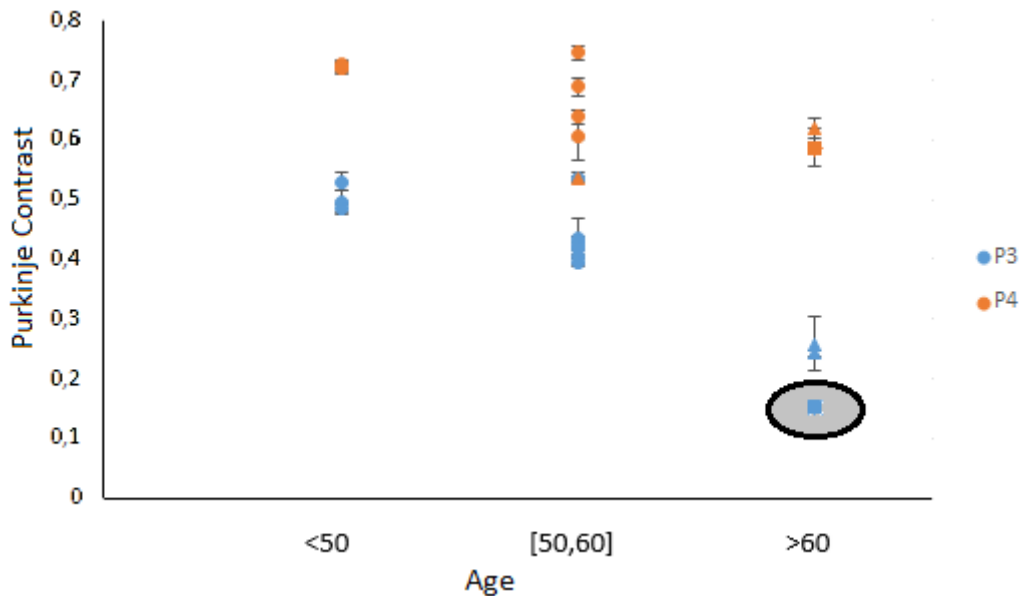
Figure 4.10. Purkinje contrasts as a function of age groups. P3 contrast in blue, P4 contrast in orange. Healthy eyes are represented with a circular marker, eyes with cataracts with a triangle and the eye with corneal opacity with a square. P3 contrast of the eye with corneal opacity is highlighted.

It can be seen that P3 contrasts decrease notably with age and that P4 contrasts remain more constant. Furthermore, the P3 contrast for the eye with the opacification in the cornea has a marked lower value with respect to the other eyes (healthy and with cataracts) of patients older than 60 years. This is in agreement with the findings of Navarro et al. [107].

Moreover, the fact that P3 contrast values are much more similar inside each group of age than P4 might indicate that age has an important impact on the P3 contrast computation while in the case of P4, this is not so important. In fact, it is known that even the lens scattering increases with age [109], there is a huge variability among individuals as the development of cataracts may differ notably among them.

In order to remove the P3 contrast dependency with age, a simple compensation by adding a constant was applied. If the subject was younger than 50 years old, no compensation was used. If the subject was between 50 and 60 years old, we added a value of 0.1 to the measured P3 contrast. Finally, if the subject was older than 60 years old, the compensation needed was found to be 0.25 (the data from the eye with corneal opacity was not taken into account for this calculation). P3 contrast values as a function of age after this correction are shown in Figure 4.11.

By doing so, P3 contrast becomes independent of the intraocular scattering associated with age. In other words, all the healthy eyes and eyes with cataracts have similar P3 contrast, indicating that those eyes have

similar corneal and anterior chamber scattering. On the other hand, the eye with abnormal high corneal densitometry has the lowest P3 contrast as expected. Therefore, we can clearly distinguish between eyes with transparent healthy corneas from those with abnormal high densitometry.
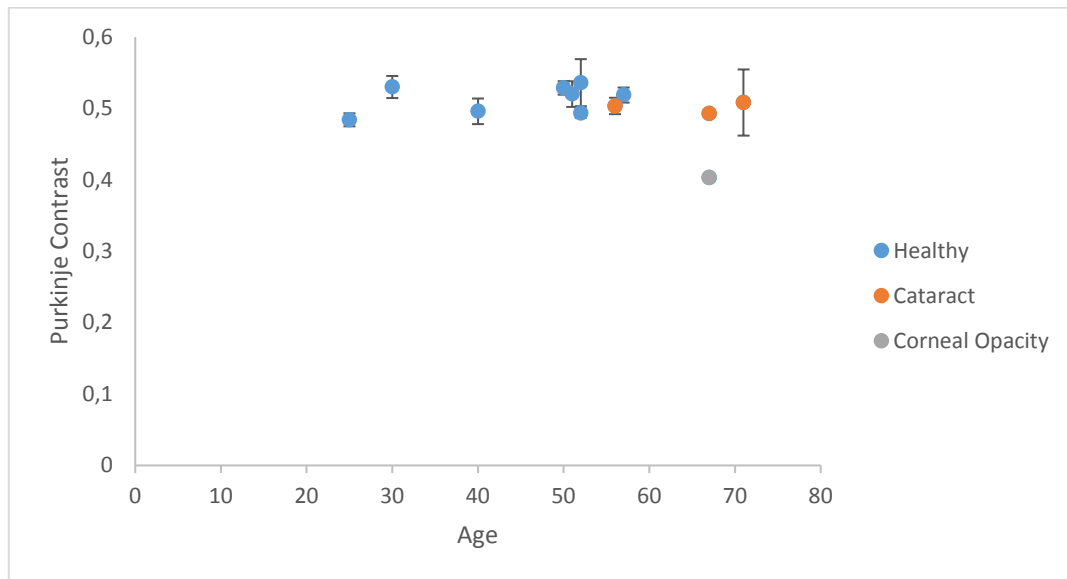
Figure 4.10. Scatterplot showing the compensated P3 contrast as a function of age. Healthy eyes in blue, eyes with cataracts in orange and the eye with corneal opacity in grey.

These preliminary results obtained at the laboratory level in real eyes indicated that our novel system was able to assess intraocular scattering in an objective way. Additionally, from the Purkinje images we knew if the intraocular scattering came from the cornea or the lens. However, only one eye with a certain degree of corneal opacification was included in the analysis and, for this reason, a clinical study with a larger sample, including eyes with cataracts and corneal disorders, was also conducted.

5 Clinical study

In this chapter, we present the results of a clinical study carried out to validate the performance of the developed system and the proposed methodology to account for scattering associated with different ocular structures in a clinical environment. The study included healthy eyes, eyes with cataracts and eyes with corneal disorders (CD). Since the number of eyes with CD was limited, we conducted an additional study with 4 healthy young eyes wearing scatter-customized contact lenses (CLs) to simulate different levels of corneal opacification. Finally, a method to make the P3 contrast independent of the lens scattering was also developed.

5.1 Methods

5.1.1 Patients

This prospective, observational, cross-sectional, non-consecutive case series study included the analysis of 46 eyes of 46 patients with different grades of nuclear cataracts (30 nuclear and 16 mixed nuclear cataracts) (age: 56.4 ± 10.0 years). For individuals who had bilateral cataract, only the left eye was selected.

Furthermore, 11 eyes from 11 patients (age: 38.8 ± 12.2 years) with CD such as keratitis, cornea Verticillata, Fuchs dystrophy and complications from laser refractive surgery (Femto-LASIK) were also included in the analysis. In patients undergoing refractive surgery, the corneal flap was created using the IntraLase femtosecond laser and LASIK was performed using the Amaris Schwind excimer laser system with the same profile treatment, at 6.3 mm optical zone, and a customized transition zone. The thickness of the flap was of 120 microns and the residual stromal bed of 300 microns. Postoperative medication comprised moxifloxacin hydrochloride (Vigamox) and dexamethasone phosphate (Dexafree) 4 times a day for 8 days and artificial tears at least 5 times a day for 2 months.

Twenty-five eyes of healthy subjects were used as control group (age: 45.6 ± 11.6 years) in the study of patients with cataracts. The inclusion criterion for the control group was restricted to eyes with a corrected distance visual acuity (CDVA) of at least 20/20. On the other hand, 17 of them were also selected according to the sample size and age, and used in the clinical study of patients with CD.

Patients with a history of ocular pathology, except cataract, CD and laser (Femto-LASIK) surgery, were excluded from the analysis as well as those with a pupil diameter smaller than 4 mm.

As commented above, an additional study was also carried out including 4 healthy eyes of 4 young patients (age: 23.75 ± 3.40 years) wearing scatter-customized contact lenses (CLs) to simulate different levels of corneal opacification.

The studies were conducted either at the University Vision Center - CUV (Terrassa, Spain) and Hospital CIMA Sanitas (Barcelona, Spain) from April to September 2017 under the supervision of 3 ophthalmologists (J.C, S.S. and L.C.). After receiving a written and verbal explanation of the nature of the study, all patients provided written informed consent (Appendixes A and B) before any examination and ethical committee approval was obtained (Appendix C). The Declaration of Helsinki tenets of 1975 (as revised in Tokyo in 2004) were followed throughout the study.

5.1.2 Cataract classification, corneal diagnostic and scattering measurement protocol

All patients underwent a detailed ophthalmologic and optometric examination. Cataracts were graded at the slit lamp, and the pupil was dilated by instilling 0.2 ml of tropicamide 1.0%. Only eyes with a low to moderate grade of nuclear and predominantly nuclear cataract in the LOCS III classification system were included: from NO1 to NO3 (nuclear opalescence) and from C1 to C2 (cortical cataracts) or P1 to P2 (posterior subcapsular cataracts).

After a detailed slit lamp examination, patients were either diagnosed as having a CD such as ephitelial disruption (keratitis) or a superficial, stromal or posterior corneal dystrophy (cornea Verticillata and Fuchs dystrophy). Patients undergoing Femto-LASIK surgery were also carefully checked at the slit lamp. In any case, post-LASIK patients with any loss of corneal transparency (haze), inflammation etc. were finally selected for the CD group.

In all cases, the protocol throughout the study included the assessment of the intraocular scattering by the HD Analyzer, C-Quant straylight meter, the Purkinje clinical prototype developed in this thesis and, finally, the Pentacam Scheimpflug camera.

Measurements were performed in a dark room by trained optometrists and technicians. Firstly, we used the HD Analyzer to measure the OSI value. In this case, measurements were done without pupil's dilation and using a diameter of 4.0 mm. Because optical quality might be dependent on the tear film quality, measurements were taken just after a blink. The spherical refractive error was automatically corrected by the DP system (from -8.00 to +6.00 D with an accuracy of 0.125 D), whereas astigmatism was corrected with an external cylindrical lens (with an accuracy of 0.25 D) to obtain the best possible retinal image. We did three consecutive measurements and the reported OSI value is the average of these individual measurements. DP measurements of patients with a pupil diameter smaller than 4 mm were not considered in the analysis.

The protocol also included the assessment of the straylight in terms of Log(S) measured with the C-Quant instrument. This test also gives an assessment of the reliability of the test outcome, specified as the expected standard deviation (SD) and Q value, which is a further quality criterion. According to the manual of the instrument, if the expected SD is less than 0.08 and Q is more than 1, the reliability of the result is considered good. If the expected SD is less than 0.08 and Q is more than 0.5, the reliability is considered acceptable. A warning is given if the expected SD is more than 0.08 or Q is less than 0.5. Eyes with outcomes fulfilling this last condition were excluded from this study.

Patient's pupil was then dilated with 0.2 ml of 1% tropicamide. After dilation, we acquired the Purkinje images with our clinical prototype. The patients were asked to put the head on the chinrest while looking at the blue light of the fixation target (FT). To ensure that the best focused image was obtained, a scanning process varying the distance between the system and the eye was carried out. The reported Purkinje contrasts for both the third and fourth Purkinje images (P3 and P4) are the average of the 3 images with the highest contrasts. Purkinje images affected by the eye lips were excluded.

Finally, densitometry using the Pentacam was also assessed in patients with cataracts, corneal disorders and of the control group. Pentacam is programmed to automatically locate the corneal apex and takes 25 images over different meridians of eye with a uniform blue light source. Grayscale unit (GSU) is used to indicate the densitometry output; the value ranges from 0 (minimum densitometry) to 100 (maximum densitometry). In the study of eyes with cataracts, the reported densitometry value is the highest densitometry value found in the lens after analyzing the 25 images registered in a single measurement. In the case of patients with CD, the reported densitometry is the highest corneal value. Corneal densitometries with a value of 100 are considered outliers and were not included in the statistical analysis to avoid biased results. Measurements were performed just after a patient's blink. In fact, Pentacam software detects if the patient blinks or the eye moves during the image acquisition.

5.1.3 Statistical analysis

The data were analyzed using the SPSS software for Windows (V.24.0. Armonk, NY: IBM Corp.). Comparisons were considered to be statistically significant for p values of less than 0.05. The Shapiro-Wilk test (for populations of less than 30) and the Kolmogorov-Smirnoff test (for populations of 30 or more) were used to evaluate the normal distribution of all variables. Descriptive data are shown as the mean ± standard deviation (SD) for normally distributed variables; the median and interquartile range (IQR) are given additionally for non-normally distributed variables.

The correlations of variables with age, i. e., contrast of Purkinje images (P3, P4), OSI, Log(S), and densitometry was analyzed using either Pearson's (r) or Spearman's (r_S) correlation coefficients for those

with normal and non-normal distributions, respectively. Agreement between pairs of variables was also studied using either Pearson's (r) or Spearman's (r_S) correlation coefficients.

An independent sample t-test was used to compare the mean values of the main outcome measures for eyes of the control group and with nuclear cataracts in terms of contrast of Purkinje images (P3, P4), OSI, Log(S), and densitometry. The same test was used to compare mean values of eyes with CD (or alternatively, with scatter-customized CLs) and the control group. In both cases, the Mann-Whitney U test was used alternatively for non-parametric variables.

An analysis of variance (ANOVA) test was also used to compare the mean values of the main outcome measures for eyes of the control group and with nuclear of different grades (LOCS III) (NO1, NO2 and NO3). For those variables that did not meet the criteria for normal distribution, the Kruskal-Wallis test was used to compare the data among subgroups. We carried out the same analysis to compare among naked eyes and eyes wearing scatter-customized CLs with different levels of scattering.

5.2   Results of healthy subjects, patients with cataracts and corneal disorders

5.2.1   Age dependence of scattering in healthy eyes

As a preliminary approach to understand how intraocular scattering changes with age in terms of the several tested variables, we carried out a first analysis considering only the 25 eyes of 25 healthy patients included in the control group. As explained above, subjects included in the control group were those with healthy eyes, without cataracts or CD, having therefore transparent cornea and lens. Of course, this does not mean that the eye is completely free of scattering, but that it is non-pathologic. The reported densitometry in this subsection corresponds to the highest value found in the lens as with age the transparency of the cornea is almost unaffected [110].

As a representative example of the technologies analyzed in this thesis, Figure 5.1 shows the Purkinje, Scheimpflug and DP images corresponding to an eye of a subject of the control group aged 30 years old.
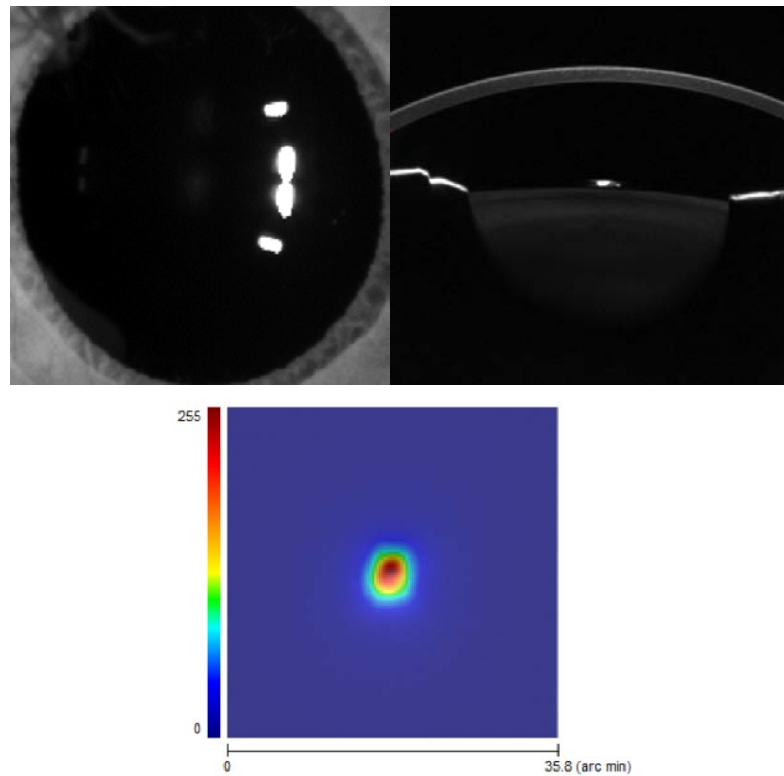
P3	P4	OSI	Log(S)	Densitometry
0.60	0.69	0.40	0.72	12.7

Figure 5.1. Purkinje (top left), Scheimpflug (top right) and DP (bottom) images of an eye of a healthy subject of the control group aged 30 years old. The specific values of the contrast of the Purkinje images (P3 and P4), OSI, Log(S) and densitometry are also given.

As a summary, patient demographics, manifest refraction as well as scattering variables are shown in Table 5.1. Sex distribution occurred with almost equal probability in the control group (48.0% male and 52.0% female). In this case, all scattering variables were normally distributed except the P3 contrast (p = 0.009), OSI (p = 0.014) and densitometry (p = 0.001).

Table 5.1. Sex and age distribution, subjective refraction, CDVA (Corrected Distance Visual Acuity) and scattering measurements in the control group: Purkinje contrasts (P3, P4), OSI, Log(S) and densitometry. The mean ± SD and the corresponding range (minimum and maximum values) are shown as well as the median and the interquartile range (IQR) for those variables non-normally distributed. The SD in terms of percentage is also given for variables related with scattering (SE: Spherical Equivalent; D: Diopters).

	Mean ± SD and range [min, max]	
Sex		
Male	12	
Female	13	
Age (years)	45.6 ± 11.63	[29 , 63]
Refraction (D)		
Sphere	-1.5 ± 2.7	[-7.5 , 2.25]
Cylinder	-0.5 ± 0.4	[-1.25 , 0]
SE	-1.8 ± 2.75	[-7.5 , 1.87]
CDVA	1.0 ± 0.00	[1.00 , 1.00]
P3	0.51 ± 0.09 (18%)	[0.35 , 0.60]
Median (IQR)	0.54 (0.17)	
P4	0.69 ± 0.03 (4%)	[0.62 , 0.74]
OSI	0.63 ± 0.34 (54%)	[0.20 , 1.67]
Median (IQR)	0.55 (0.43)	
Log(S)	0.98 ± 0.20 (20%)	[0.71 , 1.43]
Densitometry	14.23 ± 3.22 (22%)	[10.3 , 24.4]
Median (IQR)	12.57 (2.8)	

The results obtained in terms of OSI seem to be in good agreement with those published elsewhere; Martínez-Roda et al. [111] reported values of OSI of 0.55 ± 0.19 in patients within the decade between 41 and 50 years, which is slightly smaller than the value found in this study. In a posterior study [112], the same authors reported a mean OSI of 0.67 ± 0.18 for a control group of 10 eyes with a mean age of 58

years. However, in our study the variance linked to the OSI parameter is slightly larger (54%) than the values reported formerly. Anyway, values are below 1, which correspond to normal eyes with low amounts of scatter as established by other authors [76], [77].

A similar conclusion is reached in terms of Log(S). Martínez-Roda and colleagues found a Log(S) of 1.09 $\pm$ 0.08 in the control group of 10 eyes, which is actually similar to that reported here [111]. Similarly to OSI, the variance of Log(S) seems to be slightly larger (20%) in our population. A study of European drivers proposed a value of 1.4 in terms of Log(S) as a safety limit for driving, and this seems to be coherent with our findings, which are in fact much lower [113].

Regarding the results in terms of densitometry, in a first study [114] with 10 healthy patients (mean age: 22.90 $\pm$ 5.71 years), the authors found a mean densitometry of 9.0 $\pm$ 1.3. Another one [115] reported values of 9.70 $\pm$ 1.29 when 30 healthy patients were considered (mean age: 68.40 $\pm$ 9.07 years). However, in our study the mean value is of 14.23 $\pm$ 3.22.

Also from our results, the contrast of the third Purkinje image (P3) is linked to a slightly larger variance than the fourth one (P4). Interestingly, P4 is the variable with the smallest variability among the eyes included in this study (4%). This could possibly indicate that P3 is affected by other optical aspects rather that the sole contribution of the scattering of the anterior segment of the eye, since eyes with same amount of scattering can have different P3 contrast values.

Moreover, the averaged value of the P3 contrast seems to be less than that of the P4, as we have also seen in the measurements made at the laboratory (section 4.2). Regardless the fact that both Purkinje images are linked to similar levels of reflectance (around 30 times lower than P1) (see section 2.3 in the state of the art), the 3rd one is much larger so that the energy is more widespread leading to a smaller contrast value.

Figure 5.2 depicts scatterplots for all scattering parameters as a function of age. Additionally, Table 5.2 shows the correlations found between age and each variable in terms of the Pearson (r) and Spearman's (r_s) correlation coefficients for those with normal and non-normal distributions, respectively. There were statistically significant correlations between age and P4 ($r = -0.422$, $p = 0.045$), OSI ($r_s = 0.498$, $p = 0.013$), Log(S) ($r = 0.778$, $p < 0.001$) and densitometry ($r_s = 0.604$, $p = 0.001$). Only P3 contrast did not show a significant correlation with age ($r_s = -0.254$, $p > 0.05$).
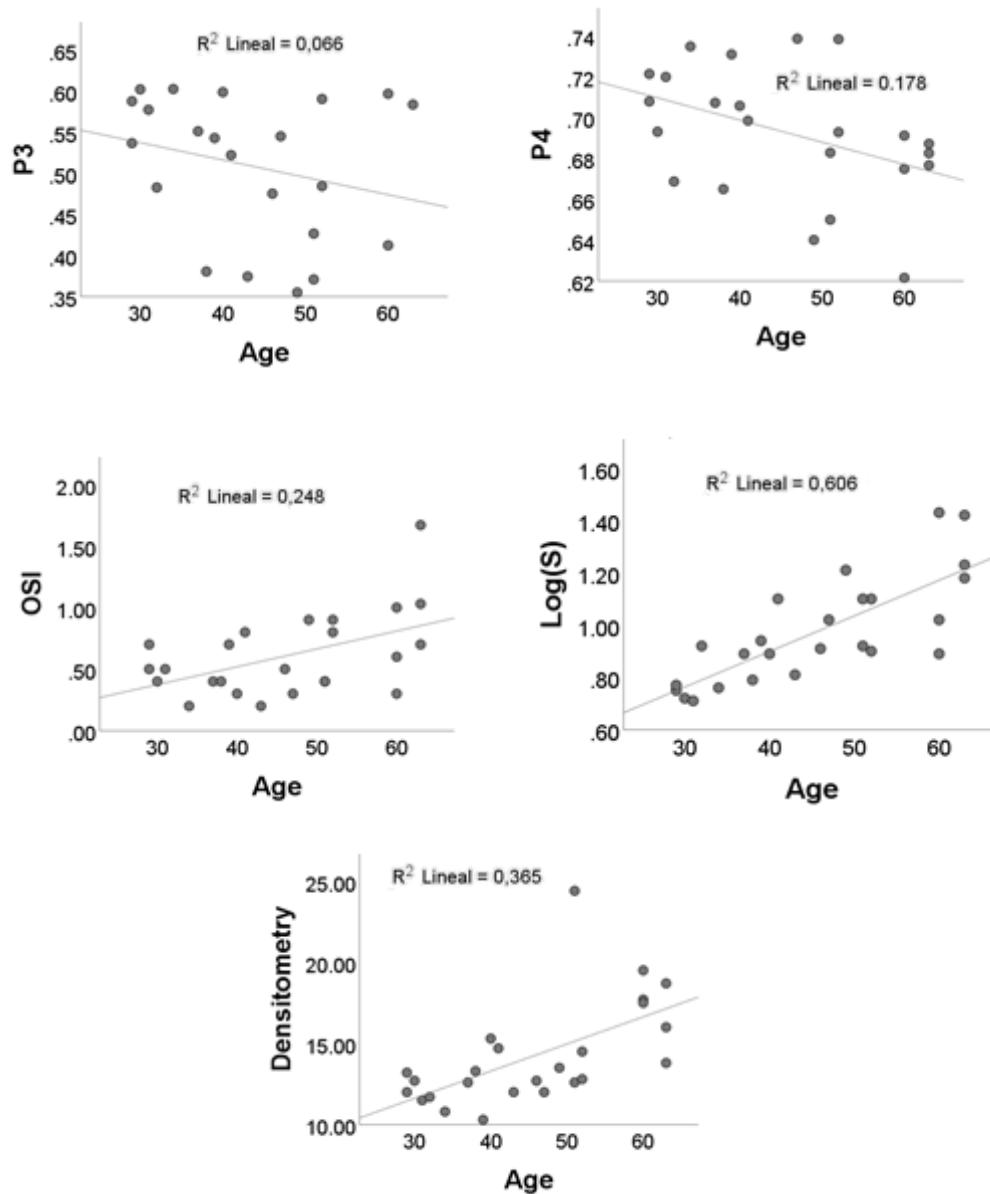
Figure 5.2. Scatterplots and corresponding linear regression (R^2) of the scattering variables as a function of age for the control eyes: Purkinje contrasts (P3, P4), OSI, Log(S) and densitometry.

Table 5.2. Pearson's† and Spearman's‡ correlation coefficients and corresponding significance (p-value) between age and scattering variables for the control eyes: Purkinje contrasts (P3, P4), OSI, Log(S) and densitometry.

		P3‡	P4†	OSI‡	Log(S) †	Densitometry‡
Age	Correlation (linear)	-.254	-.422	.442	.778	.677
	p-value (linear)	.253	.045*	.030*	<.001*	<.001*

*Statistically significant correlation.

With age, the cornea transparency is almost unaffected in the central area in absence of scar or degeneration [110] while, even in the absence of cataract, there is a steady increase in the overall light-scattering because of the lens. Studies [73], [75], [116] have used different methods to evaluate scattered light in the eye and have reported a rapid increase in forward scatter after the age of 45.

In the present study, we found significant correlations in terms of Log(S), densitometry and OSI vs. age. van den Berg et al. [10] also found that in noncataractous eyes straylight values increase strongly with age as: Log(S) = constant + log(1 + (age / 65)(4)), doubling by the age of 65 years, and tripling by the age of 77 years. Large-scale Scheimpflug studies (1040 eyes of 1685 individuals) have also revealed an exponential increase in light-scattering in the lens with age [109], in line with the findings of our study.

Additionally, Martínez-Roda et al. [111] reported a marked growth of scattered light in terms of OSI with age, with doubled values for the last decade considered (61 to 70 years) with respect to subjects aged from 31 to 40 years old. Saad et al. [12] also found that scattering increased with age when comparing OSI values of two control groups (<30 years old and >40 years).

One possible explanation for the stronger correlation found in terms of Log(S) is that it is also affected by sensory and perceptual factors. In fact, some authors have suggested that the optical deficits beyond 30 years of age are compensated during the first decades of adult life by means of sensory and perceptual factors, which through neural adaptation preserve visual function until the age of 50; and that beyond the age of 50 this compensation is less effective [111].

On the other hand, the outcomes of our study in terms of P4, which decreases with age, are in agreement with our initial hypothesis, suggesting that P4 is affected by the scattering of the lens apart from the preceding scattered light coming from the cornea and the aqueous humor. We also hypothesized that P3 contrast contains information about the scattering of the cornea and the aqueous humor. And the results found in healthy eyes seem to be in agreement with this as from Figure 5.2 it is evident that P3 contrast does not show a marked trend vs. age (the correlation is not significant). Accordingly, we can conclude that P3 does not include relevant information from the lens scattering, which is expected to increase with age [109].

This is slightly different to what we observed in the former chapter (see section 4.2), in which a P3 contrast compensation as a function of age was applied as a means of removing the likely impact of the roughness of the anterior lens surface on the contrast computation (orange peel effect). In fact, if data of healthy eyes are grouped in decades of age, a decline is not observed in terms of P3 contrast (Figure 5.3); moreover, there is a large variability within groups. We also represented P4 contrast grouped in decades of age, which shows an age dependency and, as previously commented, can be attributed to the loss of transparency of the human lens ageing.
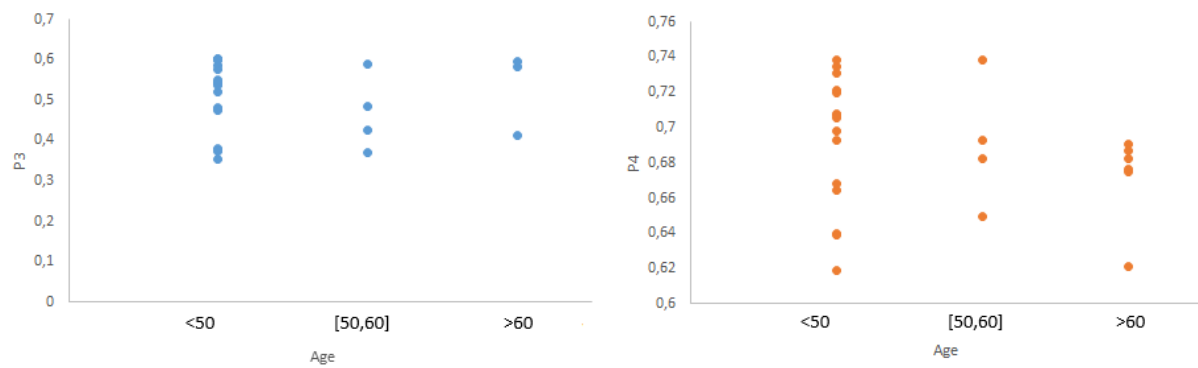
Figure 5.3. P3 (left) and P4 (right) contrasts as a function of age groups.

Bivariate correlations as well as the corresponding linear regression between pairs of variables used to assess intraocular scattering are shown in Figure 5.4 as well as in Table 5.3.

The results indicate that there is a significant correlation between densitometry and P4 ($r_s = -0.611$, p = 0.002), densitometry and Log(S) ($r_s = 0.571$, p = 0.003), and between OSI and Log(S) ($r_s = 0.450$, p = 0.027).

Interestingly, P3 contrast does not correlate significantly with any other variable (p > 0.05). Only P3 and P4 contrasts share approximately 22% of information about intraocular scattering if one takes into account the coefficient of determination (R^2) shown in Figure 5.4. From the assumption that P3 is mainly influenced by scattering coming from the cornea while P4 is also influenced from that of the lens, it could be therefore inferred that, at least in healthy patients, about 22% of the intraocular scattering has a different origin rather than scattering from the lens.

On the other hand, the P4 contrast correlates significantly with densitometry (p = 0.002). Note that densitometry - at least in the way that we measured it - is only associated with lens opacities. However, no correlation was found between P3 contrast and densitometry (p > 0.05). These statistical results support again the hypothesis that P3 does not include the lens scattering while P4 does.

The fact that OSI correlates with Log(S) and not with densitometry could be explained if one considers that both account for forward scattering as several authors have previously pointed out [76], [111], [112], while densitometry would be more affected by the lens back-scattering, similarly to slit-lamp observations.
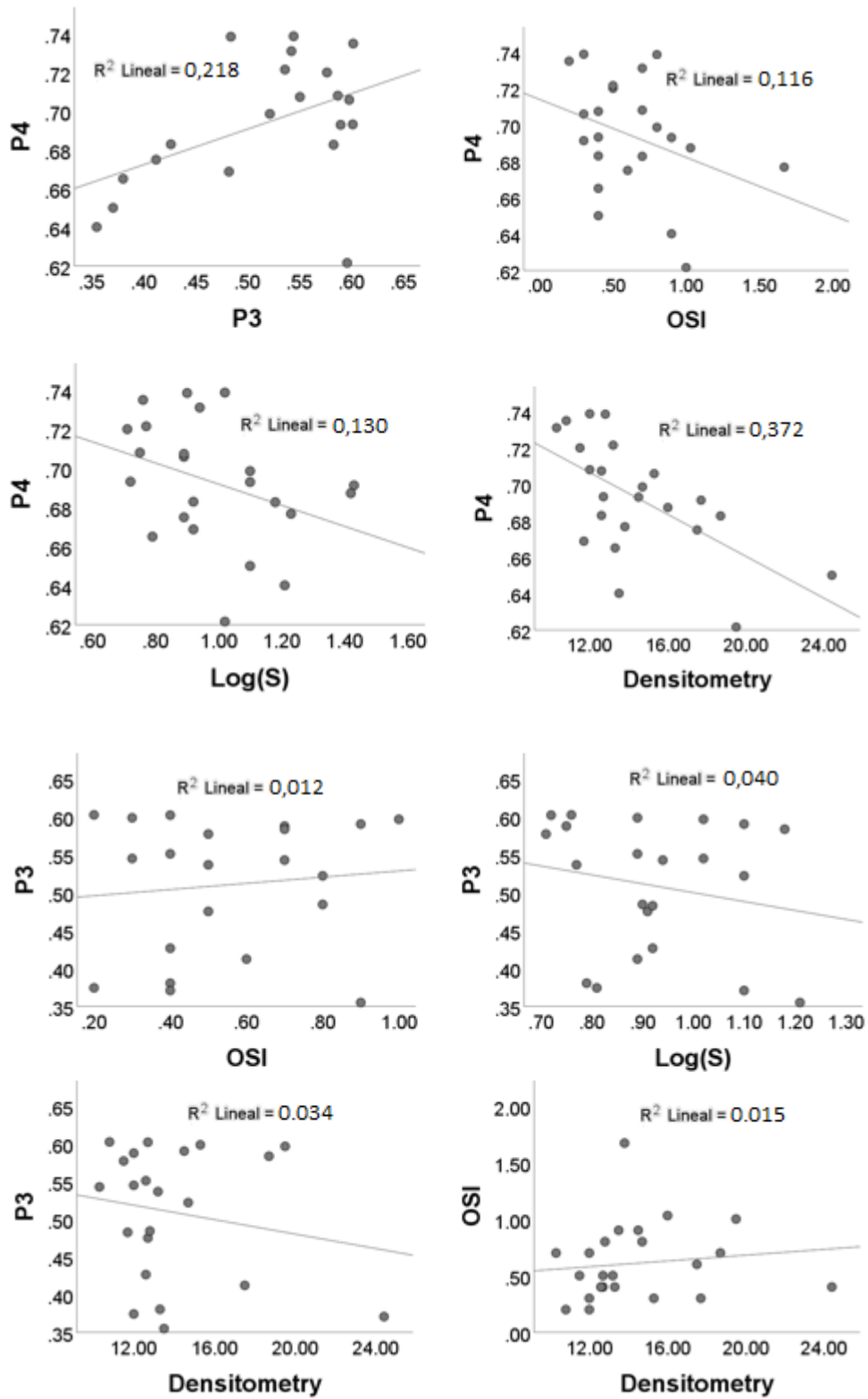
Figure 5.4. Scatterplots and corresponding linear regression (R^2) of the scattering variables as a function of age for the control eyes: Purkinje contrasts (P3, P4), OSI, Log(S) and densitometry.

Table 5.3. Pearson† and Spearman's‡ correlation coefficients and corresponding significance (p-value) between scattering variables.

	P3	P4	OSI	Log(S)	Densitometry
P3	-				
P4	.376(.102)‡	-			
OSI	-.025(.915)‡	-.341(.120) ‡	-		
Log(S)	-.288(.193)‡	-.360(.091) †	.450(.027)* ‡	-	
Densitometry	-.132(.559)‡	-.611(.002)*‡	.339(.105)‡	.571(.003)*‡	-

*Statistically significant correlation.

5.2.2   Analysis of scattering in eyes with cataracts

Figures 5.5, 5.6 and 5.7 show representative examples of the Purkinje, Scheimpflug and DP images corresponding to cataracts graded as NO1, NO2, and NO3, respectively.
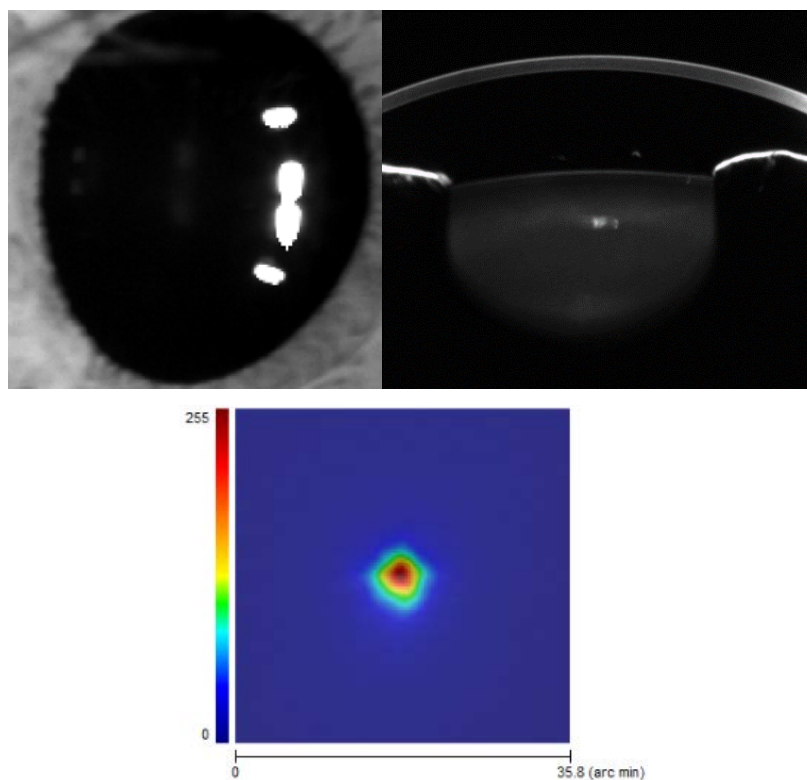
P3	P4	OSI	Log(S)	Densitometry
0.39	0.64	0.97	0.99	17.1

Figure 5.5. Purkinje (top left), Scheimpflug (top right) and DP (bottom) images of a cataract graded as NO1 of a subject aged 58 years old. The specific values of the contrast of the Purkinje images (P3 and P4), OSI, Log(S) and densitometry are also given.
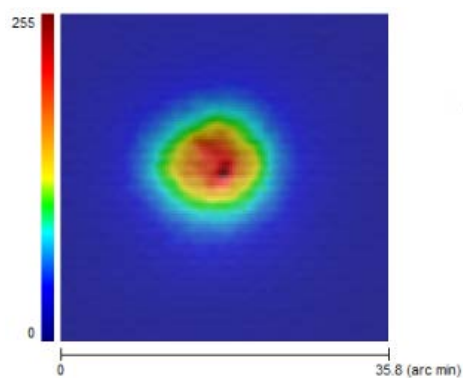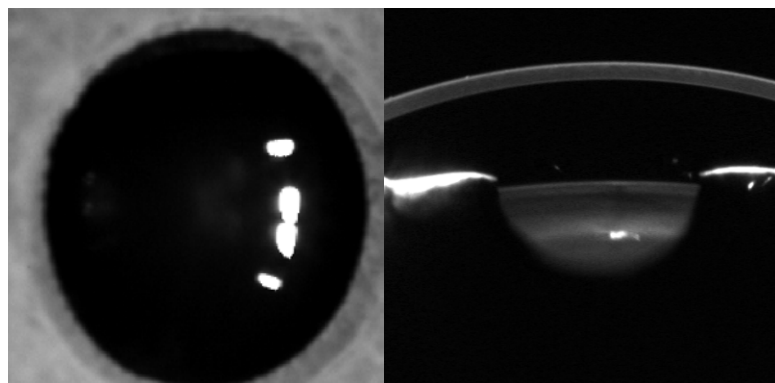
P3	P4	OSI	Log(S)	Densitometry
0.28	0.59	2.30	1.20	21.7

Figure 5.6. Purkinje (top left), Scheimpflug (top right) and DP (bottom) images of a cataract graded as NO2 of a subject aged 67 years old. The specific values of the contrast of the Purkinje images (P3 and P4), OSI, Log(S) and densitometry are also given.
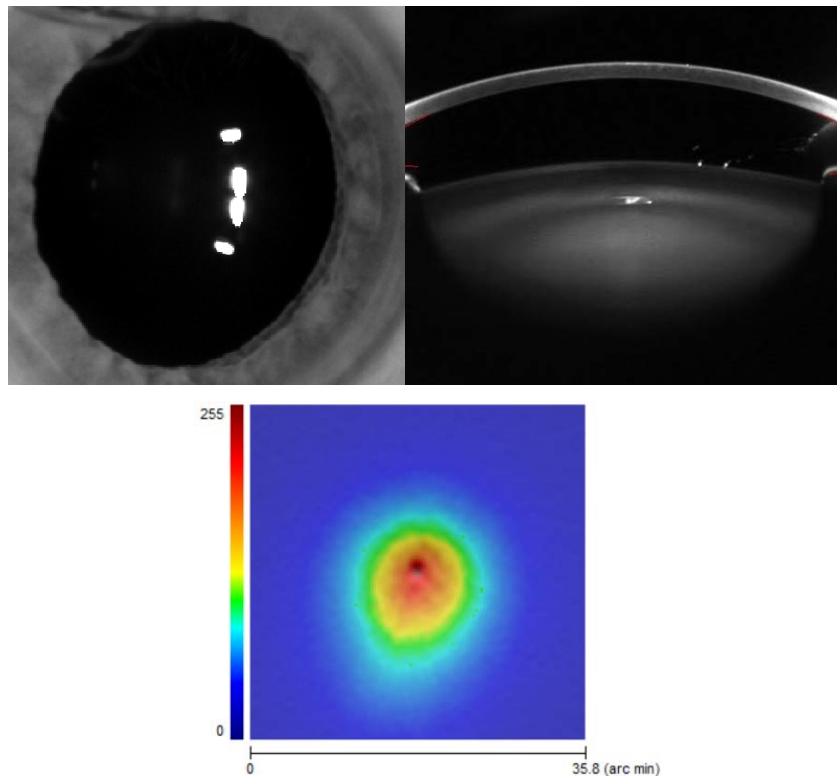
P3	P4	OSI	Log(S)	Densitometry
0.22	0.56	2.90	1.51	24.1

Figure 5.7. Purkinje (top left), Scheimpflug (top right) and DP (bottom) images of a cataract graded as NO3 of a subject aged 63 years old. The specific values of the contrast of the Purkinje images (P3 and P4), OSI, Log(S) and densitometry are also given.

Table 5.4 summarizes the patients' demographics as well as the subjective refraction, CDVA and scattering parameters for the cataract group. Data for the control group is provided again for comparison purposes. Scattering values found using each of the tested techniques are also provided. Sex distribution of the whole cohort was: 40.8% male and 59.2% female. Age distribution and results as a function of the cataract severity determined by means of the LOCS III classification system are summarized in Table 5.5.

In this case, all scattering variables were normally distributed except OSI ($p = 0.001$) and densitometry ($p = 0.008$).

Table 5.4. Sex and age distribution, subjective refraction, CDVA (Corrected Distance Visual Acuity) and scattering measurements in the cataract and control groups: Purkinje contrasts (P3, P4), OSI, Log(S) and densitometry. The mean ± SD and the corresponding range (minimum, maximum) are shown as well as the median (IQR) for those variables non-normally distributed.

	Mean ± SD and range [min, max]	
	Cataract Group	**Control Group**
Sex		
Male	17	12
Female	29	13
Age	56.4 ± 10.0 [24 , 69]	45.6 ± 11.6 [29 , 63]
Refraction [D]		
Sphere	0.3 ± 3.0 [-7.0 , 5.5]	-1.5 ± 2.7 [-7.5 , 2.5]
Cylinder	-0.8 ± 0.6 [-2.5 , 0]	-0.5 ± 0.4 [-1.25 , 0]
SE	-0.1 ± 3.0 [-7.6 , 4,6]	-1.8 ± 2.8 [-6.75 , 1.9]
CDVA	0.98 ± 0.19 [0.40 , 1.00]	1.00 ± 0.00 [1.00 , 1.00]
P3	0.38 ± 0.12 [0.16 , 0.69]	0.52 ± 0.08 [0.35 , 0.60]
P4	0.60 ± 0.07 [0.45 , 0.74]	0.69 ± 0.03 [0.62 , 0.74]
OSI	1.36 ± 0.70 [0.50 , 2.90]	0.61 ± 0.27 [0.20 , 1.20]
Median (IQR)	1.15 (0.90)	0.55 (0.40)
Log(S)	1.24 ± 0.24 [0.82 , 1.59]	0.93 ± 0.15 [0.71 , 1.21]
Densitometry	18.28 ± 3.96 [12.60 , 25.90]	14.01 ± 3.33 [10.30 , 24.40]
Median (IQR)	17.05 (5.95)	13.20 (3.65)

Table 5.5. Age distribution, CDVA (Corrected Distance Visual Acuity) and scattering measurements by grade of cataract NO (LOCS III classification): Purkinje contrasts (P3, P4), OSI, Log(S) and densitometry. The mean ± SD and the corresponding range (minimum, maximum) are shown as well as the median (IQR) for those variables non-normally distributed.

	Mean ± SD		
	Range [min, max]		
	Cataract Group (NO)		
LOCS III	**1**	**2**	**3**
Age	52.95 ± 11.94	56.3 ± 7.7	66.0 ± 2.9
	[24 , 61]	[44 , 67]	[63 , 69]
CDVA	0.99 ± 0.00	1.00 ± 0.00	0.91 ± 0.21
	[0.90 , 1.00]	[1.00 , 1.00]	[0.40 , 1.00]
P3	0.41 ± 0.14	0.37 ± 0.08	0.31 ± 0.08
	[0.16 , 0.69]	[0.23 , 0.52]	[0.22 , 0.40]
P4	0.62 ± 0.05	0.63 ± 0.09	0.57 ± 0.03
	[0.51 , 0.70]	[0.47 , 0.74]	[0.53 , 0.60]
OSI	1.00 ± 0.36	1.39 ± 0.61	2.40 ± 0.66
	[0.50 , 1.80]	[0.50 , 2.30]	[1.50 , 2.90]
Median (IQR)	0.90 (0.53)	1.20 (1.07)	2.60 (1.20)
Log(S)	1.22 ± 0.25	1.15 ± 0.19	1.34 ± 0.24
	[0.82 , 1.59]	[0.83 , 1.36]	[1.06 , 1.56]
Densitometry	17.32 ± 3.81	17.87 ± 4.12	20.38 ± 2.60
	[12.60 , 25.00]	[13.90 , 25.90]	[18.10 , 24.10]
Median (IQR)	16.35 (5.63)	16.10 (6.60)	19.65 (4.68)

In view of the results, it is interesting to note that in general all scattering parameters are in agreement with the LOCS III grade (NO). In the same way, CDVA decreases as the cataract grade increases. Surprisingly,

the mean CDVA of group NO2 (1.00) is slightly higher than that of NO1 (0.99). In fact, visual acuity is very similar among all groups of patients. It is also relevant that in terms of Log(S), the averaged value for NO2 (1.15) is slightly lower than that of NO1 (1.22). Similarly, both groups show very similar outcomes in terms of P4 and densitometry.

In a study by Artal et al. [4], the OSI was compared with the LOCS III in 53 eyes, 15 belonging to a group of healthy young subjects (28±5 years) while the others (38) corresponded to patients with diagnosed nuclear cataracts (73±7 years). In their study, the authors reported that healthy eyes have a small OSI value, typically below 1. However, the OSI for cataract groups was of 3.0 (NO2), 6 (NO3) and 9 (NO4) , respectively, from which they established a classification of eyes with different degrees of scattering based on the OSI: OSI below 1 correspond to normal eyes with low amounts of scatter, between 1 and 3 to older eyes with associated scatter of an early cataract, between 3 and 7 to developed cataracts that should undergo surgery, and higher than 7 to eyes with severe cataracts. Later, Vilaseca et al. [77] reported mean OSI values of 2.24, 3.82, and 5.74 in 123 eyes with nuclear cataracts classified as NO1, NO2 and NO3, respectively. While for eyes of the control group (117), OSI was on average lower than 1, too.

From the results found in our study, it is obvious that eyes of the control group are also linked to OSI values below 1; nevertheless, the values for eyes with cataracts are much below than those reported previously: 1.00 (NO1), 1.39 (NO2) and 2.40 (NO3). In a similar way, in our study CDVA values are also higher - 0.99 (NO1), 1.00 (NO2) and 0.91 (NO3) - than those reported by Vilaseca and coworkers (0.81, 0.53 and 0.31), meaning that ophthalmologists that graded cataracts in both studies probably had slightly different criteria.

As we anticipated in the state of the art, slit lamp gradation is linked to subjective criteria from the examiner, even when comparing with the standards of the LOCS III classification system. In fact, authors have analyzed the reliability of this test when different observers are involved in the comparison and have found that results may show variability [117]. This highlights the need to look for alternative and more reliable methods to clinically grade cataracts.

The same reasoning is valid when comparing our findings in terms of Log(S) (0.93 in healthy eyes vs. 1.24 in cataracts) with those published for the C-Quant instrument. Bal et al. [113] measured the straylight of 97 eyes with cataracts (Log(S) = 1.66) and 38 cataract-free eyes from healthy subjects (Log(S) = 1.24) and found significant differences between them (p < 0.001). In the same study, a limit for safety driving was established at Log(S) = 1.4, while we have reported a mean Log(S) of 1.24 for the whole cataract group, which is much below. This is again in line with the criteria used by ophthalmologists, much more restrictive in our study.

On the other hand, our measured densitometry values in eyes graded as NO1 and NO2 are slightly higher than those previously reported, similarly to what was found in eyes of the control group in the previous section. In fact, Pei et al. [115] reported a mean densitometry of 9.7 for healthy eyes, 10.5 for NO1, 14.1

for NO2 while we found values of 14.31, 17.32 and 17.87, respectively. Nevertheless, very similar values for cataracts graded as NO3 were reported in both studies (20.7 vs 20.38). As we already did with healthy eyes in the former section, the relationship between age and intraocular scattering was analyzed when eyes with cataracts were also included in the analysis (Figure 5.8 and Table 5.6).
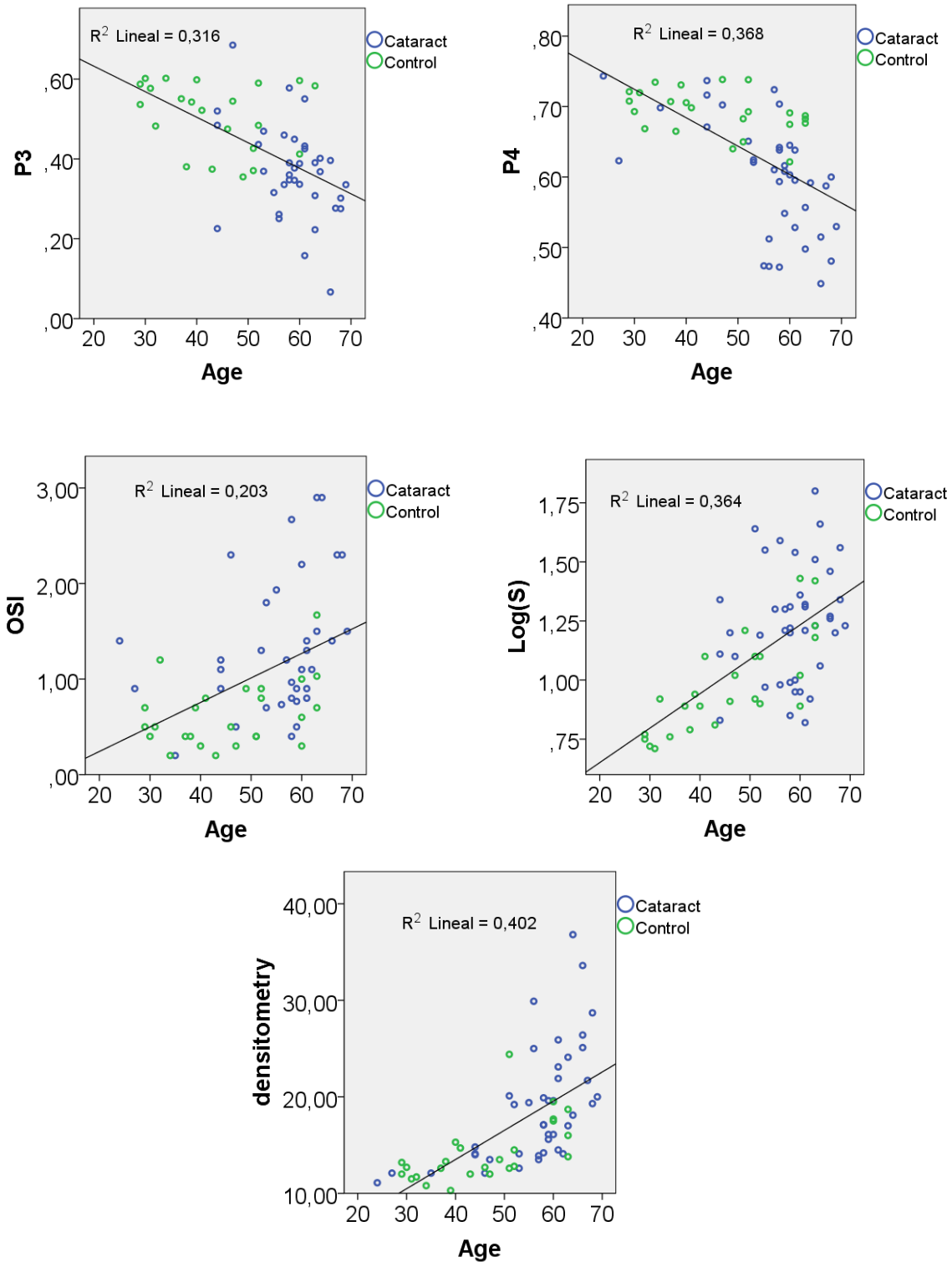
Figure 5.8. Scatterplots and corresponding linear regression (R^2) of the scattering variables as a function of age for the control eyes (in green) and with cataracts (blue): Purkinje contrasts (P3, P4), OSI, Log(S) and densitometry.

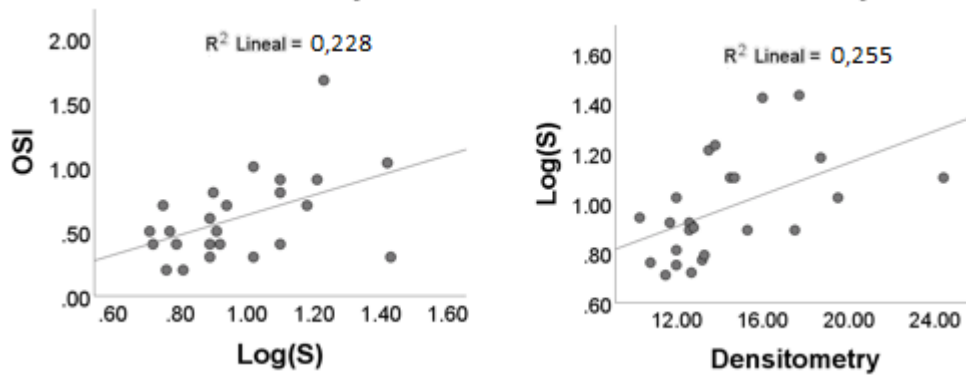**Table 5.6.** Pearson's‡ and Spearman's† correlation coefficients and corresponding significance (p-value) between age and measured variables: Purkinje contrasts (P3, P4), OSI, Log(S) and densitometry.

		P3‡	P4‡	OSI†	Log(S) ‡	Densitometry†
Age	Correlation (Linear)	-.562	-.602	.551	.603	.759
	p-value (Linear)	<.001*	<.001*	<.001*	<.001*	<.001*

As expected, there were significant correlations between all parameters and age. In the former section, we did not find a significant correlation between P3 contrast and age in healthy eyes. Accordingly, we concluded that P3 did not include relevant information from the lens scattering, which is expected to increase with age indeed. However, when analyzing together the control group and eyes with cataracts, a correlation between age and P3 contrast is found ($r = -0.562$, $p < 0.001$). Therefore, this result indicates that, unexpectedly, cataracts can have a certain influence on the P3 contrast.

Coming back to Figure 5.8, it can be seen that even the continuous growing tendency of scattering with age, beyond the 50s the data clouds appear to be more widespread in terms of all variables. Thus, for cataractous patients of the same age, we found a larger variability in terms of measured scattering. This change of data distribution occurs at the age where the risk of cataract formation starts [118], [119]; and, of course, not all patients have the same development of the cataract with age.

Figure 5.9 shows the boxplots of the measured intraocular scattering as a function of cataract severity (LOCS III). As it can be seen, we found agreement between cataract grade and any of the techniques used in this clinical study to account for scattering.
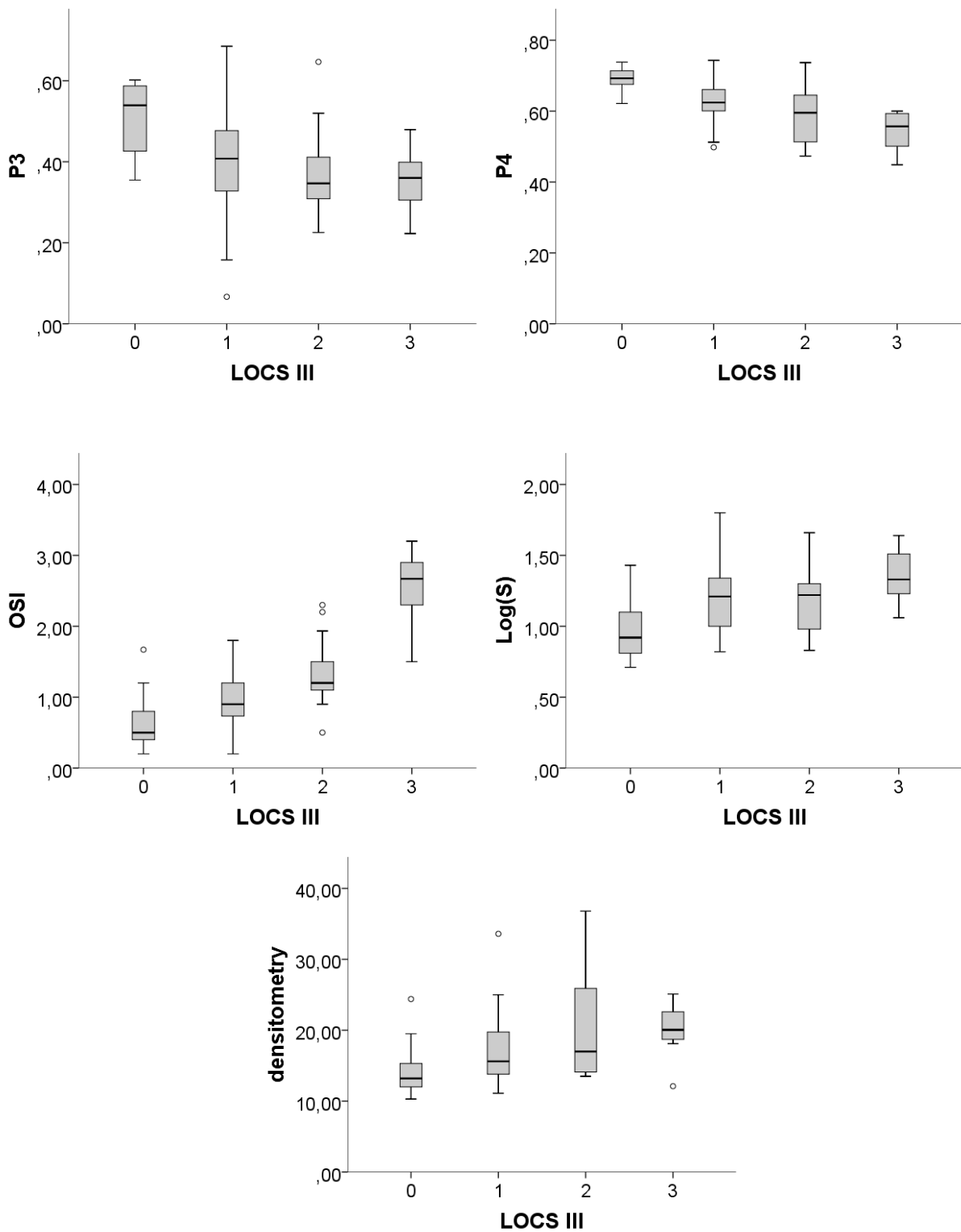
Figure 5.9. Boxplots showing each scattering parameter as a function of the LOCS III classification (NO1, NO2, and NO3) and the control group (0). Five statistical descriptors are shown in these plots: maximum, third quartile, median, first quartile and minimum as well as the outliers.

The t-test for parametric data and the Mann-Whitney test for the non-normal distributed data confirmed that there were statistically significant differences between eyes of the control and cataract groups in terms of any of the parameters analyzed (Table 5.7).

Table 5.7. Results of the t-test and Mann-Whitney test to account for differences between eyes of the control group and with nuclear cataracts in terms of contrast of Purkinje images (P3, P4), OSI, Log(S), and densitometry.

	T-test t[†] (Mann-Whitney z[‡])	p-value
P3	4.298[†]	<.001*
P4	5.346[†]	<.001*
OSI	-4,450[‡]	<.001*
Log(S)	-4.703[†]	<.001*
Densitometry	-3,827[‡]	<.001*

*Statistically significant differences.

Posteriorly, an ANOVA test for normal distributed data, and the Kruskal-Wallis test for the non-normally distributed, confirmed that there were statistically significant differences among the LOCS III groups (NO1, NO2 and NO3) (p<0.05) for all parameters analyzed (Table 5.8). Again, significant differences were also found in terms of P3 contrast (p = 0.001). As we anticipated when analyzing the age dependence, these results suggest that P3 is affected to some extent by cataracts.

Table 5.8. Results of the ANOVA and Kruskal-Wallis tests to account for differences among eyes of the control group and with nuclear cataracts graded as NO1, NO2, and NO3 (LOCS III) in terms of contrast of Purkinje images (P3, P4), OSI, Log(S), and densitometry.

	ANOVA F[†] (Kruskal-Wallis H[‡])	p-value
P3	6.290[†]	.001*
P4	13.227[†]	<.001*
OSI	31.946[‡]	<.001*
Log(S)	8.941[†]	<.001*
Densitometry	17.172[‡]	.001*

*Statistically significant differences.

Again, these results are in agreement with other studies that have previously demonstrated the correspondence between the outcomes of the commercial techniques that account for intraocular scattering and the LOCS III classification system.

As already commented, in the study by Artal et al. [4], the OSI was compared with the LOCS III in 53 eyes, 15 belonging to a group of healthy young subjects while the others (38) corresponded to patients with diagnosed nuclear cataracts and found that the correlation of the cataract gradation between OSI and LOCS III was significant. Vilaseca et al. [5] in a study with 188 eyes, including nuclear, cortical and subcapsular cataracts, also found that OSI for eyes of the control group was on average lower than 1, whereas this parameter was higher when the LOCS III cataract gradation increased.

Studies comparing Log(S) and LOCS III have also found agreement between those techniques. These parameters have been compared in 97 cataractous eyes and 38 cataract-free control subjects, where the Mann-Whitney Test revealed that straylight was significantly increased in the cataract group relative to the control group ($p<0.01$) [113]. Another study including 53 eyes with cataract and 9 young volunteers concluded that straylight differed by a statistically significant amount among different LOCS III groups ($p<0.05$) [84].

Domínguez-Vicent et al. [120] showed a positive and significant correlation ($p<0.05$) between Scheimpflug densitometry and LOCS III in a study where 95 eyes with nuclear (50) and cortical (45) cataracts were also included as well as 35 eyes without cataract as control group.

Similarly to the former section, we analyzed the existing correlations between pairs of techniques when dealing with healthy eyes and with cataracts (Figure 5.10 and Table 5.9).
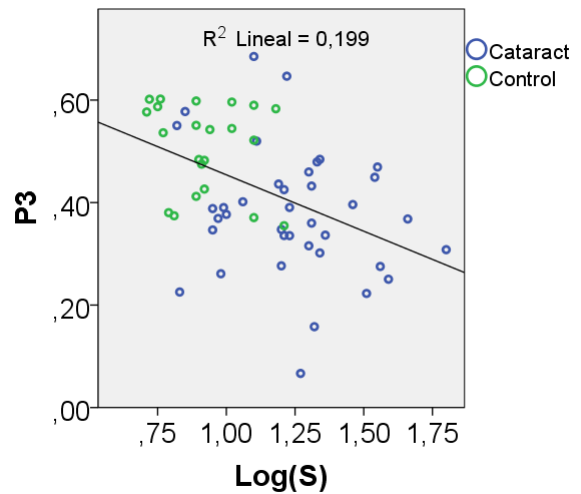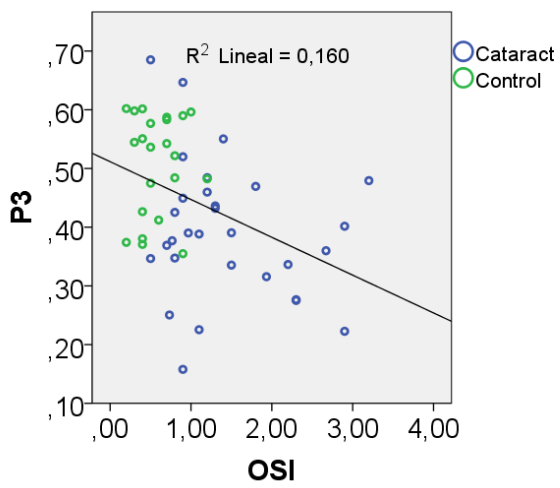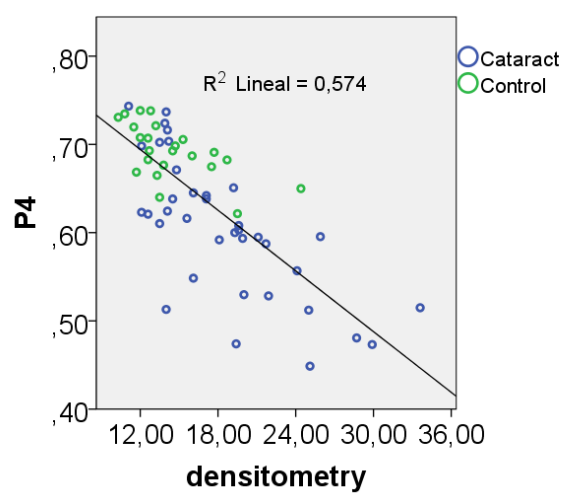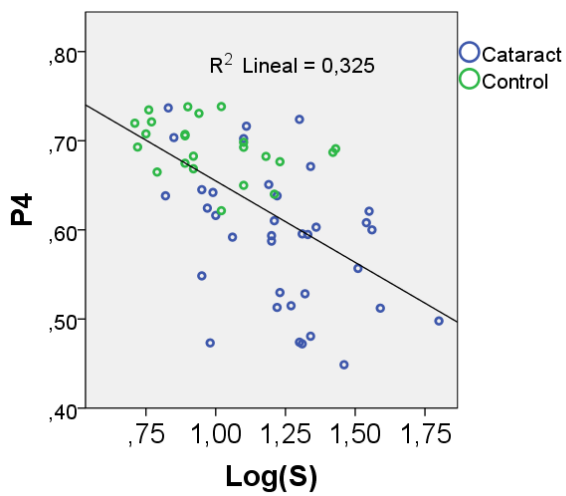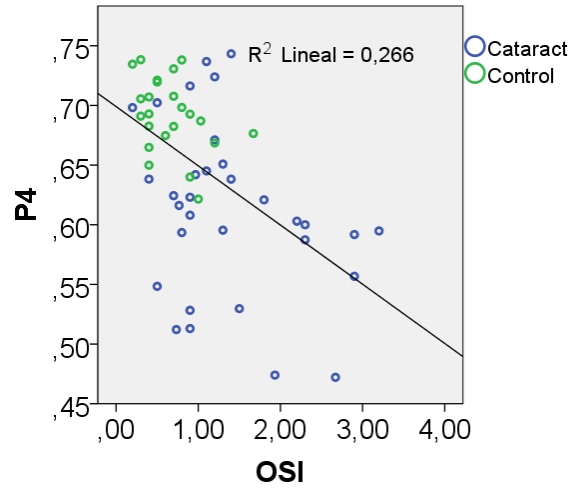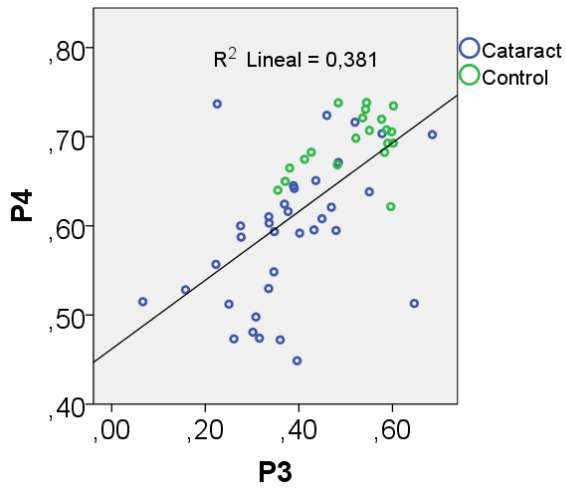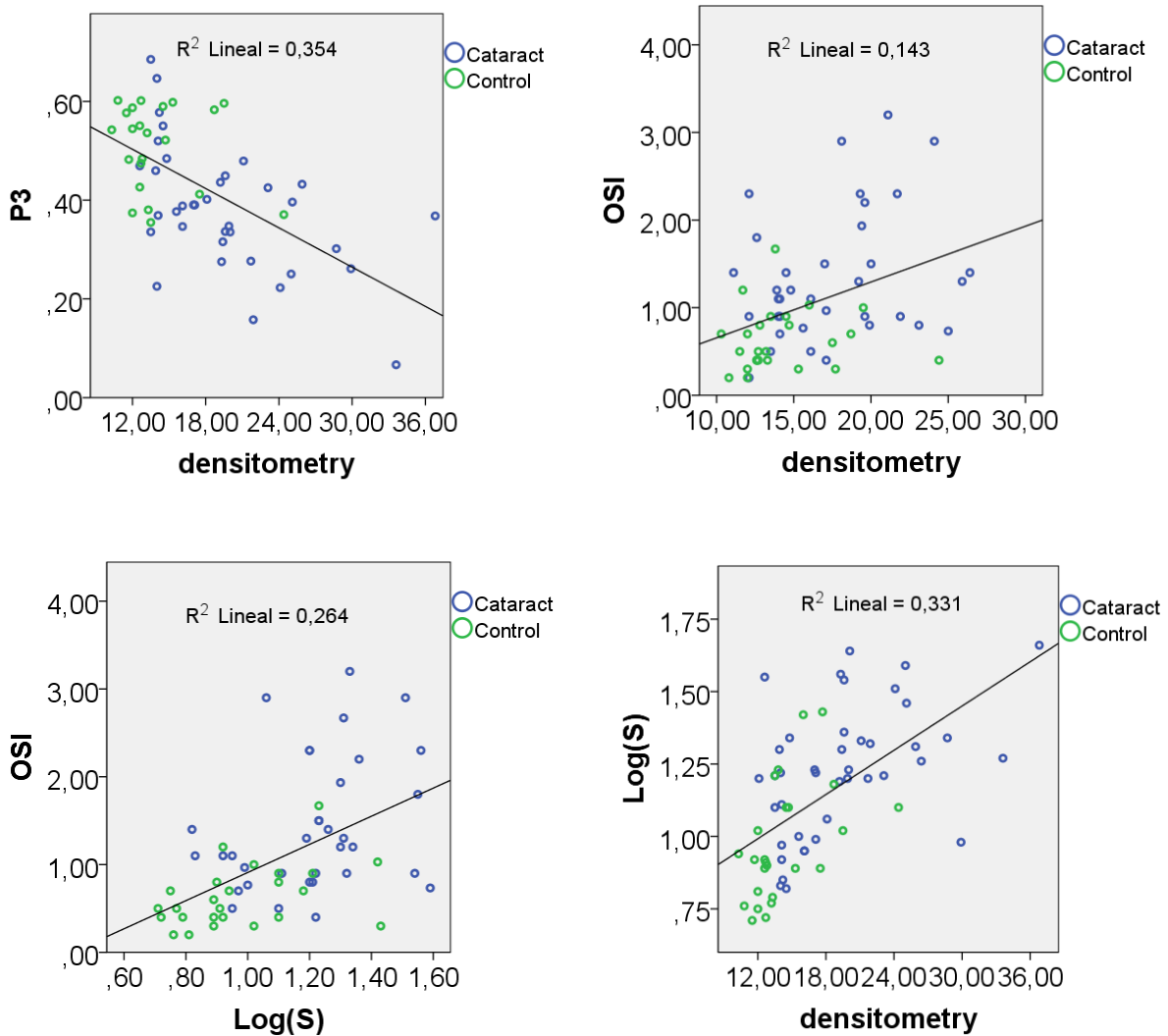
Figure 5.10. Scatterplots and corresponding linear regression (R^2) of the scattering variables for the control eyes (green) and with cataracts (blue): Purkinje contrasts (P3, P4), OSI, Log(S) and densitometry.

Table 5.9. Pearson's† and Spearman's‡ correlation coefficients and corresponding significance (p-value) between intraocular scattering parameters.

	P3	P4	OSI	Log(S)	Densitometry
P3	-				
P4	.617† (<.001)*	-			
OSI	-.403‡ (.003)*	-.504‡ (<.001)*	-		
Log(S)	-.446† (<.001)*	-.570† (<.001)*	.577‡ (<.001)*	-	
Densitometry	-.575‡ (<.001)*	-.719‡ (<.001)*	.413‡ (.001)*	.632‡ (<.001)*	-

*Statistically significant correlation.

Both Purkinje contrasts (P3 and P4) as well as OSI, Log(S) and densitometry significantly correlated between each other (p<0.05). It should be reminded that P3 contrast did not correlate with any other variable when only healthy eyes were considered; even though it is also worth noting that all correlations in terms of P3 contrast were weaker than in terms of P4 contrast.

When analyzing the outcomes of the commercial systems involved in the study, the weakest correlation was found between OSI and Scheimpflug densitometry (r = 0.413, p = 0.001). This disparity could be explained by the differences between methods. OSI is computed for a pupil diameter of 4 mm as a whole. On the contrary, Scheimpflug densitometry can be influenced by local lens opacities; additionally, the systems do not use the same wavelength (NIR vs. blue), and in some cases where eyes are greatly affected by higher order aberrations, OSI could be abnormally increased; OSI is actually computed as the ratio between the amount of light recorded inside an annular area between 12' and 20' and that recorded closer to the peak, specifically in a circular area of a radius of 1' from the central peak. Therefore, it is susceptible to artefacts related to the effect of aberrations, mainly higher order ones as defocus and astigmatism are corrected to perform the measurement with the DP system. Finally, the DP technique is related with forward scattering while Scheimpflug densitometry mainly accounts for backscattered light. As some researchers have already discussed [46], the behavior of back and forward scattering is somehow related but one cannot be derived from the other [121], [122].

Lim et al. [123] conducted a study including 70 eyes with age-related nuclear cataract and compared the objective assessment of lens density with the DP (OSI) and the Pentacam Scheimpflug camera. They reported that OSI correlated with the Scheimpflug-measured lens density (r =0 .764, p < 0.01), which is indeed a larger value than the one found in our study. However, they just included eyes with mature cataracts (LOCS III ≥ 1) and probably this resulted in the higher correlation. On the contrary, Crnej et al. [124] also compared OSI and densitometry in eyes with cataracts, reporting a lower correlation than the one found in this thesis (r = 0.32, p = 0.024). The study included 56 eyes of patients (mean age: 71 years) that had predominantly nuclear sclerotic (15), cortical (13), posterior subcapsular (11) and mixed cataracts (15).

Comparisons between OSI and Log(S) have been published previously. In a study with 78 cataractous eyes (including nuclear, cortical and posterior subcapsular cataracts) and 10 healthy eyes, Martinez-Roda and colleagues [112] found a correlation of r = 0.66, which is pretty similar to our results (r = 0.577, p < 0.001). Surprisingly, different values were published in the study carried by Crnej et al. [124] in which the authors did not find a good correlation between the 2 forward light-scatter measurements. These authors showed that the OSI values were relatively low for cortical cataracts because the center of the crystalline lens is clear, being opaque in the periphery only.

As pointed out by Barrionuevo et al. [104], who measured straylight and PSFs in 10 young subjects with an uncorrected visual acuity (UDVA) of at least 20/20, the lack of correlation could be explained by the

differences in the principle of operation of both systems. The C-Quant straylight meter is a psychophysical method that involves the optical aspects for assessment, the posterior neural processing, and the response criterion. The DP technique is a physical measurement. Furthermore, each system measures a different angle of light scatter. The straylight meter measures a 5º to 10º angle from the visual axis, and the PSF measurement angle is much below 1º as commented formerly. Another possible reason for the difference between the devices is that the DP method uses NIR light, which is partially absorbed in the retina [125],[126].

Overall, despite the slightly differences between methods, all them seem to be useful for cataract diagnosis as they are in rather agreement with the LOCS III classification. All them showed significant differences between healthy eyes and those with cataracts. Moreover, statistically significant differences were also reported among subgroups of cataracts, that is, from different grades.

On the other hand, it is also remarkable that the Purkinje system, and especially P4, does not take into account the contribution in scattering of the posterior segment of the eye (i. e., vitreous and retina) while the OSI can be affected by the retinal scattering and also by that coming from deeper layers as the choroid [126], [90].

Regarding the hypothesis that P3 provides information of the cornea and the aqueous humor, without including the lens contribution, our data suggest that the P3 contrast is affected to some extend by lens scattering. However, the correlations of P3 contrast with OSI, Log(S) and lens densitometry are weaker than those found in terms of P4 contrast, meaning that P3 is less dependent on lens scattering than P4.

From a qualitative point of view, the detailed analysis of our Purkinje images in eyes with cataracts also reveal that in some cases a ghost image appears between P3 and P4; in some cases it overlaps with P3 affecting the P3 contrast computation (Figure 5.11). Therefore, the ghost image could explain the fact that cataracts affect the P3 contrast, although it was expected to be independent of lens scattering.
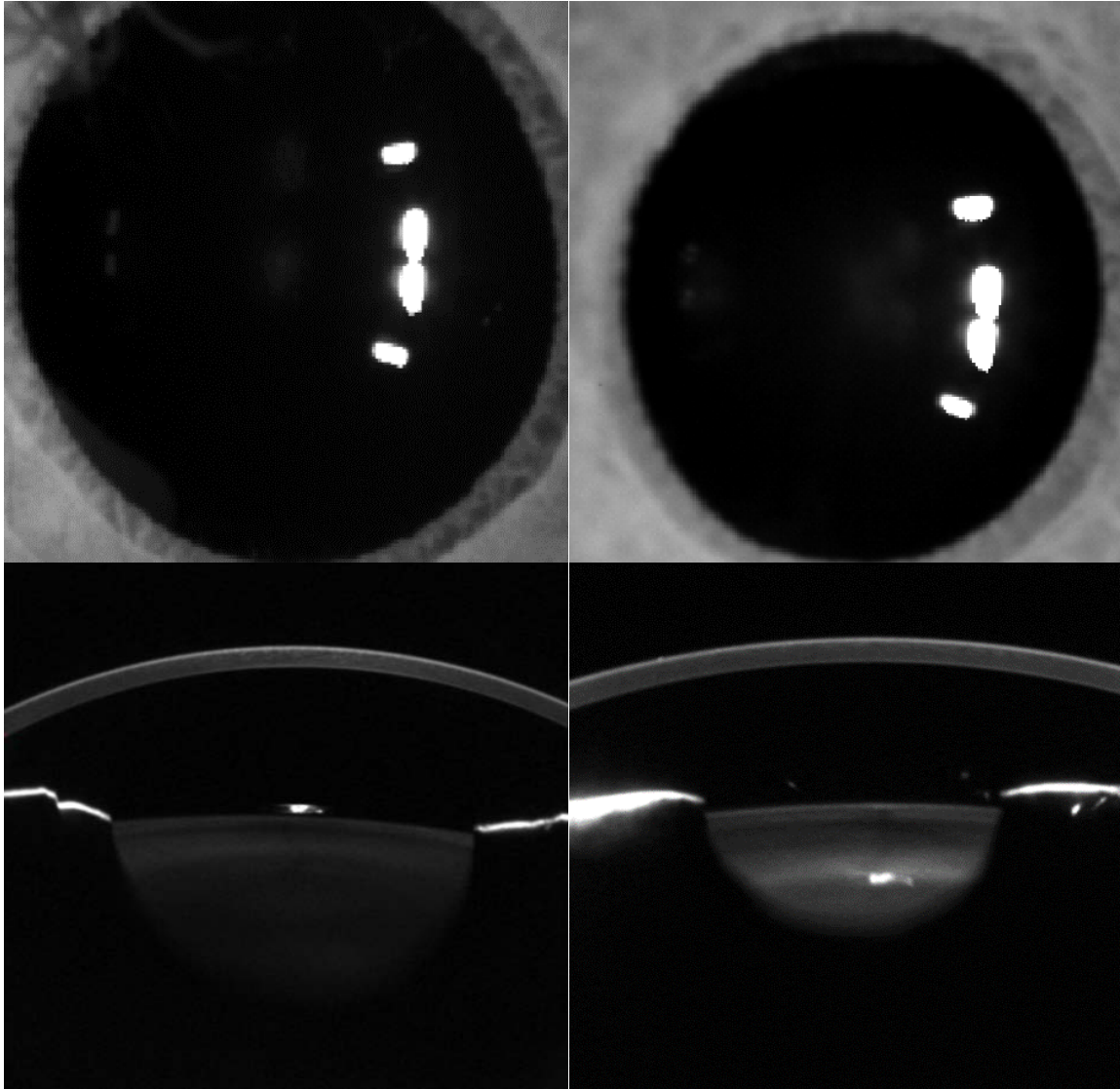
Figure 5.11. Purkinje (top) and Scheimpflug (bottom) images from an eye without (left) and with (right) the ghost image.

Our hypothesis is that the formation of a cataract implies a change in the refractive index inside the lens, which in some cases cause additional internal reflections, i. e., additional Purkinje images, causing the ghost image to appear. Note that the ghost image seems to be related with the high-density area seen in the corresponding Scheimpflug images so that it can also correspond to backscattered light from this region.

In fact, the anatomy of the human lens and changes that occur when a cataract appears have been previously discussed, and authors have suggested that a cataract can lead to discontinuity zones, already observed by means of a Scheimpflug camera [127] [Figure 5.12 (top)]. Castro and coworkers [128] have recently developed a swept-source optical coherent tomography system (SS-OCT) able to characterize different features in the crystalline lens, and those of older adults with and without a cataract have been measured. They have found that the most common and notable opacities extend parallel to either the anterior or the posterior surface of the lens and that these are always hyperreflective [Figure 5.12 (bottom)]. Therefore,

the ghost image that appears in some of the images taken with our system can probably be explained because of this.

On the other hand, the human lens roughness of its anterior surface has an age dependency, the well-known orange peel effect described by Navarro et al. [107] as previously commented, and this could have also an impact on the sharpness of P3 in some patients.
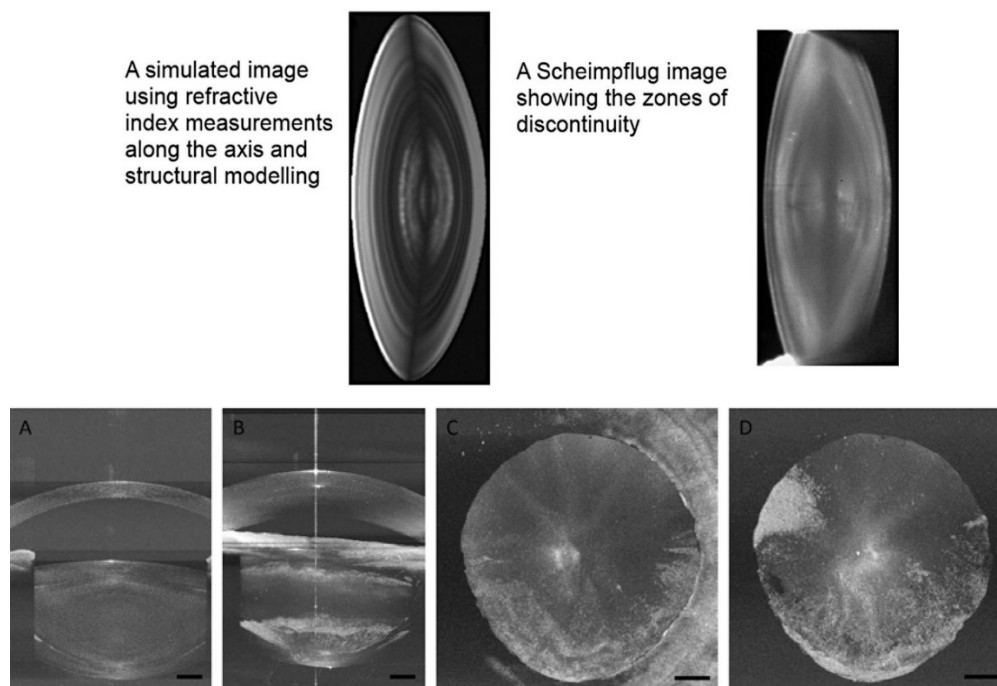
Figure 5.12. (Top) Simulation of reflected and scattered light compared to a Scheimpflug image showing zones of discontinuity in refractive index [127]. (Bottom) Cortical cataract imaged with SS-OCT in the right eye of a 63-year-old female pre–cataract surgery patient. Central cross-section (**A**), lateral projection of the volume maximum intensity (**B**), and axial projection of the anterior (**C**) and the posterior (**D**) part of the crystalline lens. The lateral projection of the maximum intensity allowed observing the extent of the opacities and their location either in the anterior or posterior cortex of the crystalline lens. Scale bars: 1 mm (Source: de Castro et al. 2018 [128]).

5.2.3 Analysis of scattering in eyes with corneal disorders

Figures 5.13, 5.14 and 5.15 show representative examples of the Purkinje, Scheimpflug and DP images corresponding to an eye undergoing refractive surgery, an eye with cornea Verticillata and another one with Fuchs dystrophy, respectively. As explained in the method section, this clinical study involved the analysis of eyes with CD and their comparison with healthy eyes. The reported densitometry in this subsection corresponds the highest value found in the cornea.
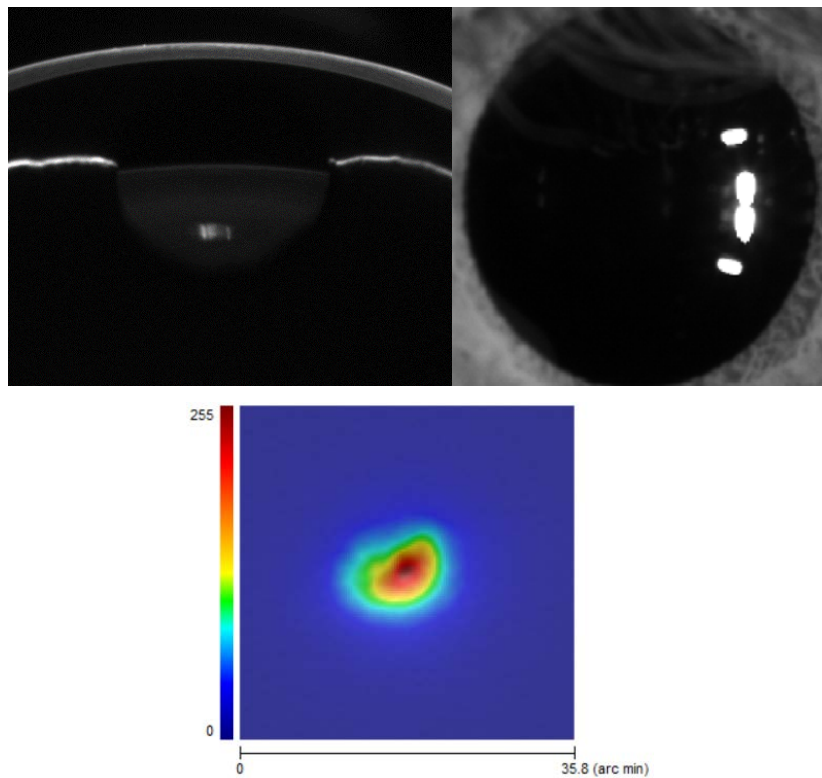
P3	P4	OSI	Log(S)	Densitometry
0.43	0.62	1.10	1.07	37.0

Figure 5.13. Purkinje (top left), Scheimpflug (top right) and DP (bottom) images of a post-LASIK eye of a subject aged 38 years old. The specific values of the contrast of the Purkinje images (P3 and P4), OSI, Log(S) and densitometry are also given.
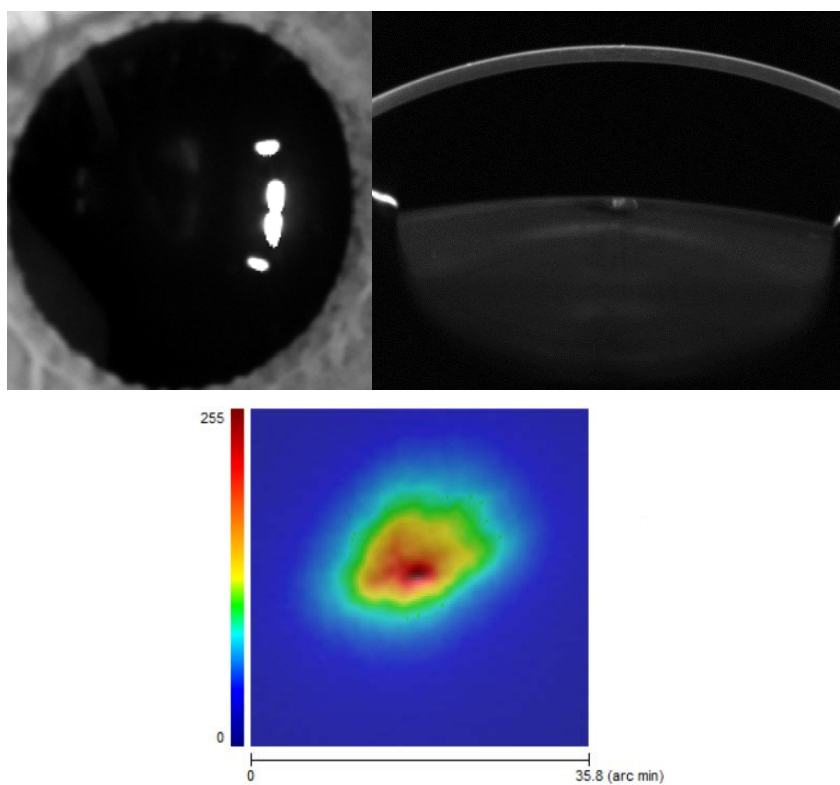
P3	P4	OSI	Log(S)	Densitometry
0.35	0.58	6.70	1.43	38.9

Figure 5.14. Purkinje (top left), Scheimpflug (top right) and DP (bottom) images of an eye with cornea Verticillata of a subject aged 65 years old. The specific values of the contrast of the Purkinje images (P3 and P4), OSI, Log(S) and densitometry are also given.
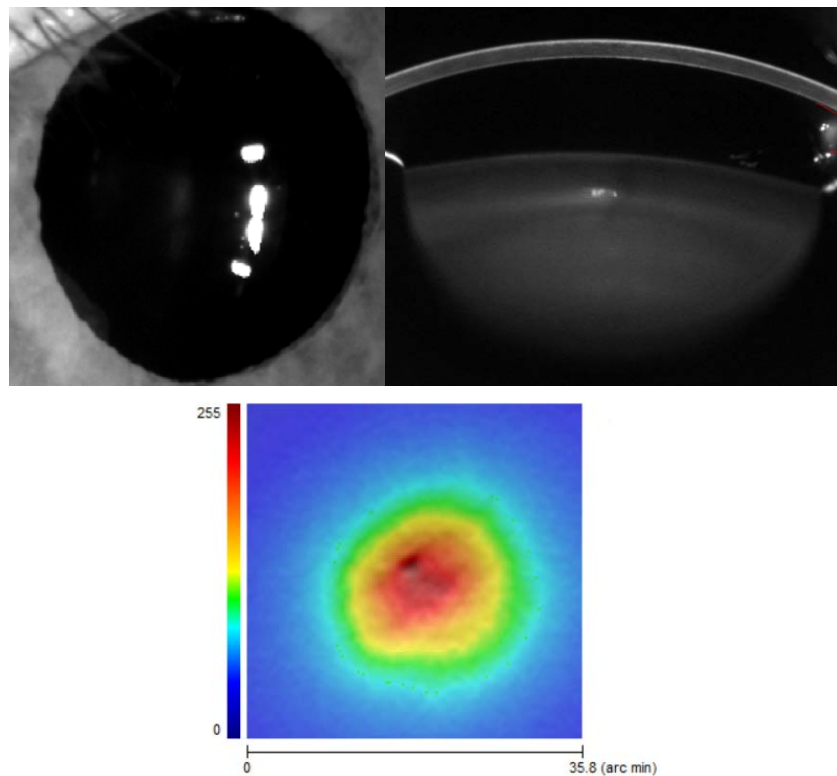
P3	P4	OSI	Log(S)	Densitometry
0.54	0.59	3.80	1.21	35.2

Figure 5.15. Purkinje (top left), Scheimpflug (top right) and DP (bottom) images of an eye with an eye with Fuchs dystrophy of a subject aged 635 years old. The specific values of contrast of the Purkinje images (P3 and P4), OSI, Log(S) and densitometry are also given

Table 5.10 summarizes the patients' demographics as well as the subjective refraction, CDVA for the control and CD groups. Scattering values found using each technique are also provided. Sex distribution occurred with the following probability: 55.5% female and 45.5% male for eyes with CD, and 52.9% female and 47.1% male for the control group. In this case, it is noticeable that the refractive error is much smaller in the CD than in the control group, since the first one included post-LASIK eyes.

Table 5.10. Sex and age distribution, subjective refraction, CDVA (Corrected Distance Visual Acuity) and scattering measurements in the CD and control groups: Purkinje contrasts (P3, P4), OSI, Log(S) and densitometry. The mean ± SD and the corresponding range (minimum, maximum) are shown as well as the median and the interquartile range (IQR) for those variables non-normally distributed (SE: Spherical Equivalent; D: Diopters).

	Mean ± SD and range [min, max]	
	CD Group	**Control Group**
Sex		
Male	5	8
Female	6	9
Age	38.8 ± 12.2 [24 , 65]	39.9 ± 8.5 [29 , 52]
Refraction [D]		
Sphere	-0.05 ± 1.42 [-3.75 , 0]	-1.44 ± 2.44 [-7.5 , 2.5]
Cylinder	-0.41 ± 0.55 [-1.50 , 0]	-0.44 ± 0.35 [-1.25 , 0]
SE	-0.23 ± 0.68 [-2.13 , 0]	-1.66 ± 2.59 [-6.75 , 0]
CDVA	0.98 ± 0.30 [0.8 , 1.0]	1.0 ± 0.0 [1.0 , 1.0]
P3	0.45 ± 0.12 [0.23 , 0.60]	0.52 ± 0.07 [0.37 , 0.60]
Median (IQR)	0.47 (0.19)	0.54 (0.11)
P4	0.62 ± 0.03 [0.58 , 0.70]	0.70 ± 0.03 [0.62, 0.74]
Median (IQR)	0.62 (0.04)	0.71 (0.05)
OSI	2.49 ± 1.78 [0.40 , 6.70]	0.55 ± 0.26 [0.20 , 1.20]
Median (IQR)	2.05 (2.03)	0.50 (0.35)
Log(S)	1.31 ± 0.23 [1.07 , 1.77]	0.89 ± 0.13 [0.71 , 1.10]
Median (IQR)	1.28 (0.36)	0.90 (0.21)
Densitometry	34.37 ± 3.78 [30.00 , 39.20]	30.28 ± 1.64 [27.60 , 33.40]
Median (IQR)	33.75 (7.55)	30.10 (2.05)

All scattering parameters analyzed rejected the null hypothesis of normal distribution (p<0.05), probably due to the smaller sample size (Table 5.11).

Table 5.11. Shapiro-Wilk test of normality for scattering measurements in the CD and control groups: Purkinje contrasts (P3, P4), OSI, Log(S) and densitometry.

	Statistic	p-value
P3	.902	.015*
P4	.923	.048*
OSI	.694	.000*
Log(S)	.918	.036*
Densitometry	.859	.002*

*Statistically significant value.

As we also did for healthy eyes and eyes with cataracts, we studied the dependence of scattering with age in eyes with CD. Figure 5.16 depicts the corresponding scatterplots. The results were fitted by using a linear regression model.
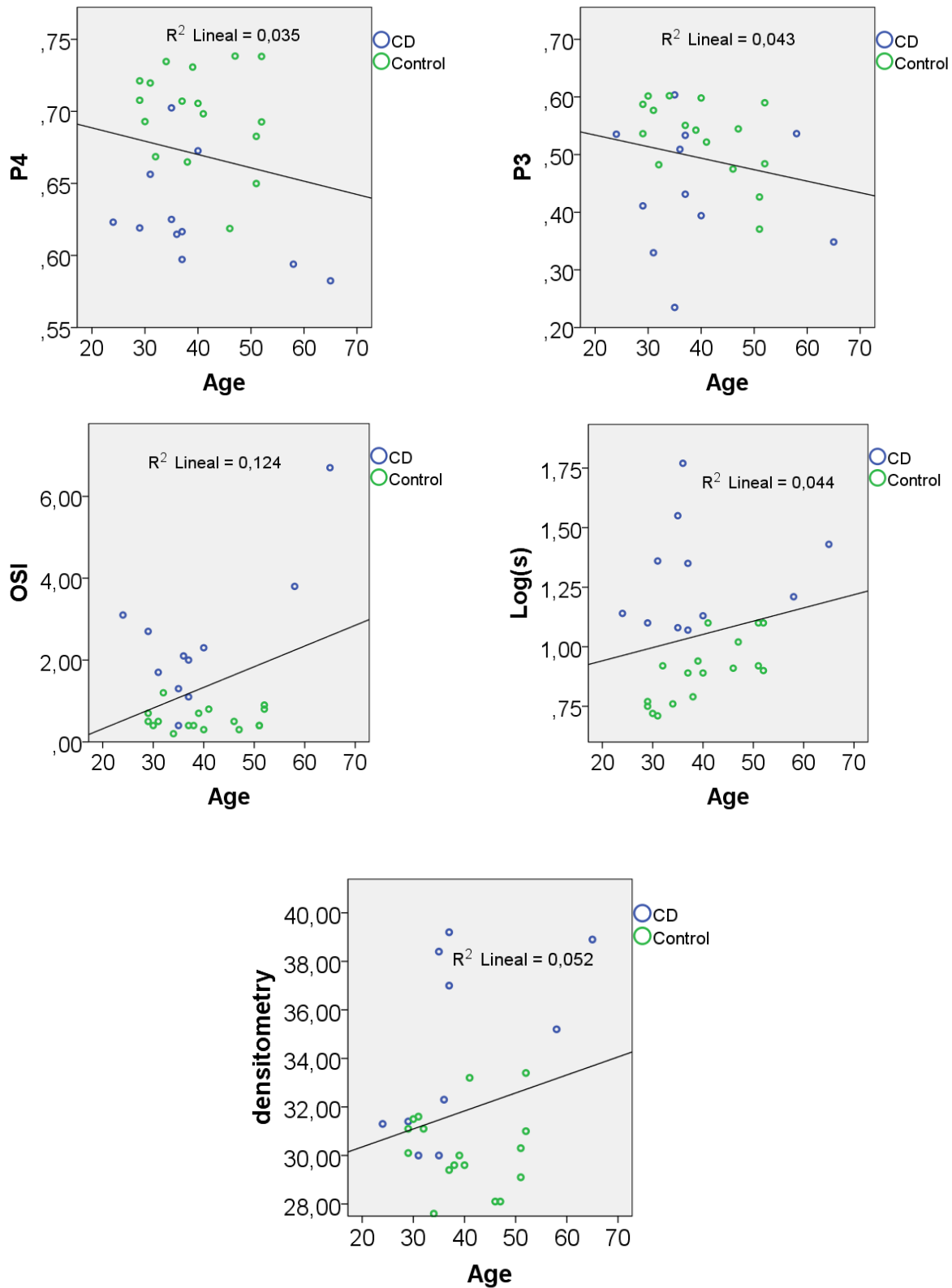
Figure 5.16. Scatterplots and corresponding linear regression (R^2) of the scattering variables as a function of age for the control eyes (in green) and with CD (blue): Purkinje contrasts (P3, P4), OSI, Log(S) and densitometry.

No statistically significant correlations could be established between scattering and age when analyzing eyes with CD (p > 0.05) (Table 5.12). This can be explained by the fact that CDs are not age-related pathologies as well as there is less data available than in the study of cataracts.

Table 5.12. Spearman's† correlation coefficients and corresponding significance (p-value) between age and measured variables: Purkinje contrasts (P3, P4), OSI, Log(S) and Densitometry.

		P3	P4	OSI	Log(S)	Densitometry
Age	Correlation (Linear)	-.187	-.117	-.021	.246	.014
	p-value (Linear)	.351	.552	.914	.207	.946

*Statistically significant correlation.

The Mann-Whitney test to compare the measured scattering between healthy eyes and eyes with CD revealed statistically significant differences in terms of all variables analyzed (p<0.05) (Table 5.13). Therefore, in view of the results P3 seems to provide information about the scattering of the cornea in eyes with CD.

Table 5.13. Results of the Mann-Whitney test to account for differences between eyes of the control group and with CD in terms of contrast of Purkinje images (P3, P4), OSI, Log(S), and densitometry.

	P3	P4	OSI	Log(S)	Densitometry
Mann-Whitney U	52.000	17.000	12.500	7.500	29.000
p-value	.030*	<.001*	<.001*	<.001*	.005*

Regardless the differences found, the P3 contrast is the variable with the lowest significance for the Mann-Whitney test. Again, this can probably be attributed to the larger variability of this parameter, which could be affected by other factors. For instance, P3 contrast is lower than P4 and the signal-to-noise ratio can be worse. Moreover, the third Purkinje image is formed much closer to the retina than the other ones, which are indeed closer to first surface of the lens; and even we use a telecentric objective lens with enlarged depth of field to acquire at the same time both images, P3 could be more influenced by defocus. Moreover, as we already commented in section 5.2.2, the roughness of the anterior lens surface could have an influence on the P3 contrast even in the absence of a cataract [107].

Bivariate correlations as well as the corresponding linear regression between pairs of variables used to assess intraocular scattering in eyes with CD are shown in Figure 5.17 and Table 5.14.
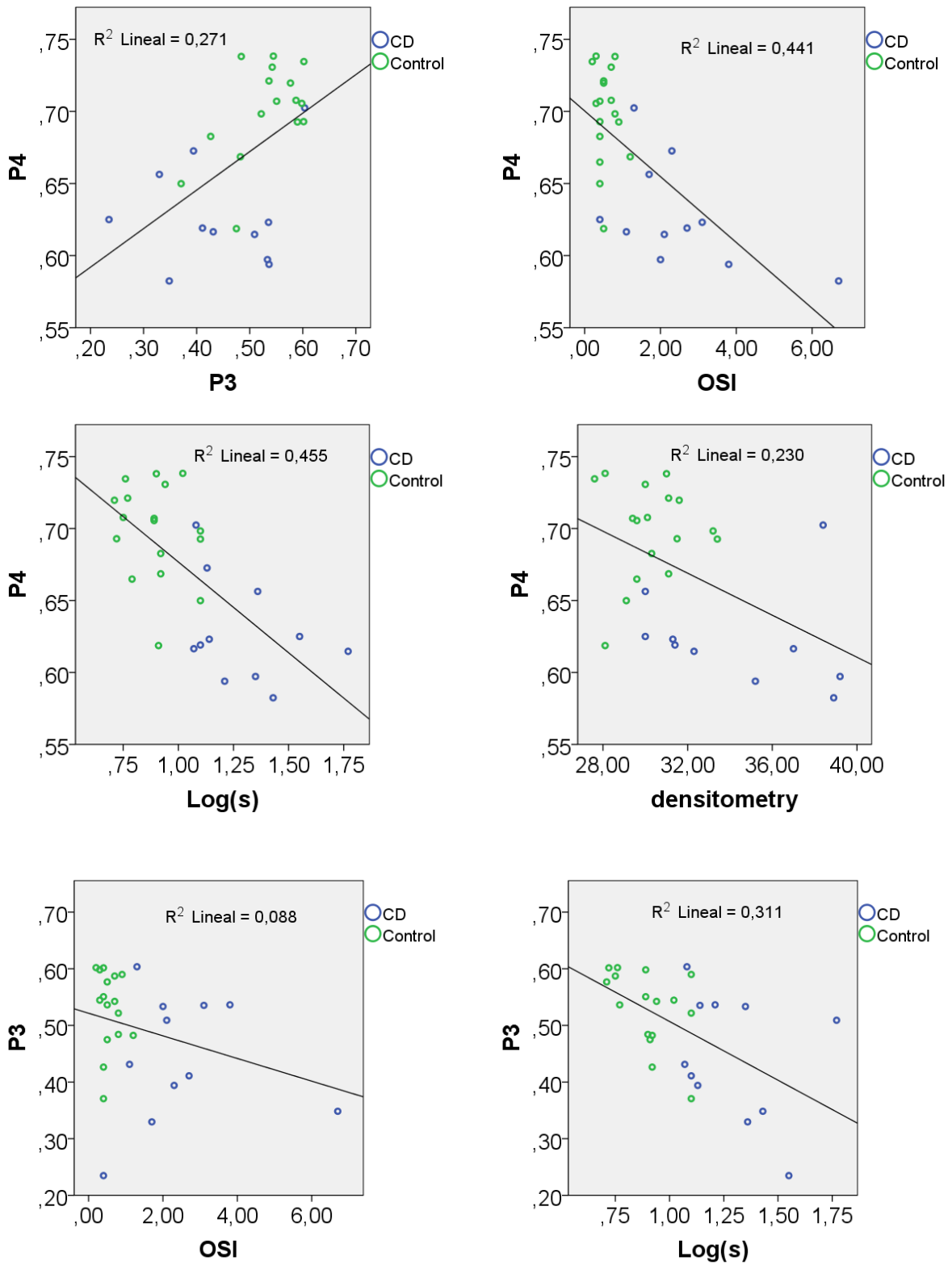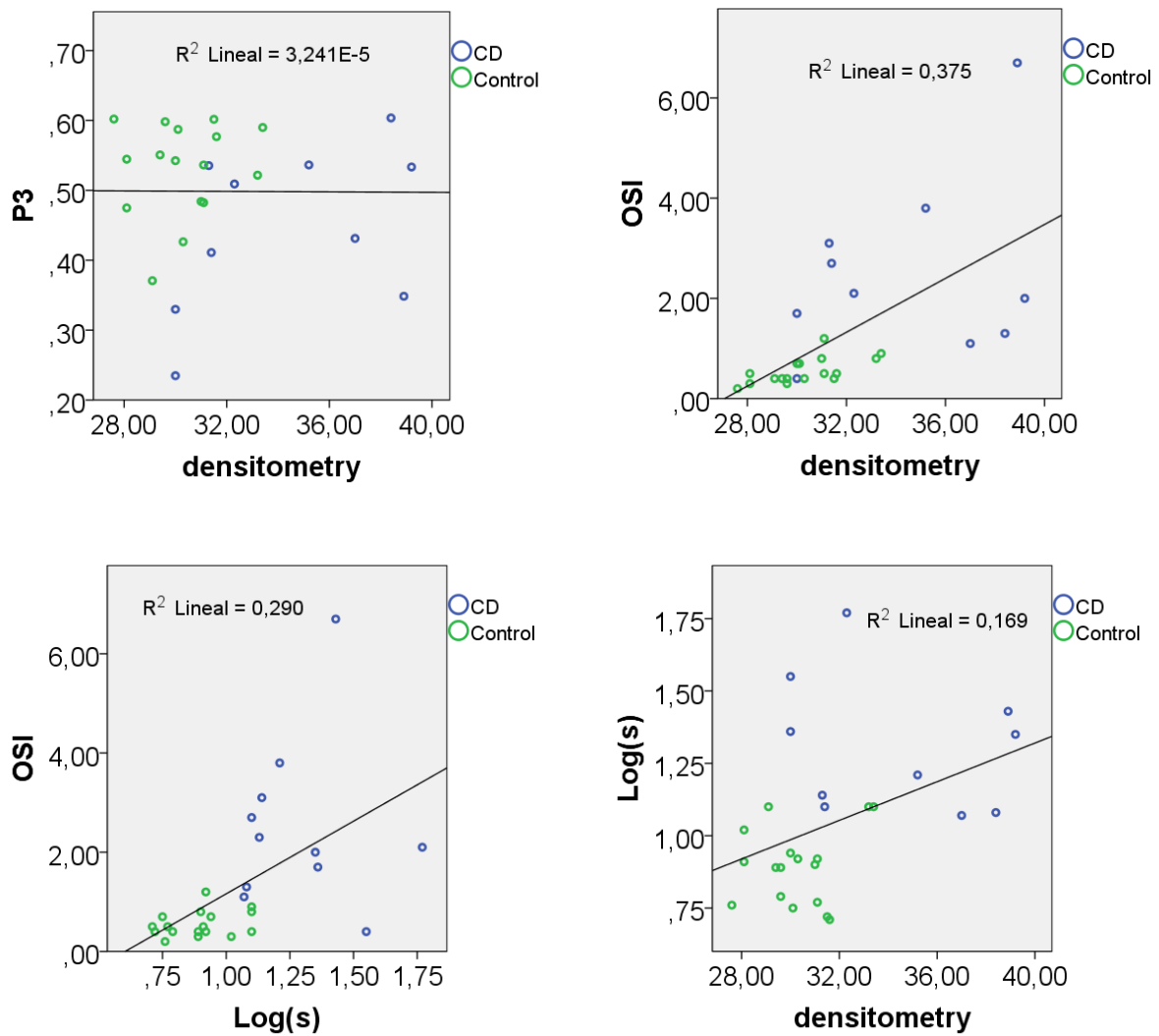
Figure 5.17. Scatterplots and corresponding linear regression (R²) of the scattering variables for the control eyes (in green) and with CD (blue): Purkinje contrasts (P3, P4), OSI, Log(S) and densitometry.

Table 5.14. Spearman's correlation coefficients and corresponding significance (p-value) between intraocular scattering parameters.

	P3	P4	OSI	Log(S)	Densitometry
P3	-				
P4	.565 (.002)*	-			
OSI	-.341(.082)	-.606 (.001)*	-		
Log(S)	-.592 (.001)*	-.686 (<.001)*	.644 (<.001)*	-	
Densitometry	<.001(.999)	-.455 (.017)*	.745 (<.001)*	.394(.042)*	-

*Statistically significant correlations.

As it can be seen, there is a significant correlation between the contrasts of P3 and P4 ($r_s = 0.565$, $p = 0.002$) and between P3 and Log(S) ($r_s = -0.592$, $p = 0.001$). In this study, we expected a strong correlation between P3 and P4 contrasts, as in the eyes of the CD group the main source of intraocular scattering should come from the cornea. Thus, these results confirm that P3 is importantly affected by corneal scattering.

The correlation between P3 and P4 contrasts obtained with healthy eyes was of $r = 0.375$ while for cataracts it was of $r = 0.617$. However, from our initial hypothesis we expected higher correlation between P3 and P4 contrasts when analyzing eyes with CD than for eyes with cataracts. The different sample size can probably have an impact on the computed correlation coefficients (note that there are only 11 eyes with CD against 46 with cataracts).

On the other hand, P3 contrast does not correlate significantly with the OSI neither the corneal densitometry ($p > 0.05$). Note that these parameters present different dependence on the location of the corneal opacification. To calculate the OSI, we acquire a DP image, in which the light source is entering in the eye using a 2-mm entrance pupil and a 4-mm exit pupil. Therefore, opacities located in the central part of the cornea are expected to have a higher impact on OSI than those localized at the periphery. Additionally, in this study the reported corneal densitometry is the highest value found in the cornea from the images taken with the Pentacam Scheimpflug camera. Thus, localized opacities could have the same impact on the reported densitometry as homogeneous opacities, or even a higher one. Figure 5.18 shows a Scheimpflug photography of a cornea with keratitis, where localized areas with clearly higher densitometry can be observed. Densitometry shows a stronger correlation with OSI ($p<0.001$) than with P4 ($p = 0.17$) and Log(S) ($p = 0.042$).
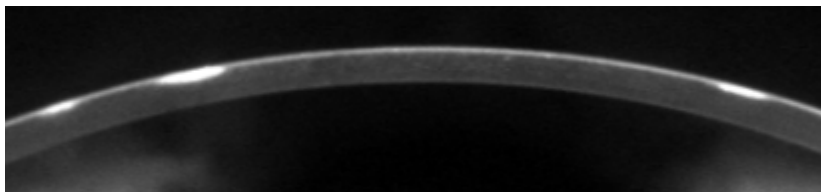
Figure 5.18. Scheimpflug photography of a cornea with keratitis in which localized areas with abnormally increased density can be observed. White areas correspond to high densitometry values.

P4 contrast correlates with all the other parameters ($p < 0.05$) validating the new method as a useful technique for assessing corneal and lens scattering in an objective way. This result is in agreement with the findings from the control group and eyes with cataracts.

On the other hand, even P3 is affected by the corneal scattering, other effects like surface roughness, backscattered light from cataracts and defocus can have an impact on the computed contrast.

As commented above, this study has some limitations because of the sample size. Accordingly, we decided to carry out another study with healthy eyes wearing scatter-customized CLs in order to be able to draw more robust conclusions when dealing with eyes with corneal scattering.

5.3   Assessment of contact lens – induced corneal scattering

5.3.1   Scatter-customized contact lenses

In order to validate the performance of the Purkinje system when used to assess corneal scattering, an additional study was conducted with eyes wearing scatter-customized CLs with different grades of diffusion.

Specifically, customized versions (different levels of scattering) of the commercial *Cataract* CL (9mm SFX, Tucson, USA) were used (Figure 5.19). The manufacturer company tagged the CLs as having 5%, 15% and 50% or higher values of scattering.

We measured the naked eyes of the volunteers as well as wearing CLs with the following degrees of scattering: low (L), medium (M), high (H) and very high (VH); L corresponds to the 5% CL, M to the 15% CL, H to 5% plus 15% CLs and VH to 15% plus 15% CLs. We also tried CLs tagged with 50% or more, but they were too opaque to measure intraocular scattering with the devices used in the study.

Figure 5.19. Eye wearing the commercial *Cataract* CL (Image from the vendor website) (top left). Scatter-customized CLs (top right). Images with the same camera without CL (bottom-left) and with a 50% CL attached to the objective lens (bottom right).

5.3.2 Measurements

We measured 4 eyes from 4 healthy young volunteers (age: 23.75 ± 3.40 years, range [21, 28]) with a corrected distance visual acuity (CDVA) of at least 20/20 (2 female and 2 male) recruited from the staff of the CD6 and the CUV.

Similarly to the former studies, we measured each eye for each corneal scattering condition with the commercial straylight meter C-Quant and the DP system HD Analyzer. These results were compared with the scattering measured by means of the Purkinje images contrasts (P3 and P4) given by our clinical prototype. Additionally, we also measured the corneal densitometry by means of the Pentacam Scheimpflug camera, but all images of eyes with CLs had a densitometry of 100 (saturated value). The measurements were consecutive for each subject, starting with the naked eye and followed by CL measurements, from low to high degree of scattering.

5.3.3 Results

As a representative example, Figure 5.20 shows the Purkinje images of a patient wearing the CLs with different scattering grades, together with the intensity profiles of P3 and P4.
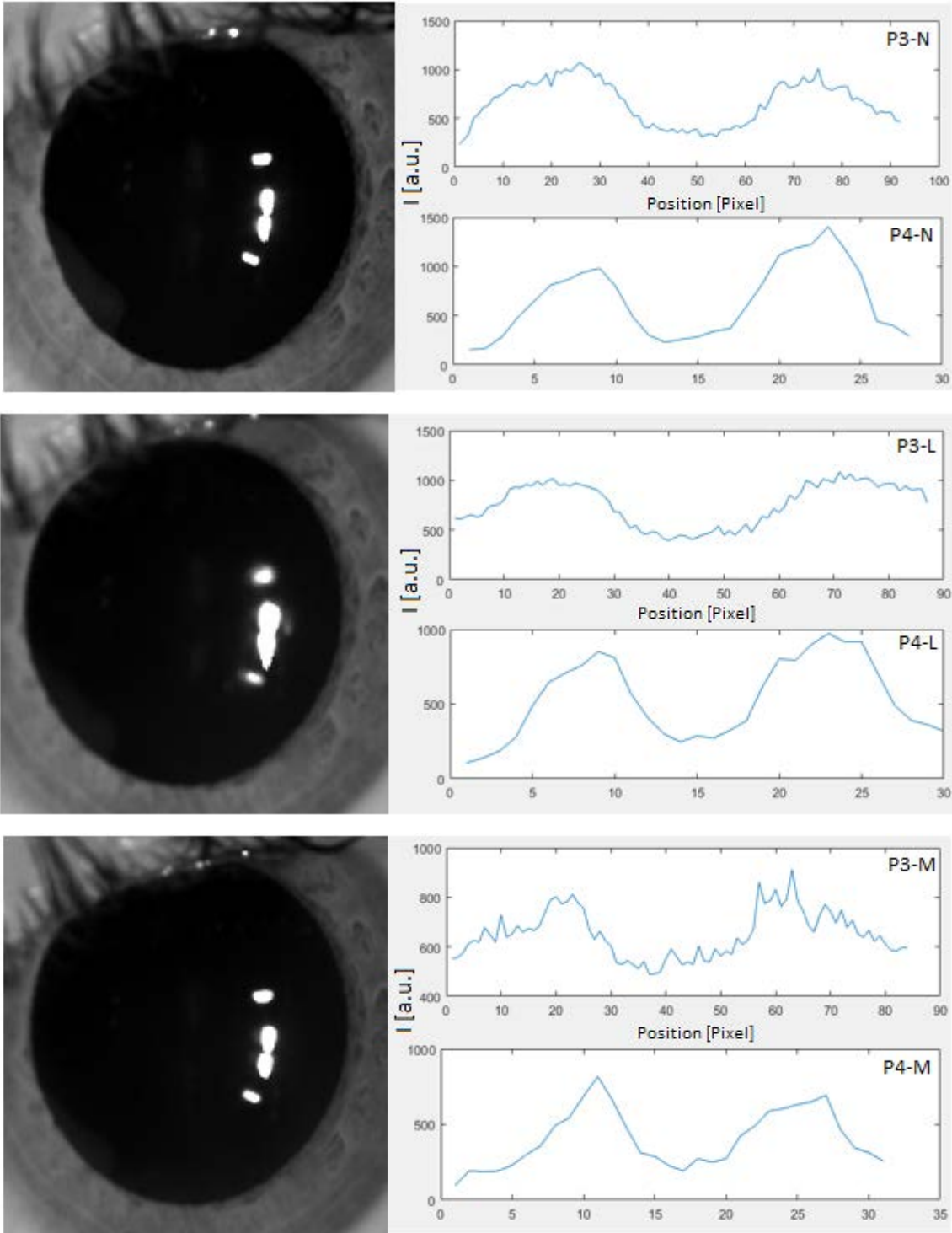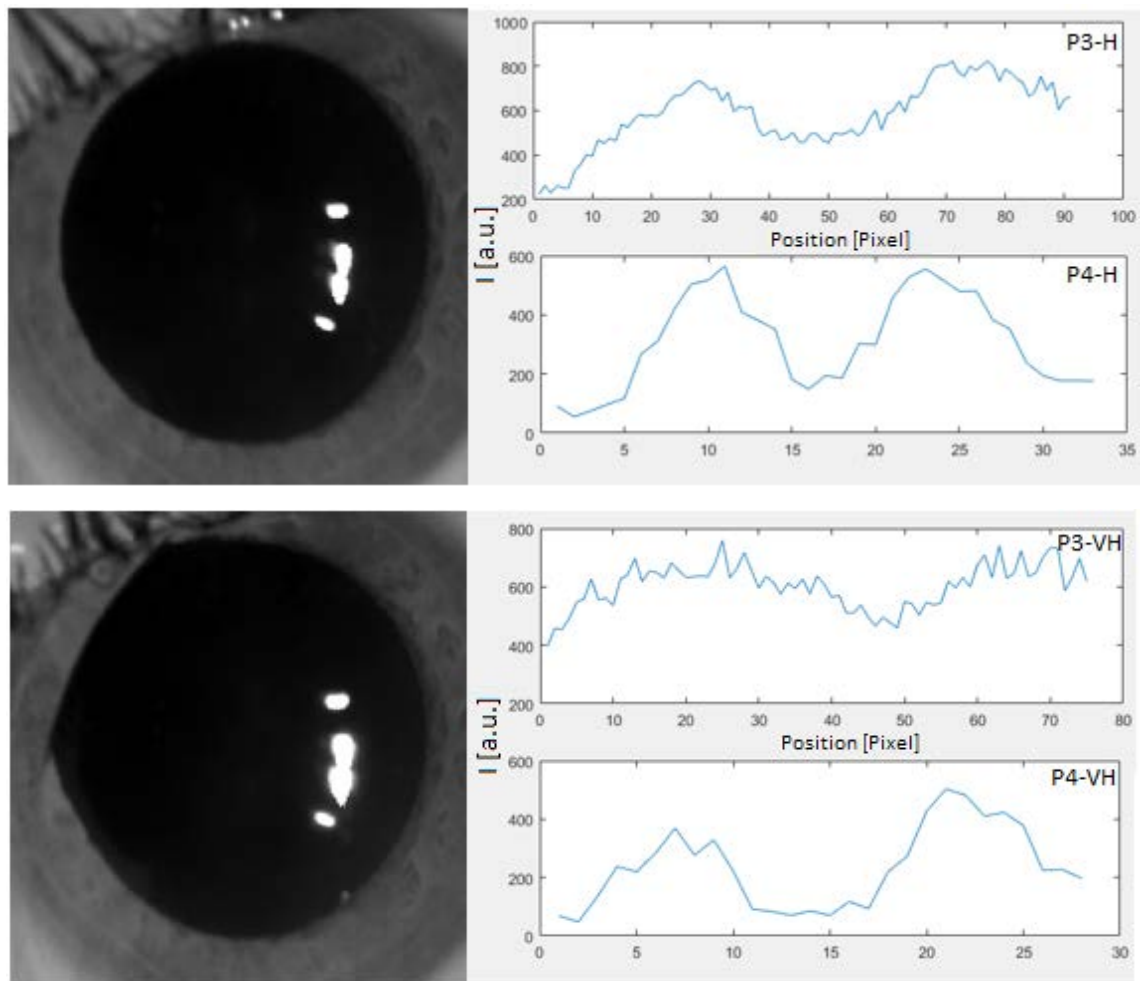
	N	L	M	H	VH
P3	0.57	0.48	0.28	0.28	0.17
P4	0.69	0.61	0.55	0.53	0.50
Log(S)	0.79	1.49	1.95	1.98	2.22
OSI	0.5	0.73	0.7	0.63	1.13

Figure 5.20. (Left) Purkinje images of an eye wearing CLs with several degrees of scattering of a subject aged 25 years old. From top to bottom: low (L), medium (M), high (H) and very high (VH). N refers to the naked eye. (Right) Corresponding P3 and P4 intensity profiles. The specific values of the P3 and P4 contrasts of the Purkinje images, OSI and Log(S) are also given.

For one specific volunteer, it was not possible to compute the contrast of the P3 image in the VH condition (Figure 5.21). It corresponded to a case in which the patient was wearing two CLs simultaneously and, as it is evident from the images, there was a bad adaptation; probably, this gave rise to an inhomogeneous tear film between them. Fortunately, this did not happen for the rest of subjects.
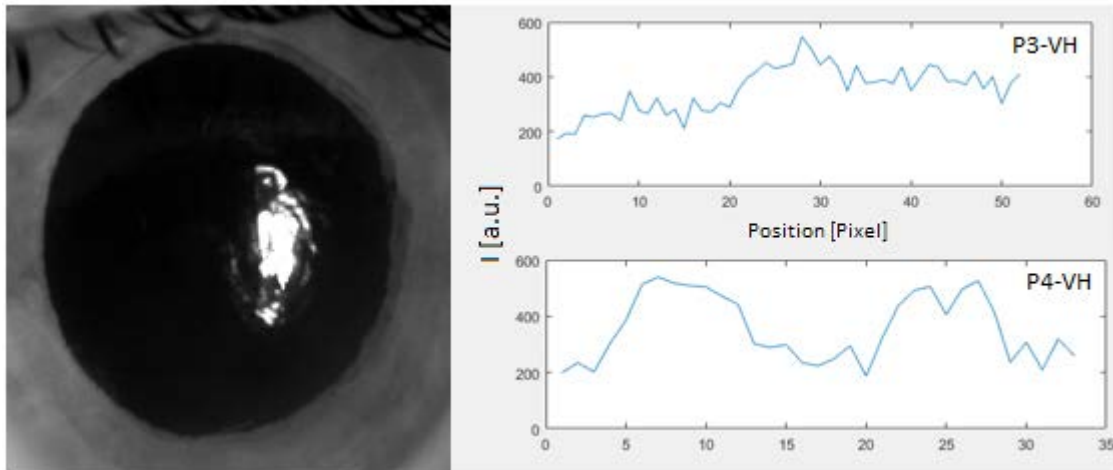
Figure 5.21. (Left) Purkinje images of an eye wearing CLs with very high (VH) scattering. (Right) Corresponding P3 and P4 intensity profiles. The P3 contrast could not be computed while the P4 was of 0.42.

The assessment of scattering for all variables and conditions are shown in Table 5.15. P3 and P4 contrasts were normally distributed ($p > 0.05$) while OSI ($p < 0.001$) and Log(S) ($p = 0.008$) were not. The results corresponding to different grades of scattering using boxplots are shown in Figure 5.22. It can be seen that scattering due to CLs affected all variables analyzed. P3 and P4 contrasts decreased as the scattering increased while the straylight in terms of Log(S) increased. In the same way, higher OSI values were found for higher scattering conditions although there was more variability for the conditions of corneal scattering labeled as H (SD = 1.17) and VH (SD = 1.36) in comparison with others with less diffusion, i. e., naked eyes (SD = 0.16), L (SD = 0.38) and M (SD = 0.29). Note that H and VH corneal scattering conditions correspond to eyes wearing two CL simultaneously. Differences in adaptation between patients, misalignments and heterogeneous tear distribution between CLs etc. can probably introduce important aberrations that can affect the central part of the PSF and thus, the OSI value. As we have seen in figure 5.21 for one of the volunteers, the P3 image could not be properly focused when wearing two CL at the same time. The OSI of this volunteer for high scattering (H) was of 3.03 and for very high scattering (VH) of 3.17, while the mean of volunteers was of 1.42 and 1.22, respectively.

The t-test (Mann-Whitney for the non-normal distributed data) revealed that there were statistically significant differences between naked eyes and eyes with scatter-customized CLs in terms of P3 contrast ($p = 0.014$), P4 contrast ($p = 0.027$), and Log(S) ($p = 0.001$), but not in terms of OSI ($p > 0.05$).

Moreover, the analysis of variance (or equivalently Kruskal Wallis test) confirmed that the contrasts of the third and fourth Purkinje images were significantly different among groups with different grades of scattering: P3 contrast ($p = 0.002$) and P4 contrast ($p = 0.006$). Similarly, in terms of Log(S) statistically significant differences were reported among the different CLs groups and naked eyes ($p = 0.004$). However, no statistically significant differences were reported among groups in terms of OSI ($p > 0.05$).

Table 5.15. Mean (± SD) and range [minimum and maximum values] for each corneal scattering condition. The median and interquartile range (IQR) are additionally given for non-normal distributed data.

	P3	P4	OSI (Median (IQR))	Log(S) (Median (IQR))
Naked	0.53±0.04 [0.49 , 0.57]	0.69±0.03 [0.66 , 0.73]	0.43±0.16 [0.20 , 0.53] 0.50 (0.25)	0.82±0.10 [0.71 , 0.96] 0.89 (0.19)
Low	0.49±0.05 [0.43 , 0.54]	0.67±0.05 [0.61, 0.71]	0.62±0.38 [0.25 , 1.10] 0.57 (0.72)	1.27±0.21 [1.02 , 1.49] 1.28 (0.41)
Medium	0.40±0.09 [0.28 , 0.49]	0.59±0.05 [0.55 , 0.65]	0.64±0.29 [0.35 , 0.90] 0.65 (0.44)	1.98±0.04 [1.94 , 2.02] 1.98 (0.07)
High	0.35±0.07 [0.28 , 0.42]	0.59±0.09 [0.51 , 0.67]	1.42±1.17 [0.50 , 3.03] 1.07 (2.12)	1.99±0.13 [1.81 , 2.11] 2.03 (0.25)
Very High	0.27±0.11 [0.05 , 0.39]	0.54±0.05 [0.41 , 0.60]	1.22±1.36 [0.20 , 3.20] 0.77 (2.41)	2.10±0.17 [1.86 , 2.22] 2.16 (0.30)
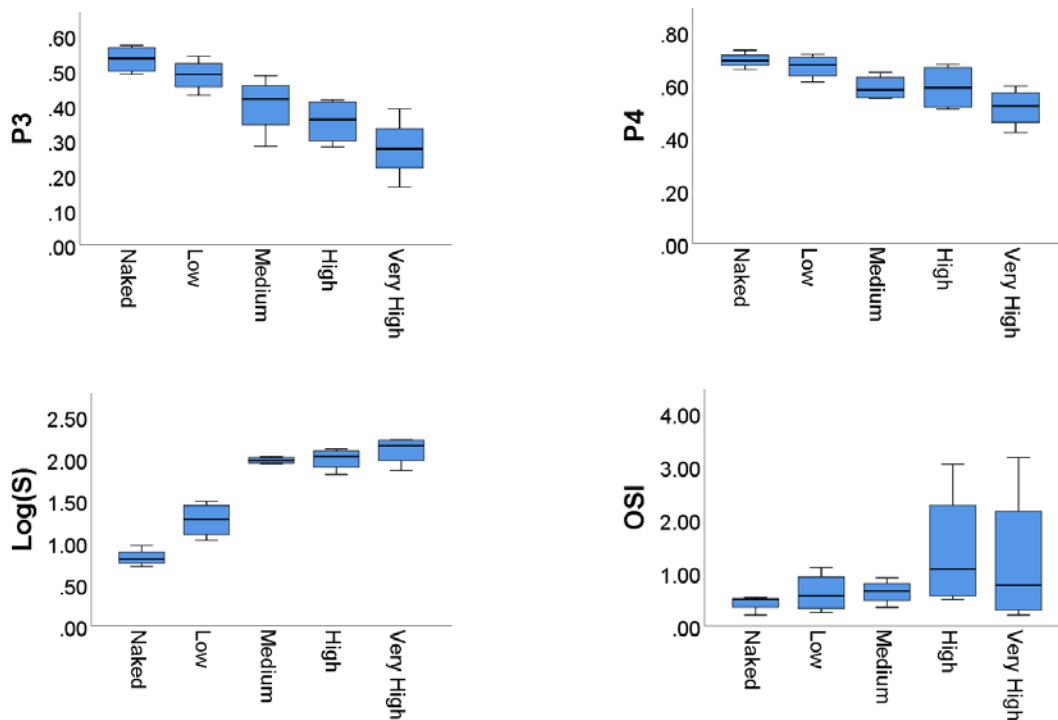
Figure 5.22. Boxplots for each variable for different groups of corneal scattering. Five statistical descriptors are shown in these plots: maximum, third quartile, median, first quartile and minimum.

Bivariate correlations and the linear regression between pairs of variables are shown in Figure 5.23. Correlation coefficients and corresponding significance levels are summarized in Table 5.16. Results indicate that there were significant correlations between all pairs of variables except OSI and P3 contrast. The highest ones were found between P3 and P4 contrasts ($r = 0.828$, $p < 0.001$) meaning that they carry the same information of scattering, which was already expected; and also, P3 contrast and Log(S) ($r = -0.830$, $p < 0.001$) and P4 contrast and Log(S) ($r = -0.810$, $p < 0.001$).

The weaker correlation of P3 contrast and OSI ($p > 0.05$) with respect to that found between P4 contrast and OSI ($p = 0.028$) could be explained by the fact that, as commented above, we were unable to compute the P3 contrast for one of the volunteers with an OSI of 3.17.

The strong correlation between both Purkinje contrasts reinforces the idea that P3 and P4 are carrying the same information about corneal scattering.
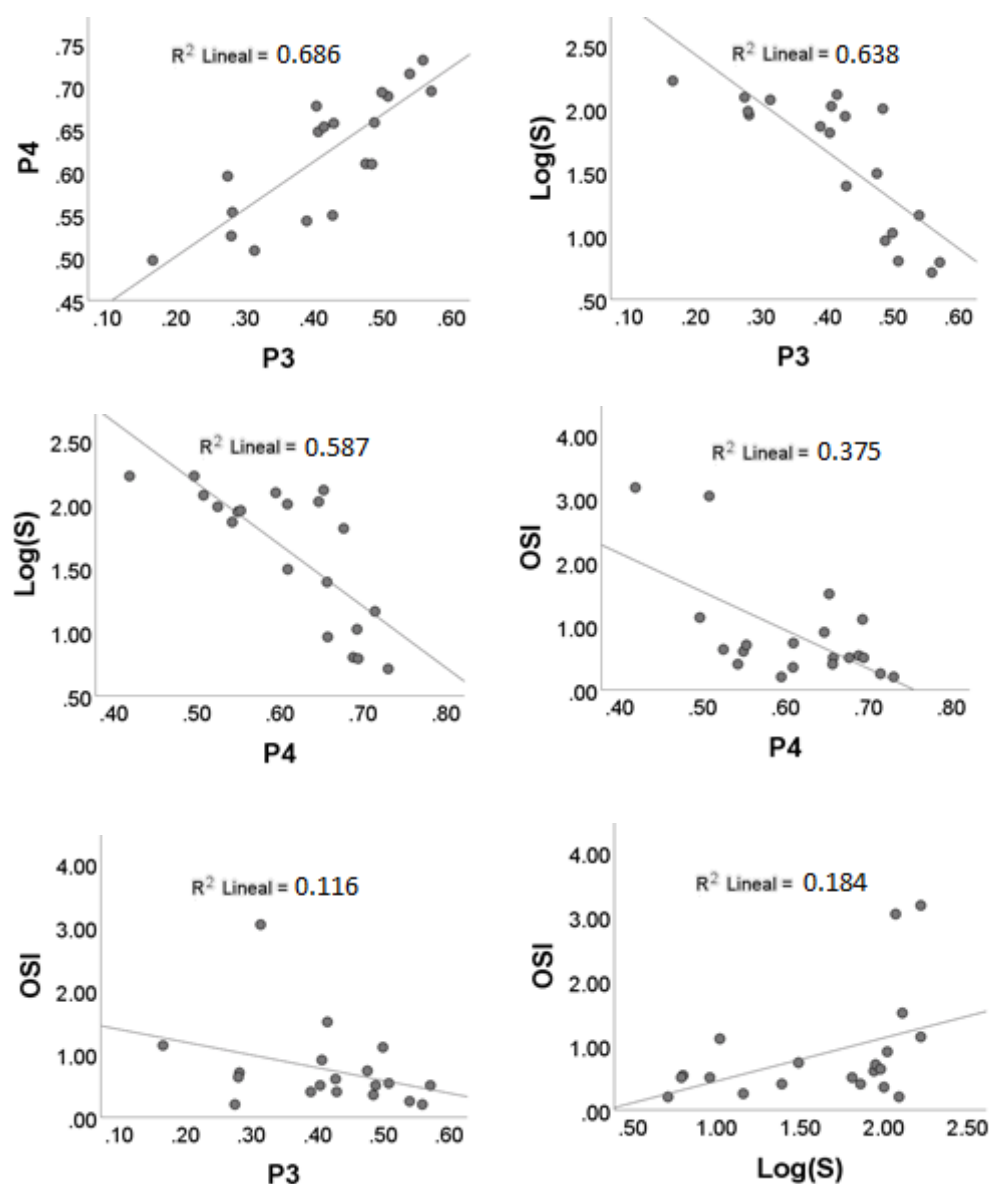
Figure 5.23. Scatterplots and linear regression (R²) between measured parameters for all groups of CLs as well as naked eyes.

Table 5.16. Pearson's† and Spearman's‡ correlation coefficients and corresponding significance (p-value) between intraocular scattering variables.

	P3	P4	OSI	Log(S)
P3	-			
P4	.828* (<.001)†	-		
OSI	-.340 (.154)‡	-.491* (.028) ‡	-	
Log(S)	-.830*(<.001)‡	-.810*(<.001)‡	.511* (.021) ‡	-

*Statistically significant correlations.

In any case, the agreement between the commercial straylight meter results - Log(S) - and our experimental Purkinje setup demonstrates the ability of our novel method to assess the corneal scattering in patients with different controlled levels of corneal scattering in terms of both P3 and P4 contrasts.

5.4 Compensation of the P3 contrast in eyes with ghost images

5.4.1 Preliminary considerations and proposed compensation

Our results make evident that the P3 contrast is affected to some extent by cataracts. This means that it carries information about the lens scattering and not only from scattered light in the cornea and the aqueous humor, as initially assumed. The formation of a cataract implies a change in the refractive index inside the lens, which in some cases could cause backscattering and additional internal reflections, i. e., additional Purkinje images, causing a ghost image to appear.

In this section, we present a new methodology to compensate for the Ghost Purkinje Image (GPI) based on the computation of a new P3 contrast (P3') in which the influence of the GPI is subtracted so that P3' becomes independent of the cataract. To do so, we firstly selected those patients whose eyes showed the GPI when measured with the Purkinje system, i. e., those with cataracts. Then, we measured the highest pixel value corresponding to the GPI (Figure 5.24). As we formerly discussed, in most of the cases the GPI is close to P3.
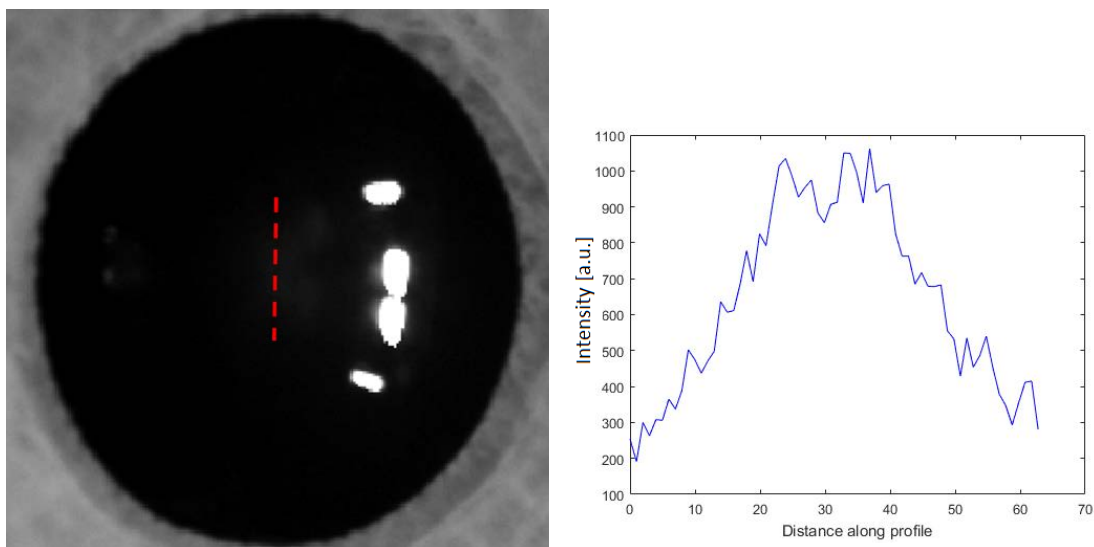
Figure 5.24. (Left) Eye with the GPI next to P3. (Right) Intensity profile of the GPI corresponding to the red dashed line. The maximum intensity of this profile is used to compute the P3' contrast.

Figure 5.25 depicts a scatterplot of the raw P3 contrast as a function of the maximum intensity of the GPI (GPI I_{max}) as well as the corresponding linear fitting. As it is shown, a significant linear correlation between the two parameters was found (r = 0.683, p < 0.001), indicating that the P3 contrast is actually influenced by the GPI light distribution.
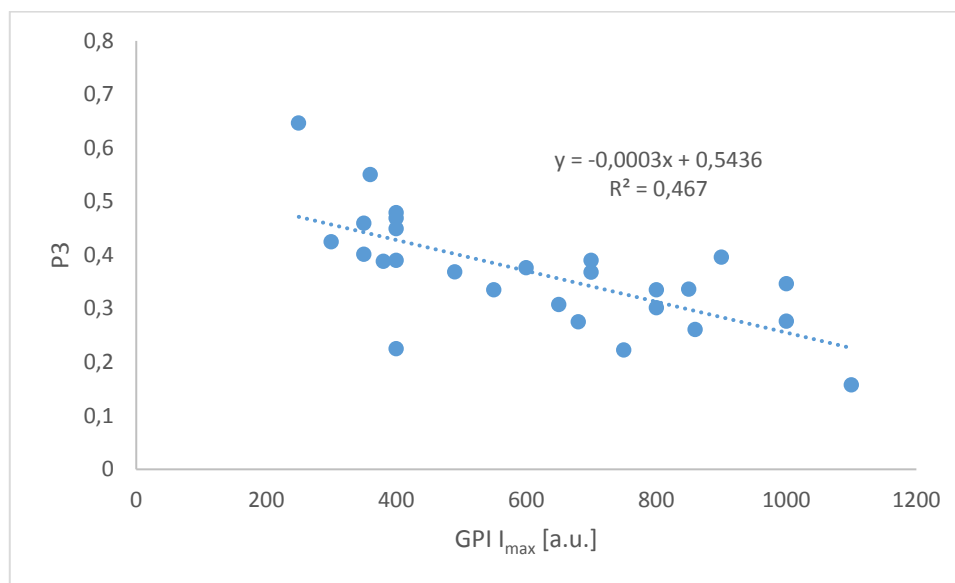
Figure 5.25. Scatterplot and corresponding linear regression (R^2) for the P3 contrast as a function of the maximum pixel value inside the GPI.

Using the linear fitting $P3 = a \cdot (GPI\ I_{max}) + b$, we computed the new P3' contrast from the raw P3 contrast in order to remove the GPI contribution, i. e., the cataract contribution, as follows:

$$P3' = P3 - a \cdot (GPI\ I_{max})$$
<div align="right">Equation 5.1</div>

where *P3'* is the compensated contrast, P3 is the raw contrast, *a* is the slope found in the linear regression and *GPI I_{max}* is the maximum intensity found in the GPI light distribution.

5.4.2 Results

Figure 5.26 depicts a scatterplot of the P3' contrast values for the eyes belonging to the control and cataract groups used in section 5.2.
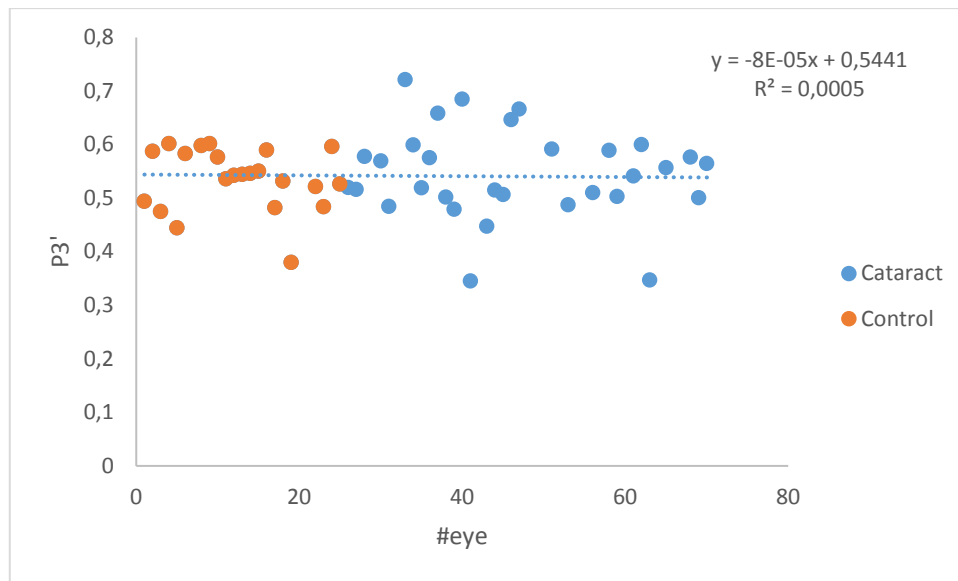
Figure 5.26. Scatterplot and corresponding linear regression (R^2) for the P3' contrast of all eyes (#eye) corresponding to the control and cataract groups. In blue eyes with cataracts, in orange control eyes.

After applying the proposed compensation, the SD of the P3 contrast for the cataracteous eyes was notably reduced: $SD_{P3} = 0.13$ vs. $SD_{P3'} = 0.07$, which is nearly the 50%, indicating that all eyes (independently of the lens transparency) have a similar value. Moreover, there were no relevant differences between P3' contrast values of control eyes and of eyes with cataracts.

A t-test confirmed that there were statistically significant differences between eyes of the control and cataract groups in terms of P3 contrast (section 5.2.2). However, there were no significant differences in terms of P3' for eyes of the control and cataract groups ($p = 0.66$), confirming that the cataract effect on the contrast of the third Purkinje image was removed with the compensation, or at least reduced.

For the sake of completeness, we included eyes of the CD group and wearing scatter-customized CLs to this analysis, which showed statistical significant differences with respect to the control eyes (section 5.3). Figure 5.27 depicts scatterplots of P4 contrast as a function of P3' and the corresponding linear regressions.
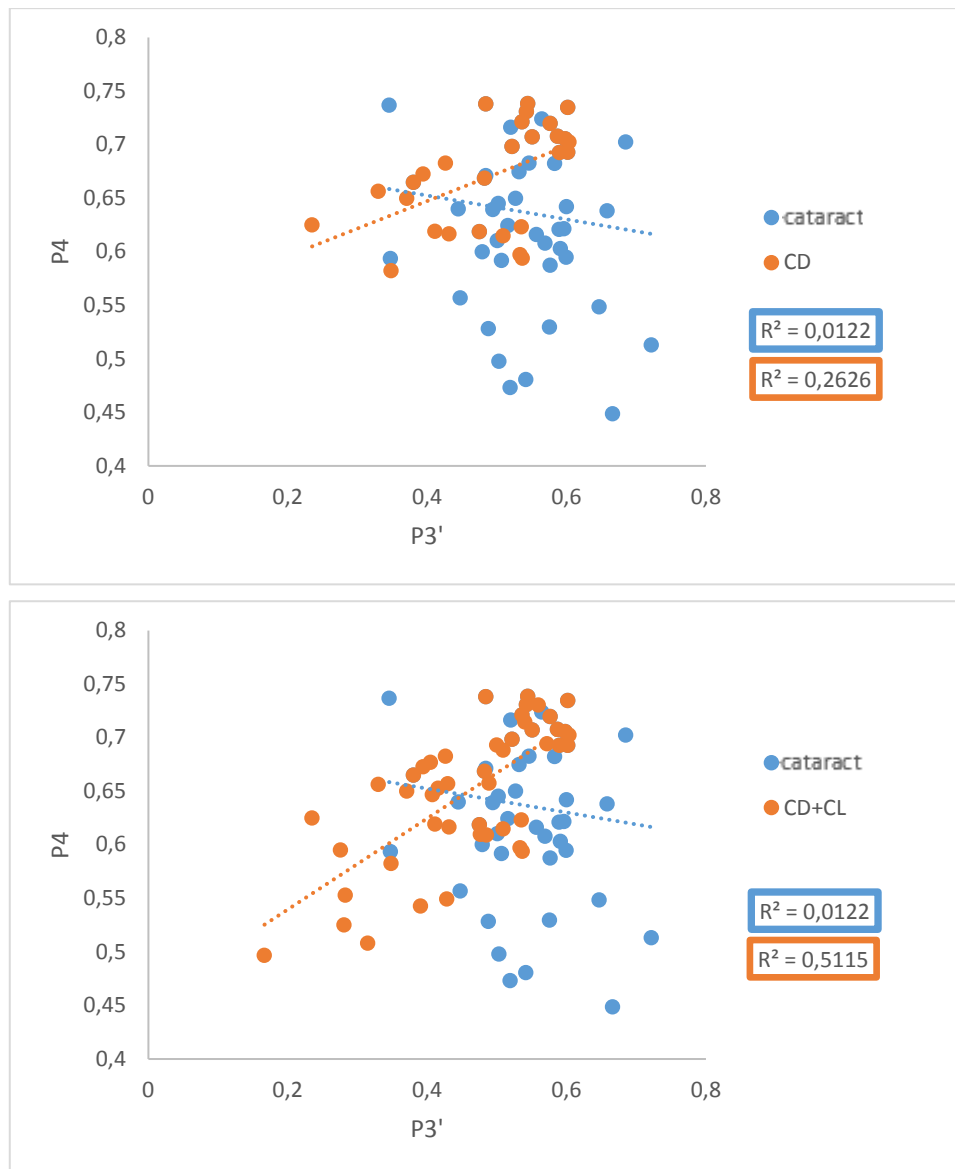
Figure 5.27. Scatterplots and corresponding linear regression (R^2) of P4 contrast as a function of P3'. (Top) Eyes with cataracts in blue, and with CD in orange. (Bottom) Eyes with cataracts in blue, eyes with CD and wearing scatter-costumized CLs in orange.

No significant correlations were found between P3' and P4 contrasts for eyes with cataracts ($r = -0.11$, $p > 0.05$). However, there were significant correlations when eyes with CD were considered ($r = 0.51$, $p = 0.005$); the correlation was even higher when data from eyes wearing scatter-customized CLs was also included in the analysis ($r = 0.716$, $p < 0.001$).

As we already did in the analysis of the eyes with cataracts, here we show a boxplot of P3' as a function of the LOCS III classification (Figure 5.28). In section 5.2.2 we found agreement between cataract grade and P3 contrast, but here, after applying the compensation of the GPI effect, the P3' value becomes independent

of the cataract severity. An ANOVA test confirmed that there were no statistical significant differences between the LOCS III groups in terms of P3' (p>0.05). Again, this confirms that P3' is not influenced by the lens scattering.
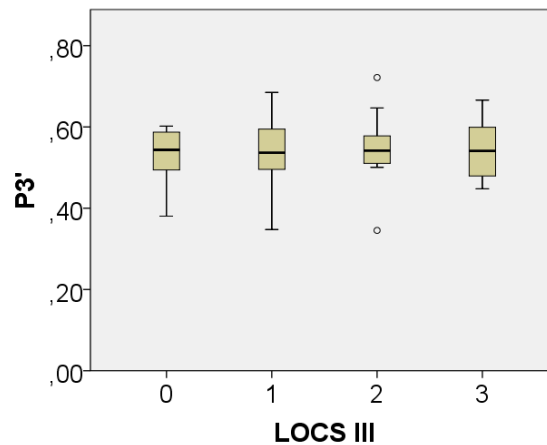
Figure 5.28. Boxplot showing P3' as a function of the LOCS III classification (NO1, NO2, and NO3) and the control group (0). Five statistical descriptors are shown in these plots: maximum, third quartile, median, first quartile and minimum as well as the outliers.

Figure 5.29 shows the boxplots of P3, P3' and P4 contrasts for eyes of the control group, with cataracts and CD, and wearing customized CLs (CL). As it can be seen, P3 contrast was higher in eyes of the control group than in the others making evident that cataracts influence P3. A t-test confirmed that there were significant statistical differences between the control and cataract groups (p < 0.001) and between the control and CL groups (p = 0.005), but there were no differences between the cataract and CL groups (p>0.05), and between cataracts and CDs (p > 0.05). Nevertheless, P3' showed similar values for those eyes with healthy corneas (control and cataract groups) (p > 0.05) while smaller values were obtained for eyes with CD and induced corneal scattering (CL), where we found statistical significant differences (p < 0.001). Finally, P4 contrast showed differences between healthy eyes and eyes with scattering (cornea or lens) (p < 0.001), but not between cataract and CL groups (p > 0.05).
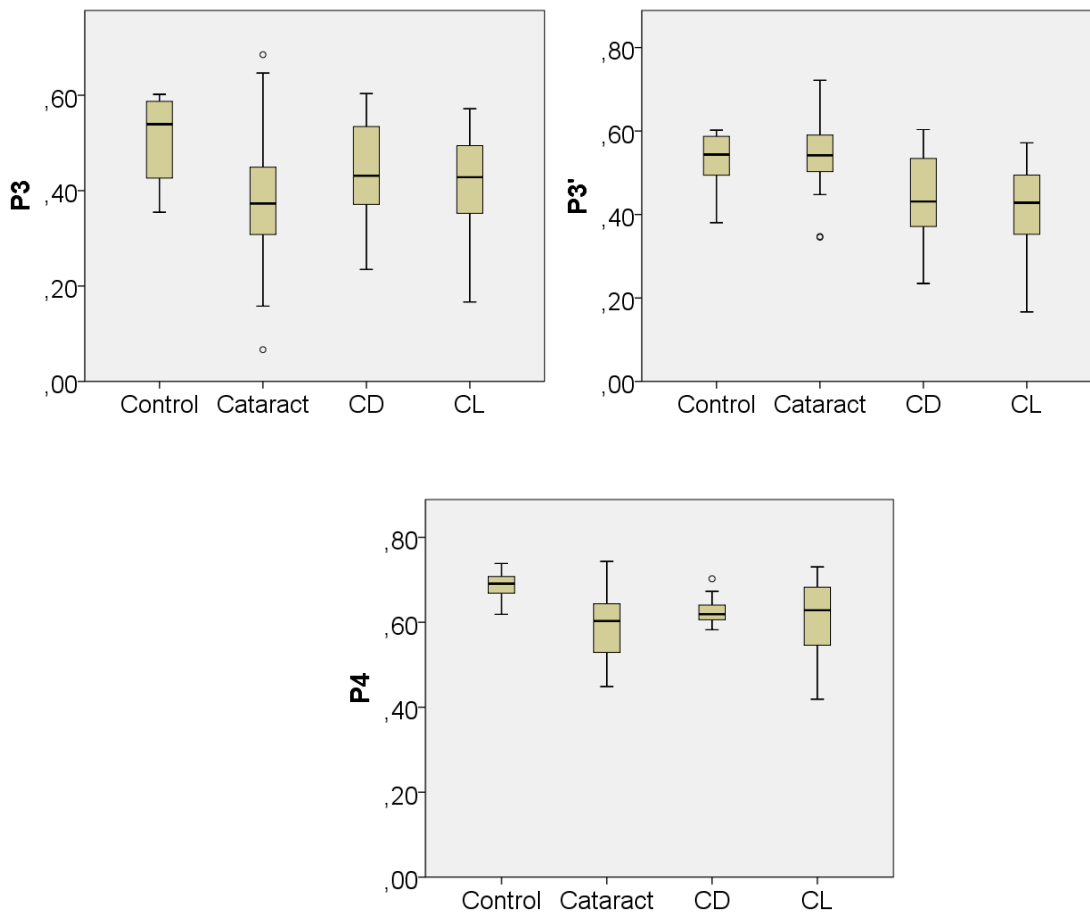
Figure 5.29. Boxplots showing P3, P3' and P4 contrasts for eyes of the control group as well as with cataract, CD or wearing customized CLs. Five statistical descriptors are shown in these plots: maximum, third quartile, median, first quartile and minimum as well as the outliers.

6 Conclusions

In this thesis, the main goal of developing a novel experimental system based on the acquisition of Purkinje images to quantify the intraocular scattering associated with the cornea and the lens individually was achieved. Specifically, the use the third (P3) and fourth (P4) Purkinje images formed by reflection of light on the first and second surfaces of the lens was proposed to do so. The hypothesis that P3 is mainly affected by the light scattered in the cornea (and also the anterior chamber) while P4 is additionally affected by the scattering produced inside the lens was demonstrated, although some corrections were finally needed in some eyes with cataracts.

The specific achievements of this thesis as well as the most relevant conclusions obtained are outlined in more detail below.

1. Purkinje system and novel method for the assessment of scattering:

a. We designed a system to acquire the third (P3) and fourth (P4) Purkinje images. For this purpose, an optimal stimulus was designed with a vertical pattern composed of two slits and a central dark fringe between them, in which only scattered light is expected to be. Different geometrical configurations to avoid overlapping among images were considered.

b. In order to validate our initial hypothesis - i. e., that P3 is mainly affected by the light scattered in the cornea while P4 is additionally affected by the scattering produced inside the lens - we performed some preliminary simulations. They allowed us to analyze the effect of scattering on the light intensity distribution of the Purkinje images validating the hypothesis of the work at a theoretical level.

c. An experimental system to work at the laboratory level was developed. It included a xenon lamp, an opaque plate with two slits, diffusors attached to the anterior and posterior surfaces of the opaque plate, a long-pass filter to work in the near infrared (NIR) avoiding therefore pupil's contraction, and a camera attached to a telecentric lens to acquire all images at the same time. A chinrest was also used to minimize the patients' movements during measurements while simultaneously improving comfort.

d. A novel method was proposed for the assessment of the scattering related with the cornea (and the anterior chamber) and the lens based on the computation of the contrasts of the P3

and P4 images. Two contrasts were computed with the Michaelson formula for each Purkinje image from the intensity profile of the stimulus, and the averaged one was finally used as the scattered light outcome.

e. We also developed a clinical prototype to work in a clinical environment. A low intensity blue light-emitting diode (LED) was added as a fixation target and an additional long-pass filter was included to avoid this light reaching the camera. We also added a stepper motor to control for the distance between the system and the patient's eye to acquire the images at the best focus position. The system was enclosed inside a black box and mounted on a breadboard, which allowed the system to be moved as a whole.

f. In order to proceed with the Ethical Committee approval and to launch the system in hospitals, irradiance and radiance measurements were done according to the standard ISO 15004-2:2007 "Ophthalmic instruments -- Fundamental requirements and test methods -- Part 2: Light hazard protection", to ensure that the system provided light emissions under the limits established by this regulation and to guarantee that patients could not be accidentally damaged under any circumstance.

2. Validation of the system at the laboratory level (proof of concept):

a. In-vitro validation:

- We firstly validated the novel technique to assess scattering related with the cornea and the lens by means of two artificial eyes. We induced different controlled levels of corneal and lens scattering by using several commercial diffusion filters. To simulate corneal opacifications, filters were placed in front of the artificial eye. To simulate lens scattering, filters with optical characteristics that resembled early and mature cataracts were placed in between two plano-convex lenses acting as the artificial lens.

- Experimental results revealed that P3 and P4 contrasts decrease as the corneal scattering increases, while the P4 contrast decreases as the lens scattering increases while the P3 contrast remains constant. Therefore, the Purkinje system was shown to be a useful tool to separate the contribution of the cornea and the lens to the total scattered light.

    b.   In-vivo validation:

- The Purkinje system was also used to assess corneal and lens scattering of a small group of volunteers (13) as a means of validating its usefulness before going to a clinical environment. Nine healthy eyes, 3 eyes with cataracts and 1 with a corneal opacity were included in the analysis.

- The eye with corneal opacification had lower P3 and P4 contrasts than healthy eyes. However, eyes with cataracts were also linked to lower P3 and P4 contrast values, although P3 contrast was expected to remain constant in this case. These results suggested that the in-vivo P3 contrast is not only affected by corneal scattering as assumed initially.

- Since a dependency of P3 contrast on age was observed (P3 contrast values decreased notably with age while P4 contrast remained more constant), we hypothesized that the roughness of the anterior lens surface (orange peel effect), which is age dependent, could play a role in the measured P3 contrast.

3.   Clinical Study:

    a.   A clinical study was conducted at the University Vision Center - CUV (Terrassa, Spain) and Hospital CIMA Sanitas (Barcelona, Spain) to validate the proposed technique. The study included the analysis of 46 eyes with nuclear cataracts graded from NO1 to NO3 (Nuclear Opalescence) at the LOCSIII classification system, and 11 eyes with corneal disorders (CD) such as keratitis, cornea Verticillata, Fuchs dystrophy and complications from laser refractive surgery (Femto-LASIK). Twenty-five and 17 eyes of healthy subjects were used as control groups in the study of patients with cataracts and with CD, respectively.

    b.   The outcomes in terms of P3 and P4 contrasts given by our novel system were compared with the intraocular scattering measured in terms of densitometry obtained with the Pentacam Scheimpflug camera, the OSI (Objective Scatter Index) from the HD Analyzer, and the Log(S) from the C-Quant straylight meter.

c. In the analysis of cataracts, all scattering parameters were in agreement with the LOCS III grade (NO). There were statistically significant differences between eyes of the control and cataract groups in terms of any of the parameters analyzed. Both Purkinje contrasts (P3 and P4) as well as OSI, Log(S) and densitometry significantly correlated between each other ($p < 0.05$). However, all correlations in terms of P3 contrast were weaker than in terms of P4 contrast.

d. There were significant correlations between all parameters and age. Although we did not find a significant correlation between P3 contrast and age in healthy eyes, a correlation between age and P3 contrast was found when considering also eyes with cataracts. This result indicated that, unexpectedly, cataracts influence to some extent the P3 contrast. From a qualitative point of view, the detailed analysis of our Purkinje images in eyes with cataracts revealed that in some cases a ghost image – which seems to be related with the hyperreflective lens areas with different refractive indexes - appears between P3 and P4 (in most of the cases it overlaps with P3) affecting thus the P3 contrast computation. Therefore, the ghost image could explain the fact that cataracts affect the P3 contrast, although it was expected to be independent of the lens scattering.

e. In the analysis of eyes with CD, no statistically significant correlations could be established between scattering and age as these are not age-related pathologies. Statistically significant differences in terms of all variables analyzed were observed between healthy eyes and eyes with CD. P4 correlated with all the other scattering parameters ($p < 0.05$) validating the new method as a useful technique for assessing corneal and lens scattering in an objective way. Although P3 and P4 contrasts showed a strong correlation between them, as expected, no significant correlations could be established between some of the other parameters probably due to differences behind the technologies employed (e. g. measured area), and the smaller sample size.

f. To overcome the former limitations, an additional study with 4 healthy eyes wearing scatter-customized CLs was carried out with the following degrees of scattering: low, medium, high and very high, to simulate different levels of corneal opacification. The contrasts of the third and fourth Purkinje images were significantly different among groups. Results showed agreement between both Purkinje contrasts and the Log(S) although not in terms of OSI, probably due to the fact that double-pass measurements were influenced by the tear film degradation due to the contact lenses. This demonstrated the ability of our

novel method to assess the corneal scattering in patients with different controlled levels of corneal scattering in terms of P3 and P4 contrasts.

4. Compensation of the P3 contrast in eyes with ghost images:

   a. A new methodology was proposed based on the maximum intensity of the Ghost Purkinje Image to remove the effect of some cataracts on the contrast of the third Purkinje Image.

   b. After applying the linear compensation, a new contrast was calculated (P3'), which is shown to provide information about the corneal scattering independently of the lens scattering, while P4 has information about the lens and corneal scattering altogether.

7   Future Work

In this chapter, some lines of research are suggested for future work related with this thesis:

1. More sophisticated strategies to remove the effect of cataracts (backscattered light and internal reflections) from the P3 contrast should be explored:

    a. Through the complementary assessment of the roughness of the anterior surface of the lens by means of techniques such as Optical Coherence Tomography (OCT).

    b. Carrying out a deeper study on the so-called hyperreflective areas and discontinuity zones of the human lens and their relationship with the Ghost Purkinje Images (GPI) found in eyes with cataracts.

    c. Developing more complex algorithms to remove the effect of the GPI on the P3 contrast considering not only the maximum intensity but information about the distance between the GPI and P3, etc.

2. A clinical study including more mature cataracts should be conducted to validate the novel technique as well as the proposed P3 contrast compensation (to remove the influence of the GPI) in a wider sample. In the study conducted in this thesis, only eyes with NO1-NO3 in the LOCSIII classification system were included.

3. Implementation of algorithms to widen the dynamic range of the system by means of the adaptation of the exposure time of the camera or the light source intensity in order to be able to quasi-simultaneously analyze the first Purkinje image, P1(+P2), besides P3 and P4. Tear film quality or defects on the corneal surface may play a role in the computed contrasts and thus, scattering, and this could be taken into account.

4. The developed Purkinje prototype could be improved by means of new technologies available. For instance, the stimulus could be generated with a micro projector or a display instead of using a static stimulus with a specific separation between fringes. This would be useful to test the effect of using different spatial frequencies on the computed contrast.

5. A revision towards a pre-industrial prototype should be carried out to obtain a fully-functional commercial device for a clinical environment. Some aspects that could be revised are the following:

   a. Development of fast algorithms to automate the acquisition process as well as the image processing and analysis.

   b. Studying if a low-cost camera is enough to assess the Purkinje image contrast fluctuations due to scattering.

   c. Looking for alternative light sources with enough emission but with a lower cost such as LEDs.

6. The Purkinje system could be coupled to a double-pass system for the assessment of scattering, providing complementary information of the corneal and lens scattered light. This study can provide a better insight into the impact of the retinal scattering or the higher order aberrations on double-pass measurements, which might be useful for the scientific community.

8 Dissemination

8.1 Journals

Santos, P.; Martínez-Roda, J.A.; Ondategui, JC; Díaz-Doutón, Vilaseca, M. (2018): "System based on the contrast of Purkinje images to measure corneal and lens scattering". Submitted to *Biomed. Opt. Express.* (May 2018).

8.2 Conferences

1. Santos, P.; Vilaseca, M.; Martínez-Roda, J.A.; Ondategui, JC; Díaz-Doutón, F.; Pujol, J. (2017): "Novel system for measuring the scattering associated to the cornea and the lens". Annual Meeting of the Association for Research in Vision and Ophthalmology, Baltimore, USA. *Invest. Ophthalmol. Vis. Sci.* 2017;58(8):2713.

2. Santos, P.; Martínez-Roda, J.A.; Ondategui, JC; Cazal, J.; Ballesta, M.; Díaz-Doutón, F.; Pujol, J.; Vilaseca, M. (2018): "Assessment of corneal scattering using Purkinje images". Annual Meeting of the Association for Reasearch in Vision and Opthalmology, Honolulu, USA.

3. Santos, P.; Martínez-Roda, J.A.; Ondategui, JC; Cazal, J.; Ballesta, M.; Díaz-Doutón, F.; Pujol, J.; Vilaseca, M. (2018): "Validation of a novel method based on the contrast of Purkinje images for the assessment of scattering in eyes with cataracts". 9th European Meeting on Visual and Physiological Optics, Athens, Greece (August 2018) (accepted).

8.3 Patents

Title: Método para medir la difusión intraocular que afecta a diferentes medios oculares del ojo y productos de programa de ordenador del mismo.

Public Inventors: Vilaseca, M.; Pujol, J.; Santos, P.

Application number: P201730663

Country: Spain

Applicant: Universitat Politècnica de Catalunya

9 Bibliography

[1]   W. H. Organization, "Fact Sheet N°282, Updated August 2014."

[2]   R. R. A. Bourne et al.," *Lancet. Glob. Heal.*, vol. 5, no. 9, pp. e888–e897, Sep. 2017.

[3]   R. Legood, P. Scuffham, and C. Cryer, "Are we blind to injuries in the visually impaired? A review of the literature.," *Inj. Prev.*, vol. 8, no. 2, pp. 155–60, Jun. 2002.

[4]   J. M. Wood, M. J. Collins, A. Chaparro, R. Marszalek, T. Carberry, P. Lacherez, and B. S. Chu, "Differential Effects of Refractive Blur on Day and Nighttime Driving Performance," *Investig. Opthalmology Vis. Sci.*, vol. 55, no. 4, p. 2284, Apr. 2014.

[5]   S. Karande and M. Kulkarni, "Poor school performance," *Indian J. Pediatr.*, vol. 72, no. 11, pp. 961–967, Nov. 2005.

[6]   S. Marcos, "A European Strategic Roadmap for Vision Research and Ophthalmology.," 2012.

[7]   S. Marcos, "Image quality of the human eye.," *Int. Ophthalmol. Clin.*, vol. 43, no. 2, pp. 43–62, Jan. 2003.

[8]   von F. Zernike, "Beugungstheorie des schneidenver-fahrens und seiner verbesserten form, der phasenkontrastmethode," *Physica*, vol. 1, no. 7–12, pp. 689–704, May 1934.

[9]   J. K. IJspeert, P. W. de Waard, T. J. van den Berg, and P. T. de Jong, "The intraocular straylight function in 129 healthy volunteers; dependence on angle, age and pigmentation.," *Vision Res.*, vol. 30, no. 5, pp. 699–707, 1990.

[10]   T. J. T. P. van den Berg, L. Franssen, and J. E. Coppens, "Ocular Media Clarity and Straylight," in *Encyclopedia of the Eye*, Elsevier, 2010, pp. 173–183.

[11]   D. P. Piñero, D. Ortiz, and J. L. Alio, "Ocular scattering.," *Optom. Vis. Sci.*, vol. 87, no. 9, pp. E682-96, Sep. 2010.

[12]   P. W. de Waard, J. K. IJspeert, T. J. van den Berg, and P. T. de Jong, "Intraocular light scattering in age-related cataracts.," *Invest. Ophthalmol. Vis. Sci.*, vol. 33, no. 3, pp. 618–25, Mar. 1992.

[13]   H. V Gimbel and A. A. Dardzhikova, "Consequences of waiting for cataract surgery.," *Curr. Opin. Ophthalmol.*, vol. 22, no. 1, pp. 28–30, Jan. 2011.

[14]   D. W. Hahn, "Light Scattering Theory," 2009.

[15]   W. Heisenberg, "Über den anschaulichen Inhalt der quantentheoretischen Kinematik und Mechanik," *Zeitschrift für Phys.*, vol. 43, no. 3–4, pp. 172–198, Mar. 1927.

[16]   P. Artal, "Image Formation in the Living Human Eye," *Annu. Rev. Vis. Sci.*, vol. 1, no. 1, pp. 1–17, Nov. 2015.

[17]   J. I. Prydal, P. Artal, H. Woon, and F. W. Campbell, "Study of human precorneal tear film thickness and structure using laser interferometry.," *Invest. Ophthalmol. Vis. Sci.*, vol. 33, no. 6, pp. 2006–11, May 1992.

[18]   R. H. Rengstorff, "The precorneal tear film: breakup time and location in normal subjects.," *Am. J. Optom. Physiol. Opt.*, vol. 51, no. 10, pp. 765–9, Oct. 1974.

[19]   T. J. Licznerski, H. T. Kasprzak, and W. Kowalik, "Application of twyman-green interferometer for evaluation of in vivo breakup characteristic of the human tear film.," *J. Biomed. Opt.*, vol. 4, no. 1, pp. 176–82, Jan. 1999.

[20]   R. Tutt, A. Bradley, C. Begley, and L. N. Thibos, "Optical and visual impact of tear break-up in human eyes.," *Invest. Ophthalmol. Vis. Sci.*, vol. 41, no. 13, pp. 4117–23, Dec. 2000.

[21]   A. Benito, G. M. Pérez, S. Mirabet, M. Vilaseca, J. Pujol, J. M. Marín, and P. Artal, "Objective optical assessment of tear-film quality dynamics in normal and mildly symptomatic dry eyes.," *J. Cataract Refract. Surg.*, vol. 37, no. 8, pp. 1481–7, Aug. 2011.

[22]   A. Behrens, J. J. Doyle, L. Stern, R. S. Chuck, P. J. McDonnell, D. T. Azar, H. S. Dua, M. Hom, P. M. Karpecki, P. R. Laibson, M. A. Lemp, D. M. Meisler, J. M. del Castillo, T. P. O??Brien, S. C. Pflugfelder, M. Rolando, O. D. Schein, B. Seitz, S. C. Tseng, G. van Setten, S. E. Wilson, and S. C. Yiu, "Dysfunctional Tear Syndrome," *Cornea*, vol. 25, no. 8, pp. 900–907, Sep. 2006.

[23]   J. J. Chen, K. Rao, and S. C. Pflugfelder, "Corneal epithelial opacity in dysfunctional tear syndrome.," *Am. J. Ophthalmol.*, vol. 148, no. 3, pp. 376–82, Sep. 2009.

[24]   J. Artigas J.M., Capilla, P., Felipe, A. y Pujol, *Óptica Fisiológica. Psicofísica de la Visión*. New York: Mc Graw-Hill, 1995.

[25]   D. M. MAURICE, "The structure and transparency of the cornea.," *J. Physiol.*, vol. 136, no. 2, pp. 263–86, Apr. 1957.

[26]   D. M. Albert and F. A. Jakobiec, *Principles and practice of ophthalmology*. W.B. Saunders Co, 2000.

[27] M. Levin, M. Campos, A. Dennison, P. De Guzman, A. M. Tabrizi, and H. Fu, "Measurement of light reflection and scatter from eyes," *Invest. Ophthalmol. Vis. Sci.*, vol. 54, no. 15, p. 1483, Jun. 2013.

[28] M. J. Costello, S. Johnsen, K. O. Gilliland, C. D. Freel, and W. C. Fowler, "Predicted Light Scattering from Particles Observed in Human Age-Related Nuclear Cataracts Using Mie Scattering Theory," *Investig. Opthalmology Vis. Sci.*, vol. 48, no. 1, p. 303, Jan. 2007.

[29] D. Whitaker, D. B. Elliott, and R. Steen, "Confirmation of the validity of the psychophysical light scattering factor.," *Invest. Ophthalmol. Vis. Sci.*, vol. 35, no. 1, pp. 317–21, Jan. 1994.

[30] T. Oshika, M. Mori, and M. Araie, "A new approach to the study of aqueous humor dynamics by measuring the intensity of Tyndall's effect.," *J. Fr. d'ophtalmologie*, vol. 13, no. 10, pp. 471–80, 1990.

[31] G. B. Arden, "The importance of measuring contrast sensitivity in cases of visual disturbance," *British Journal of Ophthalmology*, vol. 62, no. 4. pp. 198–209, 1978.

[32] A. P. Ginsburg, "A new contrast sensitivity vision test chart," *Am. J. Optom. Physiol. Opt.*, vol. 61, no. 6, pp. 403–407, 1984.

[33] H. S. Jones, M. J. Moseley, and J. R. Thompson, "Reliability of the Cambridge Low Contrast Gratings," *Ophthalmic Physiol. Opt.*, vol. 14, no. 3, pp. 287–289, 1994.

[34] D. G. Pelli, J. G. Robson, and A. J. Wilkins, "The design of a new letter chart for measuring contrast sensitivity," *Clinical Vision Sciences*, vol. 2, no. 3. pp. 187–199, 1988.

[35] K. Ehrmann, C. Fedtke, and A. Radić, "Assessment of computer generated vision charts.," *Cont. Lens Anterior Eye*, vol. 32, no. 3, pp. 133–40, Jun. 2009.

[36] J. T. Holladay, T. C. Prager, J. Trujillo, and R. S. Ruiz, "Brightness acuity test and outdoor visual acuity in cataract patients," *J. Cataract Refract. Surg.*, vol. 13, no. 1, pp. 67–69, 1987.

[37] L. L. HOLLADAY, "ACTION OF A LIGHT-SOURCE IN THE FIELD OF VIEW IN LOWERING VISIBILITY," *J. Opt. Soc. Am.*, vol. 14, no. 1, p. 1, Jan. 1927.

[38] W. S. Stiles, "The Effect of Glare on the Brightness Difference Threshold," *Proc. R. Soc. B Biol. Sci.*, vol. 104, no. 731, pp. 322–351, Mar. 1929.

[39] J. J. Vos, "On the cause of disability glare and its dependence on glare angle, age and ocular pigmentation," *Clin. Exp. Optom.*, vol. 86, no. 6, pp. 363–370, Nov. 2003.

[40]   R. C. Augusteyn, "Growth of the human eye lens.," *Mol. Vis.*, vol. 13, pp. 252–7, Feb. 2007.

[41]   Ij. J. van den Berg TJTP, "Intraocular straylight, studied using the direct comparison technique," in *CIE proceedings 22 session*, 1991, pp. 83–4.

[42]   T. J. T. P. Van Den Berg, "Importance of pathological intraocular light scatter for visual disability," *Doc. Ophthalmol.*, vol. 61, no. 3–4, pp. 327–333, Jan. 1986.

[43]   T. J. van den Berg and J. K. Ijspeert, "Clinical assessment of intraocular stray light.," *Appl. Opt.*, vol. 31, no. 19, pp. 3694–6, Jul. 1992.

[44]   B. Hohberger, R. Laemmer, W. Adler, A. G. M. Juenemann, and F. K. Horn, "Measuring contrast sensitivity in normal subjects with OPTEC 6500: influence of age and glare.," *Graefe's Arch. Clin. Exp. Ophthalmol. = Albr. von Graefes Arch. für Klin. und Exp. Ophthalmol.*, vol. 245, no. 12, pp. 1805–14, Dec. 2007.

[45]   T. J. T. P. van den Berg, J. K. Ijspeert, and P. W. T. de Waard, "Dependence of intraocular straylight on pigmentation and light transmission through the ocular wall," *Vision Res.*, vol. 31, no. 7–8, pp. 1361–1367, Jan. 1991.

[46]   P. W. T. De Waard, J. K. Ijspeert, T. J. T. P. Van den Berg, and P. T. V. M. De Jong, "Intraocular light scattering in age-related cataracts," in *Investigative Ophthalmology and Visual Science*, 1992, vol. 33, no. 3, pp. 618–625.

[47]   T. J. T. P. van den Berg, L. Franssen, B. Kruijt, and J. E. Coppens, "History of ocular straylight measurement: A review.," *Zeitschrift für medizinische Phys.*, vol. 23, no. 1, pp. 6–20, Feb. 2013.

[48]   J. E. Coppens, L. Franssen, L. J. van Rijn, and T. J. T. P. van den Berg, "Reliability of the compensation comparison stray-light measurement method.," *J. Biomed. Opt.*, vol. 11, no. 3, p. 34027, Jan. 2006.

[49]   L. Franssen, J. E. Coppens, and T. J. T. P. van den Berg, "Compensation comparison method for assessment of retinal straylight.," *Invest. Ophthalmol. Vis. Sci.*, vol. 47, no. 2, pp. 768–76, Feb. 2006.

[50]   L. T. Chylack, J. K. Wolfe, D. M. Singer, M. C. Leske, M. A. Bullimore, I. L. Bailey, J. Friend, D. McCarthy, and S. Y. Wu, "The Lens Opacities Classification System III. The Longitudinal Study of Cataract Study Group.," *Arch. Ophthalmol. (Chicago, Ill. 1960)*, vol. 111, no. 6, pp. 831–6, Jun. 1993.

[51]   T. J. van den Berg, "Light scattering by donor lenses as a function of depth and wavelength.," *Invest.*

Ophthalmol. Vis. Sci., vol. 38, no. 7, pp. 1321–32, Jun. 1997.

[52]   T. J. van den Berg and H. Spekreijse, "Light scattering model for donor lenses as a function of depth.," *Vision Res.*, vol. 39, no. 8, pp. 1437–45, Apr. 1999.

[53]   T. Shcheimpflug, (1904) "*Method of distorting plane images by means of lenses or mirrors.*," US751347A.

[54]   R. Jain and S. Grewal, "Pentacam: Principle and Clinical Applications," *Curr. J. Glaucoma Pract. with DVD*, pp. 20–32, May 2009.

[55]   P. Rosales and S. Marcos, "Pentacam Scheimpflug quantitative imaging of the crystalline lens and intraocular lens.," *J. Refract. Surg.*, vol. 25, no. 5, pp. 421–8, May 2009.

[56]   M. A. Vivino, S. Chintalagiri, B. Trus, and M. Datiles, "Development of a Scheimpflug slit lamp camera system for quantitative densitometric analysis.," *Eye (Lond).*, vol. 7 (Pt 6), pp. 791–8, Jan. 1993.

[57]   J. Waser, *Quantitative Chemistry*. W.A. Benjamin, 1964.

[58]   J.-S. Kim, S.-H. Chung, and C.-K. Joo, "Clinical application of a Scheimpflug system for lens density measurements in phacoemulsification.," *J. Cataract Refract. Surg.*, vol. 35, no. 7, pp. 1204–9, Jul. 2009.

[59]   M. B. Datiles, R. R. Ansari, and G. F. Reed, "A clinical study of the human lens with a dynamic light scattering device.," *Exp. Eye Res.*, vol. 74, no. 1, pp. 93–102, Jan. 2002.

[60]   R. R. Ansari, "Ocular static and dynamic light scattering: a noninvasive diagnostic tool for eye research and clinical practice.," *J. Biomed. Opt.*, vol. 9, no. 1, pp. 22–37, Jan. .

[61]   E. H. Petra Schwille, "Petra Schwille and Elke Haustein Fluorescence Correlation Spectroscopy 1 Fluorescence Correlation Spectroscopy An Introduction to its Concepts and Applications."

[62]   A. Einstein, "Über die von der molekularkinetischen Theorie der Wärme geforderte Bewegung von in ruhenden Flüssigkeiten suspendierten Teilchen," *Ann. Phys.*, vol. 322, no. 8, pp. 549–560, 1905.

[63]   M. Azharuddin, J. Khandelwal, H. Datta, A. K. Dasgupta, and S. O. Raja, "Dry eye: a protein conformational disease.," *Invest. Ophthalmol. Vis. Sci.*, vol. 56, no. 3, pp. 1423–9, Mar. 2015.

[64]   G. M. Thurston, D. L. Hayden, P. Burrows, J. I. Clark, V. G. Taret, J. Kandel, M. Courogen, J. A. Peetermans, M. S. Bowen, D. Miller, K. M. Sullivan, R. Storb, H. Stern, and G. B. Benedek, "Quasielastic light scattering study of the living human lens as a function of age.," *Curr. Eye Res.*,

vol. 16, no. 3, pp. 197–207, Mar. 1997.

[65] L. Rovati, F. Fankhauser, and J. Ricka, "Design and performance of a new ophthalmic instrument for dynamic light-scattering measurements in the human eye," *Rev. Sci. Instrum.*, vol. 67, no. 7, p. 2615, Aug. 1996.

[66] H. S. Dhadwal and J. Wittpenn, "In vivo dynamic light scattering characterization of a human lens: cataract index.," *Curr. Eye Res.*, vol. 20, no. 6, pp. 502–10, Jun. 2000.

[67] R. R. Ansari, M. B. Datiles III, J. F. King, and D. Leftwood, "<title>Measuring lens opacity: combining quasi-elastic light scattering with Scheimpflug imaging system</title>," in *BiOS '98 International Biomedical Optics Symposium*, 1998, pp. 35–42.

[68] F. Díaz-Doutón, A. Benito, J. Pujol, M. Arjona, J. L. Güell, and P. Artal, "Comparison of the retinal image quality with a Hartmann-Shack wavefront sensor and a double-pass instrument.," *Invest. Ophthalmol. Vis. Sci.*, vol. 47, no. 4, pp. 1710–6, Apr. 2006.

[69] W. J. Donnelly, K. Pesudovs, J. D. Marsack, E. J. Sarver, and R. A. Applegate, "Quantifying scatter in Shack-Hartmann images to evaluate nuclear cataract.," *J. Refract. Surg.*, vol. 20, no. 5, pp. S515-22, Jan. .

[70] T. Mihashi, Y. Hirohara, K. Bessho, N. Maeda, T. Oshika, and T. Fujikado, "Intensity analysis of Hartmann-Shack images in cataractous, keratoconic, and normal eyes to investigate light scattering.," *Jpn. J. Ophthalmol.*, vol. 50, no. 4, pp. 323–33, Jan. .

[71] J. Santamaría, P. Artal, and J. Bescós, "Determination of the point-spread function of human eyes using a hybrid optical-digital method.," *J. Opt. Soc. Am. A.*, vol. 4, no. 6, pp. 1109–14, Jun. 1987.

[72] P. Artal, S. Marcos, D. R. Williams, and R. Navarro, "Odd aberrations and double-pass measurements of retinal image quality," *J. Opt. Soc. Am. A*, vol. 12, no. 2, p. 195, Feb. 1995.

[73] M. Vilaseca, E. Peris, J. Pujol, R. Borras, and M. Arjona, "Intra- and Intersession Repeatability of a Double-Pass Instrument," *Optom. Vis. Sci.*, vol. 87, no. 9, pp. 675–681, Sep. 2010.

[74] J. A. Martínez-Roda, M. Vilaseca, J. C. Ondategui, A. Giner, F. J. Burgos, G. Cardona, and J. Pujol, "Optical quality and intraocular scattering in a healthy young population," *Clin. Exp. Optom.*, vol. 94, no. 2, pp. 223–229, Mar. 2011.

[75] A. Saad, M. Saab, and D. Gatinel, "Repeatability of measurements with a double-pass system," *J. Cataract Refract. Surg.*, vol. 36, no. 1, pp. 28–33, Jan. 2010.

[76] P. Artal, A. Benito, G. M. Pérez, E. Alcón, A. De Casas, J. Pujol, and J. M. Marín, "An objective

scatter index based on double-pass retinal images of a point source to classify cataracts.," *PLoS One*, vol. 6, no. 2, p. e16823, Jan. 2011.

[77] M. Vilaseca, M. J. Romero, M. Arjona, S. O. Luque, J. C. Ondategui, A. Salvador, J. L. Güell, P. Artal, and J. Pujol, "Grading nuclear, cortical and posterior subcapsular cataracts using an objective scatter index measured with a double-pass system.," *Br. J. Ophthalmol.*, vol. 96, no. 9, pp. 1204–10, Sep. 2012.

[78] S. A. Lim, J. Hwang, K.-Y. Hwang, and S.-H. Chung, "Objective assessment of nuclear cataract: Comparison of double-pass and Scheimpflug systems," *J. Cataract Refract. Surg.*, vol. 40, no. 5, pp. 716–721, May 2014.

[79] D. R. Williams, D. H. Brainard, M. J. McMahon, and R. Navarro, "Double-pass and interferometric measures of the optical quality of the eye.," *J. Opt. Soc. Am. A. Opt. Image Sci. Vis.*, vol. 11, no. 12, pp. 3123–35, Dec. 1994.

[80] T. J. T. P. van den Berg, "To the Editor: Intra- and Intersession Repeatability of a Double-Pass Instrument," *Optom. Vis. Sci.*, vol. 87, no. 11, pp. 920–921, Nov. 2010.

[81] H. Ginis, G. M. Pérez, J. M. Bueno, and P. Artal, "The wide-angle point spread function of the human eye reconstructed by a new optical method.," *J. Vis.*, vol. 12, no. 3, Jan. 2012.

[82] H. S. Ginis, G. M. Perez, J. M. Bueno, A. Pennos, and P. Artal, "Wavelength dependence of the ocular straylight.," *Invest. Ophthalmol. Vis. Sci.*, 2013.

[83] H. Ginis, O. Sahin, A. Pennos, and P. Artal, "Compact optical integration instrument to measure intraocular straylight.," *Biomed. Opt. Express*, vol. 5, no. 9, pp. 3036–41, Sep. 2014.

[84] O. Sahin, A. Pennos, H. Ginis, L. Hervella, E. A. Villegas, B. Cañizares, J. M. Marin, I. Pallikaris, and P. Artal, "Optical Measurement of Straylight in Eyes With Cataract," *J. Refract. Surg.*, vol. 32, no. 12, pp. 846–850, Dec. 2016.

[85] A. Pennos, H. Ginis, A. Arias, D. Christaras, and P. Artal, "Performance of a differential contrast sensitivity method to measure intraocular scattering.," *Biomed. Opt. Express*, vol. 8, no. 3, pp. 1382–1389, Mar. 2017.

[86] A. Jóźwik, D. Siedlecki, and M. Zając, "Analysis of Purkinje images as an effective method for estimation of intraocular lens implant location in the eyeball," *Opt. - Int. J. Light Electron Opt.*, vol. 125, no. 20, pp. 6021–6025, Oct. 2014.

[87] I. Escudero-Sanz and R. Navarro, "Off-axis aberrations of a wide-angle schematic eye model," *J.*

Opt. Soc. Am. A, vol. 16, no. 8, p. 1881, Aug. 1999.

[88]   Y.-L. Chen, B. Tan, and J. Lewis, "Simulation of eccentric photorefraction images," *Opt. Express*, vol. 11, no. 14, p. 1628, Jul. 2003.

[89]   E. Hecht and Eugene, "Optics 2nd edition," *Opt. 2nd Ed. by Eugene Hecht Reading, MA Addison-Wesley Publ. Company, 1987*, 1987.

[90]   J. M. Bueno, D. De Brouwere, H. Ginis, I. Sgouros, and P. Artal, "Purkinje imaging system to measure anterior segment scattering in the human eye.," *Opt. Lett.*, vol. 32, no. 23, pp. 3447–9, Dec. 2007.

[91]   A. de Castro, P. Rosales, and S. Marcos, "Tilt and decentration of intraocular lenses in vivo from Purkinje and Scheimpflug imaging," *J. Cataract Refract. Surg.*, vol. 33, no. 3, pp. 418–429, Mar. 2007.

[92]   S. Maedel, N. Hirnschall, N. Bayer, S. Markovic, J. Tabernero, P. Artal, F. Schaeffel, and O. Findl, "Comparison of intraocular lens decentration and tilt measurements using 2 Purkinje meter systems," *J. Cataract Refract. Surg.*, vol. 43, no. 5, pp. 648–655, May 2017.

[93]   Y. Nishi, N. Hirnschall, A. Crnej, V. Gangwani, J. Tabernero, P. Artal, and O. Findl, "Reproducibility of intraocular lens decentration and tilt measurement using a clinical Purkinje meter.," *J. Cataract Refract. Surg.*, vol. 36, no. 9, pp. 1529–35, Sep. 2010.

[94]   J. Tabernero, E. Chirre, L. Hervella, P. Prieto, and P. Artal, "The accommodative ciliary muscle function is preserved in older humans," *Sci. Rep.*, vol. 6, no. 1, p. 25551, Jul. 2016.

[95]   T. J. T. P. van den Berg, L. Franssen, and J. E. Coppens, "Straylight in the human eye: testing objectivity and optical character of the psychophysical measurement," *Ophthalmic Physiol. Opt.*, vol. 29, no. 3, pp. 345–350, May 2009.

[96]   J. J. Vos and T. J. T. P. van den Berg, "Report on disability glare," 1999.

[97]   K. Kim, "Monte Carlo Simulation and Experimental analysis of Dense Medium Light scattering, with Applications to Corneal Light Scattering," (Doctoral dissertation) University of Florida, 2003.

[98]   I. Kelly-Pérez, N. C. Bruce, L. R. Berriel-Valdos, A. Werner, and J. A. Delgado Atencio, "Computational model of the effect of light scattering from cataracts in the human eye.," *J. Opt. Soc. Am. A. Opt. Image Sci. Vis.*, vol. 30, no. 12, pp. 2585–94, Dec. 2013.

[99]   H. L. Liou and N. A. Brennan, "Anatomically accurate, finite model eye for optical modeling.," *J. Opt. Soc. Am. A. Opt. Image Sci. Vis.*, vol. 14, no. 8, pp. 1684–95, Aug. 1997.

[100] G. C. De Wit, L. Franssen, J. E. Coppens, and T. J. T. P. Van Den Berg, "Simulating the straylight effects of cataracts," *J. Cataract Refract. Surg.*, vol. 32, no. 2, pp. 294–300, 2006.

[101] A. D. Edelstein, M. A. Tsuchida, N. Amodaj, H. Pinkard, R. D. Vale, and N. Stuurman, "Advanced methods of microscope control using μManager software.," *J. Biol. methods*, vol. 1, no. 2.

[102] "ISO 15004-2:2007 - Ophthalmic instruments -- Fundamental requirements and test methods -- Part 2: Light hazard protection."

[103] A. Agrawal, J. Baxi, W. Calhoun, C.-L. Chen, H. Ishikawa, J. S. Schuman, G. Wollstein, and D. X. Hammer, "Optic Nerve Head Measurements With Optical Coherence Tomography: A Phantom-Based Study Reveals Differences Among Clinical Devices," *Investig. Opthalmology Vis. Sci.*, vol. 57, no. 9, p. OCT413, Jul. 2016.

[104] P. A. Barrionuevo, E. M. Colombo, M. Vilaseca, J. Pujol, and L. A. Issolio, "Comparison between an objective and a psychophysical method for the evaluation of intraocular light scattering," *J. Opt. Soc. Am. A*, vol. 29, no. 7, p. 1293, 2012.

[105] C. M. Oliveira, C. Ribeiro, and S. Franco, "Corneal imaging with slit-scanning and Scheimpflug imaging techniques," *Clin. Exp. Optom.*, vol. 94, no. 1, pp. 33–42, Jan. 2011.

[106] S. Ní Dhubhghaill, J. J. Rozema, S. Jongenelen, I. Ruiz Hidalgo, N. Zakaria, and M.-J. Tassignon, "Normative Values for Corneal Densitometry Analysis by Scheimpflug Optical Assessment," *Investig. Opthalmology Vis. Sci.*, vol. 55, no. 1, p. 162, Jan. 2014.

[107] R. Navarro, J. A. Méndez-Morales, and J. Santamaría, "Optical quality of the eye lens surfaces from roughness and diffusion measurements.," *J. Opt. Soc. Am. A.*, vol. 3, no. 2, pp. 228–34, Feb. 1986.

[108] D. De Brouwere, "Corneal Light Scattering following Excimer Laser Surgery," (Doctoral dissertation) University of Crete, 2008.

[109] R. Michael and A. J. Bron, "The ageing lens and cataract: a model of normal and pathological ageing.," *Philos. Trans. R. Soc. Lond. B. Biol. Sci.*, vol. 366, no. 1568, pp. 1278–92, Apr. 2011.

[110] S. M. Salvi, S. Akhtar, and Z. Currie, "Ageing changes in the eye.," *Postgrad. Med. J.*, vol. 82, no. 971, pp. 581–7, Sep. 2006.

[111] J. A. Martínez-Roda, M. Vilaseca, J. C. Ondategui, M. Aguirre, and J. Pujol, "Effects of aging on optical quality and visual function," *Clin. Exp. Optom.*, vol. 99, no. 6, pp. 518–525, Nov. 2016.

[112] J. A. Martínez-Roda, M. Vilaseca, J. C. Ondategui, L. Almudí, M. Asaad, L. Mateos-Pena, M. Arjona, and J. Pujol, "Double-pass technique and compensation-comparison method in eyes with

cataract," *J. Cataract Refract. Surg.*, vol. 42, no. 10, pp. 1461–1469, Oct. 2016.

[113] T. Bal, T. Coeckelbergh, J. Van Looveren, J. J. Rozema, and M.-J. Tassignon, "Influence of Cataract Morphology on Straylight and Contrast Sensitivity and Its Relevance to Fitness to Drive," *Ophthalmologica*, vol. 225, no. 2, pp. 105–111, 2011.

[114] B. J. Kirkwood, P. L. Hendicott, S. A. Read, and K. Pesudovs, "Repeatability and validity of lens densitometry measured with Scheimpflug imaging," *J. Cataract Refract. Surg.*, vol. 35, no. 7, pp. 1210–1215, Jul. 2009.

[115] X. Pei, Y. Bao, Y. Chen, and X. Li, "Correlation of lens density measured using the Pentacam Scheimpflug system with the Lens Opacities Classification System III grading score and visual acuity in age-related nuclear cataract," *Br. J. Ophthalmol.*, vol. 92, no. 11, pp. 1471–1475, Nov. 2008.

[116] T. J. T. P. Van Den Berg, L. J. (René) Van Rijn, R. Michael, C. Heine, T. Coeckelbergh, C. Nischler, H. Wilhelm, G. Grabner, M. Emesz, R. I. Barraquer, J. E. Coppens, and L. Franssen, "Straylight Effects with Aging and Lens Extraction," *Am. J. Ophthalmol.*, vol. 144, no. 3, p. 358–363.e1, Sep. 2007.

[117] A. C. Tan, S. C. Loon, H. Choi, and L. Thean, "Lens Opacities Classification System III: Cataract grading variability between junior and senior staff at a Singapore hospital," *J. Cataract Refract. Surg.*, vol. 34, no. 11, pp. 1948–1952, Nov. 2008.

[118] E. Prokofyeva, A. Wegener, and E. Zrenner, "Cataract prevalence and prevention in Europe: a literature review," *Acta Ophthalmol.*, vol. 91, no. 5, pp. 395–405, Aug. 2013.

[119] K.-S. Na, Y.-G. Park, K. Han, J. W. Mok, and C.-K. Joo, "Prevalence of and Risk Factors for Age-Related and Anterior Polar Cataracts in a Korean Population," *PLoS One*, vol. 9, no. 6, p. e96461, Jun. 2014.

[120] A. Domínguez-Vicent, U. Birkeldh, L. Carl-Gustaf, M. Nilson, and R. Brautaset, "Objective Assessment of Nuclear and Cortical Cataracts through Scheimpflug Images: Agreement with the LOCS III Scale," *PLoS One*, vol. 11, no. 2, p. e0149249, Feb. 2016.

[121] K. Kamiya, H. Kobashi, A. Igarashi, N. Shoji, and K. Shimizu, "Effect of Light Scattering and Higher-order Aberrations on Visual Performance in Eyes with Granular Corneal Dystrophy," *Sci. Rep.*, vol. 6, no. 1, p. 24677, Jul. 2016.

[122] L. Xu, Y. Wang, J. Li, Y. Liu, W. Wu, H. Zhang, Y. Wu, and G. A. Khan, "Comparison of Forward Light Scatter Changes Between SMILE, Femtosecond Laser-assisted LASIK, and Epipolis LASIK:

Results of a 1-Year Prospective Study," *J. Refract. Surg.*, vol. 31, no. 11, pp. 752–758, Nov. 2015.

[123] S. A. Lim, J. Hwang, K.-Y. Hwang, and S.-H. Chung, "Objective assessment of nuclear cataract: comparison of double-pass and Scheimpflug systems.," *J. Cataract Refract. Surg.*, vol. 40, no. 5, pp. 716–21, May 2014.

[124] A. Crnej, N. Hirnschall, C. Petsoglou, and O. Findl, "Methods for assessing forward and backward light scatter in patients with cataract," *J. Cataract Refract. Surg.*, vol. 43, no. 8, pp. 1072–1076, Aug. 2017.

[125] J. Tomás, D. P. Piñero, and J. L. Alió, "Intra-observer repeatability of optical quality measures provided by a double-pass system," *Clin. Exp. Optom.*, vol. 95, no. 1, pp. 60–65, 2012.

[126] D. Christaras, H. Ginis, A. Pennos, and P. Artal, "Scattering contribution to the double-pass PSF using Monte Carlo simulations," *Ophthalmic Physiol. Opt.*, vol. 37, no. 3, pp. 342–346, May 2017.

[127] M. Bahrami, M. Hoshino, B. Pierscionek, N. Yagi, J. Regini, and K. Uesugi, "Optical properties of the lens: An explanation for the zones of discontinuity," *Exp. Eye Res.*, vol. 124, pp. 93–99, Jul. 2014.

[128] A. de Castro, A. Benito, S. Manzanera, J. Mompeán, B. Cañizares, D. Martínez, J. M. Marín, I. Grulkowski, and P. Artal, "Three-Dimensional Cataract Crystalline Lens Imaging With Swept-Source Optical Coherence Tomography," *Investig. Opthalmology Vis. Sci.*, vol. 59, no. 2, p. 897, Feb. 2018.

Appendix A

"Hoja de información al Paciente"

HOSPITAL CIMA Barcelona	Estudio observacional: Hoja de información al paciente Código del estudio observacional:	Página 1 de 3 Versión: 1 Fecha: 11/07/2017

1. Datos del estudio	
Título del estudio	Validación del sistema basado en el Contraste de las Imágenes de Purkinje para medir la difusión de la córnea y del cristalino
Código del promotor	
Nombre del promotor	CUV-CD6

2. Datos del investigador principal	
Nombre y apellidos del investigador principal	Meritxell Vilaseca Ricart
Núm. de colegiado/da	
Unidad de especialización	
Nombre del centro	Centre Universitari de la Visió de la Universitat Politècnica de Catalunya - BarcelonaTech.

3. Introducción

Nos dirigimos a usted para informarle sobre un estudio de investigación en el que se le invita a participar. El estudio ha estado aprobado por el Comitè d'Ética i Investigació de l'Hospital Universitari Mútua Terrassa, de acuerdo con la legislación vigente, y se realiza respetando los principios enunciados en la declaración de Helsinki y a las normas de buena práctica clínica.

Nuestra intención es que usted reciba la información correcta y suficiente para qué pueda evaluar y juzgar si quiere o no participar en este estudio. Por esto, léase esta hoja informativa con atención y nosotros le aclararemos las dudas que le puedan surgir después de la explicación. Además, puede consultar con las personas que considere oportuno.

4. Participación voluntaria

Tiene que saber que su participación en este estudio es voluntaria y que puede decidir no participar o cambiar su decisión y retirar el consentimiento en cualquier momento, sin que esto afecte la relación con su óptico optometrista ni se produzca ningún prejuicio en su tratamiento.

5. Descripción general del estudio

El objetivo del estudio es validar una nueva técnica para medir la difusión intraocular. La difusión intraocular es la luz que se dispersa dentro del ojo debido a opacificaciones de los medios oculares, como por ejemplo lesiones corneales y cataratas. Tiene un efecto directo en la percepción del contraste y, por lo tanto, afecta a la visión del paciente.

El estudio consistirá en evaluar la difusión intraocular del paciente utilizando diferentes equipos comerciales (biomicroscopio, HD Analyzer, C-Quant y Pentacam) i con el sistema experimental que se quiere validar basado en las imágenes de Purkinje per comparar los resultados obtenidos. Las medidas tendrán una durada de 15~20 minutos.

Las medidas que se harán durante el estudio son no invasivas y no tienen ningún riesgo.

HOSPITAL CIMA
Barcelona

Estudio observacional:
Hoja de información al paciente
Código del estudio observacional:

Página 2 de 3
Versión: 1
Fecha: 11/07/2017

El número total de sujetos que se incluirán en el estudio será de ~150.

6. Beneficios y riesgos derivados de su participación en el estudio

El beneficio derivado esperado de su estudio es mejorar el diagnóstico de patologías relacionadas con la difusión intraocular.
Esta nueva técnica ha estado testeada previamente en el entorno de laboratorio con resultados satisfactorios.

7. Tratamientos alternativos

NO APLICABLE

8. Seguro *(cuando sea necesario)*
NO APLICABLE

9. Confidencialidad

El tratamiento, la comunicación y la cesión de los datos de carácter personal de todos los sujetos participantes se ajustará al que dispone la Llei Orgànica 15/1999, de 13 de desembre, de protección de datos de carácter personal, y su reglamento de desarrollo. De acuerdo a lo establecido en la legislación mencionada, usted puede ejercer sus derechos de acceso, modificación, oposición y cancelación de datos, para esto se tendrá que dirigir al óptico optometrista del estudio.

Sus datos serán tratados informáticamente y se incorporaran a un fichero automatizado de datos de carácter personal que ha estado registrado en la Agencia Española de Protección de Datos.

Sus datos recogidos para el estudio estarán identificados por un código y sólo su óptico optometrista del estudio y colaboradores podrán relacionar estos datos con usted y con su historia clínica. Por lo tanto, su identidad no será revelada a ninguna persona salvo excepciones, en caso de urgencia médica o requerimiento legal.

Solo se transmitirán a terceros y a otros países, previa notificación a la Agencia Española de Protección de Datos, los datos recogidos para el estudio que en ningún caso contendrán información que le pueda identificar directamente, como nombre y apellidos, iniciales, dirección, número de la seguridad social, etc. En el caso de que se produzca esta cesión, será para los mismos fines del estudio descrito y garantizando la confidencialidad como mínimo con el nivel de protección de la legislación vigente en nuestro país.

El acceso a su información personal quedará restringido al óptico optometrista del estudio / colaboradores, autoridades sanitarias, al Comité de Ética de la Investigación del Hospital Universitario Mútua Terrassa y personal autorizado, cuando lo necesiten per comprobar leo datos y procedimientos del estudio, pero siempre manteniendo la confidencialidad de acuerdo con la legislación vigente.

	Estudio observacional:	Página 3 de 3
HOSPITAL CIMA Barcelona	Hoja de información al paciente Código del estudio observacional:	Versión: 1 Fecha: 11/07/2017

10. Compensación económica

Su participación en el estudio no le supondrá ningún gasto y le serán reintegrados los gastos extraordinarios (p. ej. dietas y desplazamientos). No tendrá que pagar por los productos sanitarios del estudio.

11. Otra información relevante

Cualquier información nueva referente a los productos sanitarios utilizados en el estudio y que pueden afectar a su disposición a participar en el estudio, que se descubra durante su participación, le será comunicada por su óptico optometrista lo antes posible.

Si usted decide retirar el consentimiento para participar en este estudio, ningún datp nuevo será añadido en la base de datos y puede exigir la destrucción de todas las muestras identificables previamente retenidas para evitar la realización de nuevos análisis, aunque los responsables del estudio podrán seguir utilizando la información recogida sobre usted hasta este momento, a no ser que usted se oponga expresamente.

También tiene que saber que usted puede ser retirado del estudio en caso de que los responsables del estudio lo consideren oportuno, ya sea por motivos de seguridad, por cualquier acontecimiento adverso que se ocurra por los productos sanitarios o técnicas en estudio o porque consideren que no está cumpliendo con los procedimientos establecidos. En cualquiera de los casos, usted recibirá una explicación adecuada del motivo que ha ocasionado su retirada del estudio.

Si usted es retirado del estudio, per algún de los motivos expresados, su óptico optometrista le prescribirá un tratamiento adecuado a su defecto refractivo.

En signar el full de consentimiento adjunto, se compromete a cumplir con los procedimientos del estudio que le han expuesto.

12. Nombre i teléfono de contacto de la persona de referencia para los pacientes del CIMA

Appendix B

"Consentimiento informado por escrito para el paciente"

UNIVERSITAT POLITÈCNICA DE CATALUNYA BARCELONATECH Centre Universitari de la Visió	Estudio observacional: Consentimiento informado por escrito para el paciente Código del estudio observacional:	Página 1 de 1 Versión: 1 Fecha: 11/07/2017

1. Datos del estudio	
Título del estudio	Validación del sistema basado en el Contraste de las Imágenes de Purkinje para medir la difusión de la córnea y del cristalino
Código del estudio	
Código del promotor	
Nombre del promotor	CUV-CD6

2. Datos del investigador principal	
Nombre y apellidos del investigador principal	Meritxell Vilaseca Ricart
Núm. de colegiado/da	
Unidad de especialización	

Yo, (nombre y apellidos)

He leído la hoja de información que se me ha proporcionado.
He podido hacer preguntas sobre el estudio.
He recibido suficiente información sobre el estudio.
He hablado con: (nombre del investigador o la investigadora)

Comprendo que mi participación es voluntaria.
Comprendo que puedo retirarme del estudio:
1. Cuando quiera.
2. Sin tener que dar explicaciones.
3. Sin que esto repercuta en mis atenciones médicas.

Presto libremente mi conformidad por participar en el estudio y doy mi consentimiento para el acceso y utilización de mis datos en las condiciones detalladas en la hoja de información.

Firma del paciente	Firma del investigador/a
Nombre y apellidos Fecha (escrita por el paciente)	Nombre y apellidos Fecha

Este documento se firmará por duplicado. El investigador o investigadora se quedará una copia i el paciente otra

Appendix C

"Informe del Comité Ético de Investigación con Medicamentos"

FUNDACIÓ ASSISTENCIAL MÚTUA TERRASSA
CEIm

MútuaTerrassa

INFORME DEL COMITÉ ÉTICO DE INVESTIGACIÓN CON MEDICAMENTOS

Dr. Jordi Nicolás Picó.
Presidente del Comité Etico de Investigación con Medicamentos de:
FUNDACIÓ ASSISTENCIAL MÚTUA TERRASSA

CERTIFICA:

Que este Comité ha evaluado en la reunión del día 26 de abril de 2017 (Acta 04/2017) el estudio titulado "Validación del sistema basado en el Contraste de las Imágenes de Purkinje para medir la difusión de la córnea y del cristalino".

y considera que,

Se cumplen los requisitos necesarios de idoneidad del protocolo en relación con los objetivos del estudio y están justificados los riesgos y molestias previsibles para el sujeto.
La capacidad del investigador y los medios disponibles son apropiados para llevar a cabo el estudio.
Son adecuados tanto el procedimiento para obtener el consentimiento informado.

Y este Comité acepta que dicho protocolo sea realizado por el Sr. Pau Santos Vives, la Dra. Meritxell Vilaseca Ricart, el Dr. Juan C.Ondategui Parra y el Dr. Joan A. Martínez-Roda..

Lo que firmo en Terrassa a 26 de abril de 2017.

Firmado:
Dr. Jordi Nicolás
Presidente del CEIm